Advances in Biamperometry with Applications in Ocular Toxicology

by

Mehdi Rahimi

A thesis
presented to the University of Waterloo
in fulfillment of the
thesis requirement for the degree of
Doctor of Philosophy
in
Chemistry

Waterloo, Ontario, Canada, 2013

I hereby declare that I am the sole author of this thesis. This is a true copy of the thesis, including any required final revisions, as accepted by my examiners.

I understand that my thesis may be made electronically available to the public.

Abstract

This thesis presents advances in biamperometry, together with applications cyclic biamperometry, in *in vitro* ocular cytotoxicity assessment. For the cytotoxicity/viability assessment, cultured human corneal epithelial cells have been used as a model. The assay involves electrochemical measurement of the respiratory activity of the cells, and relating the extent of cell respiration to cell viability. This measurement is done by capturing electrons from the components of the respiratory chain and transferring these electrons to a non-native terminal recipient.

In this study, three lipophilic redox mediators, including 2,6-dichlorophenolindophenol, menadione (vitamin K3) and N,N,N',N'-tetramethyl-p-phenylenediamine were evaluated. The mediators were compared with each other under their optimal conditions and 2,6-dichlorophenolindophenol was selected for further studies.

To demonstrate the cytotoxicity assessment, three well-characterized toxicants, including benzalkonium chloride, sodium dodecylsulfate, and hydrogen peroxide, were used and it has been shown that the electrochemical assay is able to detect the cytotoxicity of the test chemicals near their cytotoxicity threshold reported in the literature.

In addition, culturing human corneal epithelial cells on growth inserts, in an attempt to construct 3D corneal tissues to be used in ocular cytotoxicity assessment, is discussed.

Differential pulse biamperometry is also introduced. This electrochemical method involves application of differential pulse waveforms in the biamperometric electrochemical cells. Various parameters affecting the response of the method as well as potential applications for future studies are discussed.

The results of the experiments performed in these studies have been published in peer-reviewed journals. Cyclic biamperometry and its applications in micro-interdigitated electrodes, which were mainly investigated during my M.Sc. studies, were published in *Analytical Chemistry* (References 14, 28). Applications of cyclic biamperometry in *in vitro* ocular cytotoxicity assessment, which forms the second Chapter of this thesis was published in *Analytical and Bioanalytical Chemistry* (Reference 78) . Currently, preparation of the manuscript for publishing the results presented in the fourth Chapter of this thesis is under progress.

Acknowledgements

It was a privilege having Dr. Susan R. Mikkelsen, an enthusiastic scientist and a great teacher, as my M.Sc. and Ph.D. supervisor. I would like to thank her for her strong work ethic and commitment to the education of her students both in the field of analytical chemistry and life in general. Not only has she nurtured the development of my mind in the field of electrochemistry but she also taught me how to be a good teacher. Her advice, support and encouragements have inspired me and given me the motivation to make this contribution.

I would also like to thank Dr. Jacob G. Sivak, one of my advisory committee members, for giving me the opportunity to work and learn in his lab. I am also thankful to him for his wisdom, support and advice during the course of my studies. My sincerest thanks go to Dr. D. J. McCanna for teaching me cell culture preparations and Dr. D. A. Donkor for his help with the confocal microscopy studies.

Thank you to my advisory committee members, Dr. P. D. Josephy, Dr. T. Gorecki, and Dr. M. A. Monteiro for consenting to be on my advisory committee and for their support these last few years.

I am also thankful to Dr. V. Karanassios for his help, support and guidance during these years. Whenever I had a chance to talk to him I learned something new.

With great affection and admiration I dedicate this thesis to my parents and my siblings without whose support it would have been impossible to accomplish such a feat.

Table of Contents

List of Figures ix

List of Tables xii

List of Abbreviations xiii

1 Introduction 1

1.1 Conventional Electrochemistry in Two- and Three-Electrode Cells 1

1.2 Biamperometry 4

1.2.1 History of Biamperometry 5

1.3 Modern Developments and Applications of Biamperometry 7

1.3.1 Application of Cyclic Biamperometry at Micro-Interdigitated Electrodes 10

1.4 Selectivity, Interference and Limitations in Biamperometry and Conventional Three-Electrode Systems 12

1.5 Electrochemical Measurement of Cell Viability 13

1.5.1 Identification of Bacteria Based on Amperometric Measurement of Respiratory Activity 14

1.5.2 Assessment of Metabolic Activity in Eukaryotic Cells Based on Amperometric Measurement of Respiratory Activity 16

1.6 Cell-Based Cytotoxicity Assays Used for Ocular Cytotoxicity Assessment . 17

1.6.1 The Neutral Red Uptake (NRU) Assay 19

1.6.2 The Neutral Red Release (NRR) Assay . . . 19
1.6.3 The Red Blood Cell (RBC) Hemolysis Test . . . 20
1.6.4 Fluorescein Leakage Test . . . 20
1.6.5 The Silicon Microphysiometer (SM) or The Cytosensor Microphysiometer Assay . . . 20
1.7 Thesis Organization . . . 21

2 Human Corneal Epithelial Cell Viability Assessment Using Cyclic Biamperometry 22

2.1 Viability Assessment of Human Corneal Epithelial Cells Based On Monitoring Metabolic Activities Using Cyclic Biamperometry . . . 22
2.2 Materials and Methods . . . 24
2.2.1 Chemicals and Instrumentation . . . 24
2.2.2 Methods . . . 24
2.3 Results and Discussion . . . 25

3 Electrochemical Measurement of Trans-epithelial Resistance 36

3.1 Cultivation and Study of 3D Corneal Constructs . . . 36
3.1.1 Bovine Corneal Opacity and Permeability (BCOP) Assay . . . 36
3.1.2 The Isolated Rabbit Eye (IRE) Test . . . 37
3.1.3 The Isolated Chicken Eye (ICE) Test . . . 37
3.1.4 The ScanTox™ Assay . . . 38
3.1.5 The Hen's Egg Test on the Chorioallantoic Membrane (HET-CAM) Assay . . . 38
3.1.6 The Chorioallantoic Membrane Vascular Assay (CAMVA) . . . 38
3.1.7 The EpiOcular™ Assay . . . 39
3.1.8 The SkinEthic *in Vitro* Reconstituted Human Corneal Epithelium (HCE™) Model . . . 39
3.1.9 The Ocular Irritection® Assay . . . 40
3.2 Measurement of Trans-epithelial Resistance . . . 40

3.3 Materials and Methods 43
3.3.1 Chemicals and Instrumentation 43
3.3.2 Methods 44
3.4 Results and Discussion 44

4 Differential Pulse Biamperometry **57**
4.1 Introduction 57
4.2 Materials and Methods 66
4.2.1 Chemicals and Instrumentation 66
4.2.2 Methods 66
4.3 Results and Discussion 68

5 Summary and Suggestions for Future Research **81**
5.1 Summary of Original Contributions 81
5.2 Suggestions for Future Research 83

Appendix A Daily Raw Data for Trans-epithelial Resistance Measurement **85**

Appendix B Staining HCECs with ZO-1 and Counter Staining with Hoechst **89**

Appendix C Time Constant Calculations of Differential Pulse Biamperometry in Microsoft Excel 2010 **92**

References **97**

List of Figures

1.1 Classical controlled-potential apparatus for two- and three-electrode cells . 2
1.2 Schematic representation of a biamperometric cell 5
1.3 Apparatus for coulometric titration of cyclohexene with bromine. 6
1.4 A typical cyclic biamperogram representing the peak potentials and the peak currents. 7
1.5 Comparison of cyclic voltammograms and cyclic biamperograms 8
1.6 Peak current vs. square root of scan rate in CV and CB 9
1.7 A typical comb-like planar micro-interdigitated electrode array 11
1.8 A plot of cyclic biamperometry at micro-interdigitated electrodes 12
1.9 Schematic representation of a mitochondrial electron transport chain. . . . 15
1.10 Structures of the lipophilic mediators. Menadione, DCIP and TMPD . . . 17

2.1 Cathodic peak current against concentration of ferricyanide obtained from HCEC suspensions. 26
2.2 A typical biamperometric signal in 1X PBS containing 5.00 mM glucose in the absence and the presence of HCECs 27
2.3 Comparison of standard-size gold disk electrodes and the gold disk micro-electrodes 27
2.4 Cathodic peak current vs. concentration of ferricyanide in the presence of 1.0×10^7 cells/mL 28
2.5 Optimization of menadione concentration. 29
2.6 Optimization of DCIP concentration. 30

2.7 Optimization of TMPD concentration. 31
2.8 Comparison of mediators at their optimal concentrations. 32
2.9 Effect of irritants on the respiratory activity of HCECs. 33

3.1 EVOM^2 fork electrodes for measurement of trans-epithelial resistance. . . . 42
3.2 Polystyrene cell culture inserts 43
3.3 Resistance of inserts vs. time (first trial) 45
3.4 Relative TER values after exposure to BAC 46
3.5 Relative TER values after exposure to SDS 46
3.6 Relative TER values after exposure to H_2O_2 47
3.7 Resistance of treated inserts before and after a 24-h recovery 48
3.8 Respiratory activity of stratified cell constructs 49
3.9 TER measurement for ferricyanide-exposed stratified cell constructs 50
3.10 Resistance of stratified constructs vs. time (second trial) 51
3.11 Micrographs of the stratified multilayer HCECs grown on the inserts (magnification: 10X). 52
3.12 Micrographs of the stratified multilayer HCECs grown on the inserts (magnification: 63X) 53
3.13 Micrographs of the HCEC monolayers stained with Hoechst and ZO-1 . . . 54
3.14 Effect of BAC on membrane tight-junctions of HCECs 55

4.1 Commonly-used potential waveforms in voltammetric analysis 58
4.2 Classical differential pulse waveforms. 60
4.3 Decay of charging current with time after application of a potential difference. 60
4.4 Plots of measured potential at W_1 (vs. an Ag/AgCl reference electrode) against the applied voltage in CB 62
4.5 An equivalent circuit for a biamperometric cell 63
4.6 Calculated vs. experimental values of $(Z_1/Z_2)/(Z_1/Z_2+1)$ 65
4.7 Comparison of DPV and DPB graphs 68

4.8 Typical potential profiles for DPB measured against an external Ag/AgCl reference electrode. 69
4.9 Different pulse shapes for DPB at different base voltages. 70
4.10 Log RC vs. the base voltage for each pulse in DPB 72
4.11 Peak current vs. mole fraction of ferricyanide for a series of solutions with a constant total concentration of ferri- and ferrocyanide. 73
4.12 Peak current vs. ferricyanide concentration for DPB and DPV 75
4.13 Peak current vs. inverse square root of pulse width for DPB and DPV . . . 76
4.14 Peak current versus $(1-\sigma)/(1+\sigma)$ for DPB and DPV 77
4.15 Selectivity issues for DPB when more than one redox couple is present in the medium 78
4.16 Potential of W_1 vs. an external Ag/AgCl electrode during a CB scan . . . 79

B.1 Making gridlines and cutting the culture flask with a glass cutter. 89
B.2 Placement of the cell-carrying squares in 96-well plates for staining. 90
B.3 Staining HCEC monolayers using various fixatives. 91

C.1 A single DPB pulse 93
C.2 Rearrangement and normalizing voltage values in a single pulse. 94
C.3 Solver Parameters dialogue box 95
C.4 RC value resulting in the minimal squared difference for a single pulse. . . 96

List of Tables

4.1 Examples of double layer capacitance values for different electrode materials, different electrolytes and at different applied potentials. 61

4.2 Comparison of experimental and predicted voltage scan rates at W_1. 64

4.3 y-Intercepts and the corresponding standard deviations for DPB and DPV 74

A.1 Trans-epithelial resistance of the corneal constructs in the second trial . . . 86

List of Abbreviations

μIDEs	micro-interdigitated electrodes
ν	scan rate
τ'	the moment of current measurement just before the application of the pulse in DPV
τ	the moment of current measurement just after the application of the pulse in DPV
A	area, auxiliary electrode, ammeter
C	capacitance, counter electrode, concentration
C_{dl}	double-layer capacitance
C_{O}	concentration of the oxidized species
C_{R}	concentration of the reduced species
D	diffusion coefficient
D_{O}	diffusion coefficient of the oxidized species
D_{R}	diffusion coefficient of the reduced species
E	potential
E_{pa}	anodic peak potential
E_{pc}	cathodic peak potential
F	Faraday constant

f	frequency
i	current
i_{pa}	anodic peak current
i_{pc}	cathodic peak current
n	number of electrons transferred in a redox reaction
R	resistance, reference electrode
R_{Ω}	resistance of the bulk solution
R_{ct}	charge-transfer resistance
t	time
V	voltage
Z	impedance
BAC	benzalkonium chloride
BCOP	bovine corneal opacity and permeability
CAMVA	chorioallantoic membrane vascular assay
CB	cyclic biamperometry
CV	cyclic voltammetry
DCIP	dichlorophenol indophenol
DPB	differential pulse biamperometry
DPP	differential pulse polarography
DPV	differential pulse voltammetry
ECVAM	European Centre for the Validation of Alternative Methods
HCEC	human corneal epithelial cell
HET-CAM	hen's egg test on the chorioallantoic membrane

ICE	isolated chicken eye
IRE	isolated rabbit eye
LDH	lactate dehydrogenase
MDCK	Madin-Darby canine kidney
MTT	methylthiazol tetrazolium test
NRR	neutral red release
NRU	neutral red uptake
PBS	phosphate buffered saline
RBC	red blood cell
rcf	relative centrifugal force
SDS	sodium dodecylsulfate
SM	silicon microphysiometer
TER	trans-epithelial resistance
TMPD	N,N,N',N'-tetramethyl-p-phenylenediamine
W	working electrode
WST	water-soluble tetrazolium

Chapter 1

Introduction

1.1 Conventional Electrochemistry in Two- and Three-Electrode Cells

Electrochemical reactions occur at interfaces (e.g. electrode-solution interfaces) across which a potential difference, sufficiently large for transfer of electrons, exists. Exchange of electrons alters the concentrations of electroactive materials in the vicinity of the interface. Hence, a concentration gradient develops at the interface which extends toward the bulk of the solution. The region in which the electroactive analyte effectively moves under the influence of this concentration gradient is known as the diffusion layer. The dimensions of the diffusion layer, although changing during the course of a reaction, are restricted to a very small region adjacent to the interface.

Controlling electrochemical reactions for acquisition of useful data requires a good understanding of various processes occurring in this interfacial region. In addition, the aim of the experiment often dictates the design of the electrochemical cell.[1]

Conventional electrochemical cells, designed for controlled-potential experiments, employ two or three types of electrodes. A two-electrode cell consists of (i) a working electrode where the reaction of interest occurs and (ii) a reference electrode against which the potential of the working electrode is controlled. The reference electrode in these type of cells also functions as the counter electrode where an opposite redox reaction completes the circuit. The magnitude of the current flowing through the counter electrode is equal to that flowing through the working electrode but opposite in direction. Figure 1.1(a) shows a classical two-electrode controlled-potential apparatus.

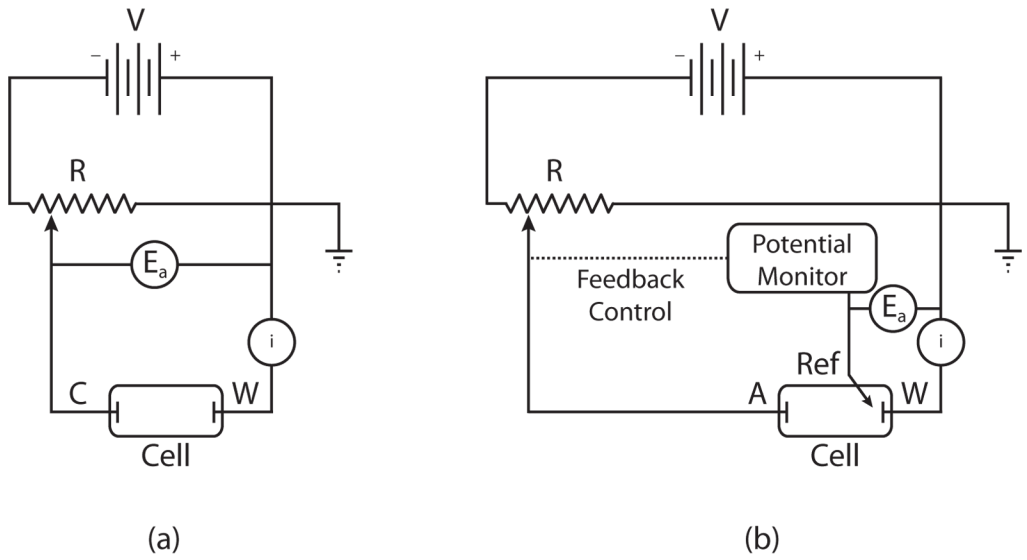

Figure 1.1: Classical controlled-potential apparatus for (a) two- and (b) three-electrode cells. E_a illustrates the controlled potential window, W, C and A are the working, the counter and the auxiliary electrodes.[1]

One major drawback of conventional controlled-potential two-electrode cells is the large distance between the desired potential control point (the working electrode-solution interface) and the actual potential control point (the counter electrode-solution interface). Therefore, when the iR drop* across the bulk of the solution is significant, i.e. when large current flows through the cell or when the resistance of the solution is high (e.g. in non-aqueous solutions), the potential of the working electrode must be increased by the magnitude of the iR drop or the control over the potential of the working electrode will be lost.[1] Another drawback can occur when significant current flows at the reference electrode, because the composition of this half-cell can change with time, and this causes a change in the reference potential. This is generally not important with disposable, single-use 2-electrode cells.

To address these issues, the simultaneous functions of the counter electrode can be assigned to two separate electrodes. This forms the basis of a conventional controlled-potential three-electrode cell, the apparatus of which is illustrated in Figure 1.1(b).

A conventional three-electrode cell consists of (i) a working electrode where the oxidation or reduction of analyte produces the current response; (ii) a reference electrode against

*iR drop, also known as the Ohmic drop, is the decrease in the magnitude of the voltage across a resistor R when the current i is passing through it ($V = iR$).

which the potential of the working electrode is controlled, and (iii) an auxiliary electrode where the opposing redox reaction completes the circuit.[1]

Exchange of electrons between the analyte and the electrode surface generates a current known as the faradaic current. It is this current that is considered the analytical response in the aforementioned electrochemical cells. Faradaic current, however, is not the only source of electron flow in the electrode leads. It is widely accepted that an electrode-solution interface behaves similarly to an electrical circuit containing a resistor (impedance) in parallel with a capacitor.[2] In other words, any change in the magnitude of the applied potential at the interface triggers the flow of a transient current known as the charging current. Ideally, charging current is the only interfering current (background). In practice, however, chemical impurities in the electrolyte and the components of the electrical measurement device generate non-specific currents known as noise. The magnitude of the background current and the noise impose the detection limit of an amperometric electroanalytical method.[2]

Over decades, various electrochemical methods have been developed for different purposes; however, for analytical applications, improving the signal to background ratio has been a major goal pursued through application of different waveforms to various cell geometries.[3]

Methods based on applications of pulse waveforms (e.g. differential pulse voltammetry) offer very sensitive analytical responses and low detection limits. The detection limits are enhanced when the analysis is preceded by a preconcentration step (e.g. in anodic stripping differential pulse voltammetry).

Good detection limits, a large linear dynamic range ($10^{-8} - 10^{-3}$ M), the low cost of equipment, and the rapidity and simplicity of voltammetric methods make them very suitable for quantitation of pharmaceuticals. In addition, an extremely large number of organic compounds are electroactive due to the presence of certain electroactive groups. Functional groups with excellent electrochemically-addressable properties in these compounds are nitro, nitroso, azo, azoxy, quinone, azomethine, activated carbonyls and activated double bonds.[1] This has led to manufacturing of hundreds of electrochemical sensors for different analytes based on voltammetry.[4–7] However, as fabrication of micro and nano-scale sensors has become more popular, new challenges have emerged. One such challenge is the fabrication of a functioning reference electrode on the same size scales as the working electrode(s). Therefore, development of miniaturized reusable reference electrodes for use in micro sensors is still a subject of research.[8–11]

In some studies, quasi-reference electrodes have been used.[12,13] Quasi-reference electrodes (e.g. simply a platinum wire), have usually been used in non-aqueous media and/or when the possibility of interference due to contamination by the reference electrode materials exists.[2] In these studies the potential of the quasi-reference electrode is controlled by

the solution composition, and should be checked and reported against an accepted reference electrode. Users assume that during the course of the reaction this potential does not change significantly.

Two-electrode cells, with the counter electrode functioning as both auxiliary and reference, are often employed. Miniaturized electrochemical cells, for example, have current response magnitudes in the range of nA or less in aqueous electrolytes. In such cases, the potential variations of the counter electrode are often less than 1 mV and, therefore, this electrode can also be used as a reference probe.[1] However, when the auxiliary electrode is positioned in proximity to the working electrode, as in miniaturized electrochemical cells, the products generated at the former electrode may easily reach and interfere at the latter electrode. Therefore, neglecting the reaction at the counter/auxiliary electrode, which is the default approach in conventional three-electrode cells, is not always an acceptable practice.

In conventional potentiostatic or potentiodynamic amperometric methods, the potential difference between the working electrode surface and the bulk solution is controlled because this value is measured against a reference electrode or half-cell, the potential of which is assumed constant. This assumption is not always valid, especially with regard to metallic quasi-reference electrodes, which can be easily fouled, and are subject to the potential dictated by the analyte solution.

Elimination of the reference electrode, using two conducting working electrodes instead of conventional two- or three-electrode cells, is one of the main topics of this thesis: biamperometry.

1.2 Biamperometry

Biamperometry, also called amperometry with two polarizable electrodes, involves the application of a small constant voltage ($\sim$ 150 mV) across two typically metallic electrodes and measurement of the resulting current. Usually, an aqueous solution forms the electrolyte and the electrodes are noble metals (e.g. Au or Pt) of approximately equal surface area,[14] as shown in Figure 1.2.

Generation of faradaic current in biamperometric cells depends on the presence of two species (frequently two halves of a reversible redox couple) that can undergo opposite redox reactions within the applied voltage. This current is proportional to the concentration of the limiting reactant when the other species is present in great excess.[14]

In biamperometry, control of individual electrode-to-solution potentials is impossible and it has been found that distribution of the applied voltage between the electrode-solution

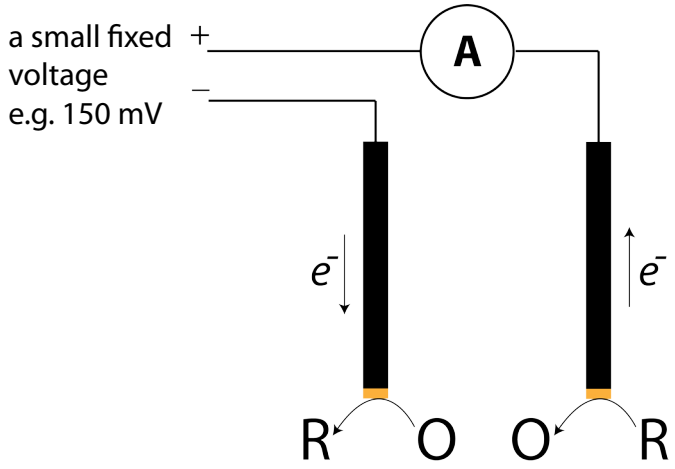

Figure 1.2: Schematic representation of a biamperometric cell

interfaces follows the concentration ratio of the oxidized-to-reduced species in the bulk of the solution, provided that the diffusion coefficients of the two species are equal and the electron transfer rates are fast. As a result, the faradaic currents at the electrodes are equal in magnitude but opposite in direction.[14]

1.2.1 History of Biamperometry

The biamperometric cell, as we know it today, was discovered accidentally while preparing the electrochemical titration of iodine with thiosulfate using a "conventional" approach.[15] The endpoints in early biamperometric titrations were marked by diminishment of the faradaic current to zero after addition of just-enough titrant; hence, the dead-stop endpoint was suggested by Foulk and Bawden along with the introduction of the cell in 1926.[15] Biamperometry has since been used in electrometric titration of various analytes including, but not limited to copper, organic peroxide, vitamin C, cyclamate and uranium.[16–21]

Early biamperometric titrators were intended for the volumetric determination of analyte concentration.[15] However, integration of biamperometric circuits into a coulometric titrator, in which total charge, rather than current, is measured allowed the endpoints to be marked more accurately.[22]

Figure 1.3 shows a schematic representation of a coulometric titrator with an integrated biamperometric circuit. In this scheme cyclohexene is titrated with bromine in the following reactions:[22]

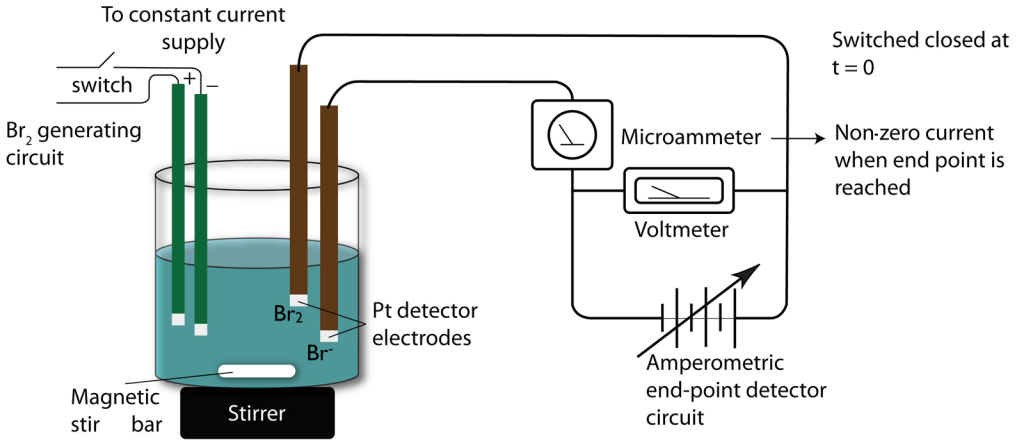

Figure 1.3: Apparatus for coulometric titration of cyclohexene with bromine.[22]

$$2Br^- \longrightarrow Br_2 + 2e^- \tag{1.1}$$

$$Br_2 + \text{cyclohexene} \longrightarrow \textit{trans}\text{-1,2-dibromocyclohexane} \tag{1.2}$$

The solution of cyclohexene contains 0.15 M KBr and 3.0 mM mercuric acetate in a mixed solvent of acetic acid, methanol and water. Mercuric acetate catalyzes the addition of Br_2 to the cyclohexene.[22]

This titration is carried out at a constant current in the stirred solution. Bromine molecules immediately react with cyclohexene to produce *trans*-1,2-dibromocyclohexane. Just after depletion of cyclohexene, the presence of excess bromine, indicator of the end-point, is marked by the generation of a current in the biamperometric circuit on the right-hand side of the figure. Because in the left-hand circuit the applied current is kept constant, the experimenter can determine the initial concentration of cyclohexene based on the amount of charge transferred within the time required to reach the endpoint.[22]

It is worth mentioning that applications of biamperometric cells have not been limited to titrations; these cells have been integrated into various devices including flow injection cells,[23] a glucose sensor (Accu-Chek® from Roche Diagnostics[24]), sensor chips,[25] and an auto-dimming electrochromic rear-view mirror.[26]

1.3 Modern Developments and Applications of Biamperometry

Previous work in this laboratory considered the application of a triangular voltage waveform, similar to that in cyclic voltammetry (CV), across the two biamperometric electrodes. This forms the basis of a recently introduced electrochemical method called cyclic biamperometry (CB).[14]

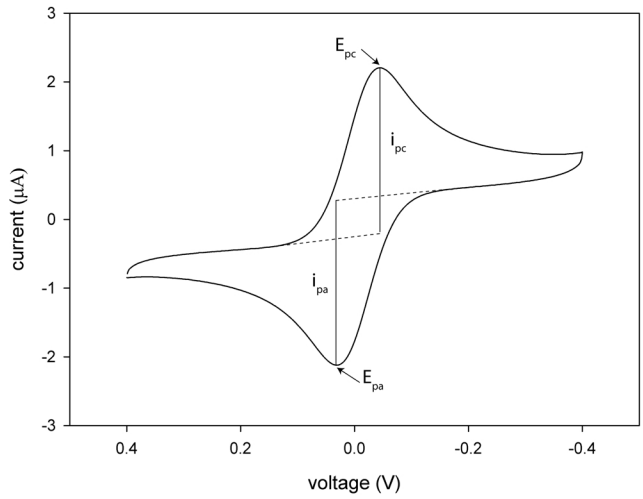

Figure 1.4: A typical cyclic biamperogram representing the peak potentials and the peak currents. Conditions: 1.00 mM ferricyanide and 5.00 mM ferrocyanide in 0.100 M KCl, 25 mV/s scan rate using two gold disk electrodes (1.6 mm dia.) at room temperature.[14]

CB registers the current as a function of the applied voltage. The peak currents and the peak voltages are defined in a similar way to those in cyclic voltammetry; however, lack of a reference electrode in the circuitry results in formation of a "biamperogram" that is centered on the origin as shown in Figure 1.4. The peak currents in CB are proportional to the concentration of the limiting half of the redox couple when the other half is present

in great excess. Also, these currents are proportional to the square root of the applied voltage scan rate.[14]

Unlike in CV, where the potential of the working electrode is controlled against the potential of the reference electrode, in CB only the applied voltage window can be controlled. In other words, the experimenter has no control over the potentials of the individual electrode-solution interfaces.

The main difference between CB and CV, except for the absence of the reference electrode in the former, is that the current response in CV is proportional to the total concentration of the redox couple, not to the limiting species; because the starting point of the scan in CV is often selected at a potential value where only one form of the two species can be present at the surface of the electrode. Figure 1.5 illustrates the similarities and the differences between the two methods.[14]

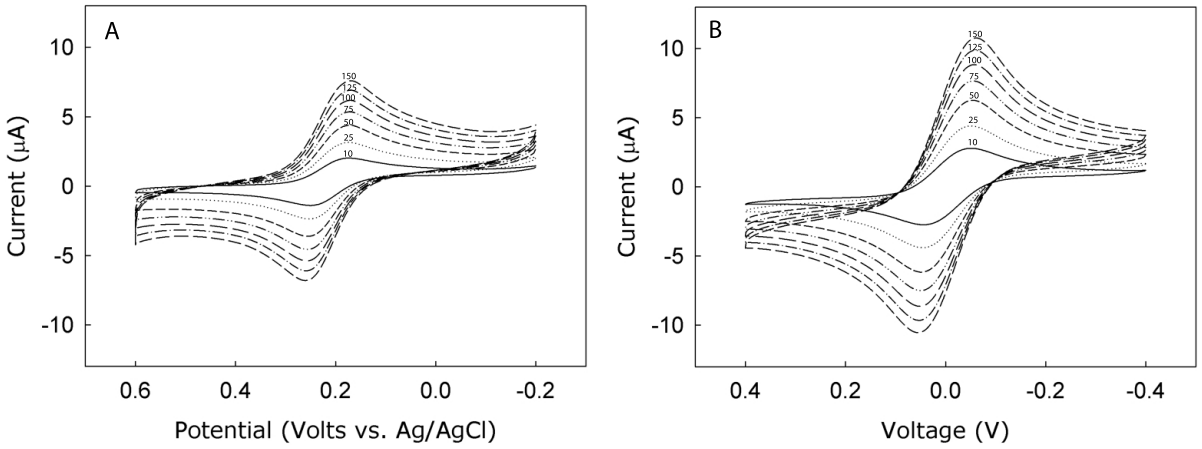

(a) Cyclic voltammetry (b) Cyclic biamperometry

Figure 1.5: Cyclic voltammograms of 1.00 mM ferricyanide in 0.100 M KCl (A) and cyclic biamperograms for a solution containing 1.00 mM ferricyanide in 5.00 mM ferrocyanide and 0.100 M KCl (B) The applied scan rates were 10, 25, 50, 75, 100, 125 and 150 mV/s. Standard-size gold disk electrodes (dia: 1.6 mm) were used.[14]

The cathodic and anodic peak potentials in the CV experiment (Figure 1.5(a)) are symmetrical with respect to the formal potential of the redox couple (0.214 ± 0.001 V vs Ag/AgCl), while the CB peaks (Figure 1.5(b)) are symmetrical about zero applied voltage (–0.003 ± 0.001 V).[14]

The peak currents in both cases are linearly proportional to the square root of the scan rate as shown in Figure 1.6. The slopes of these lines are 1.46×10^{-5} and 2.62×10^{-5}

$A/(V/s)^{1/2}$ for CV and CB, respectively with the corresponding R^2 values of 0.999 and 0.999.[14]

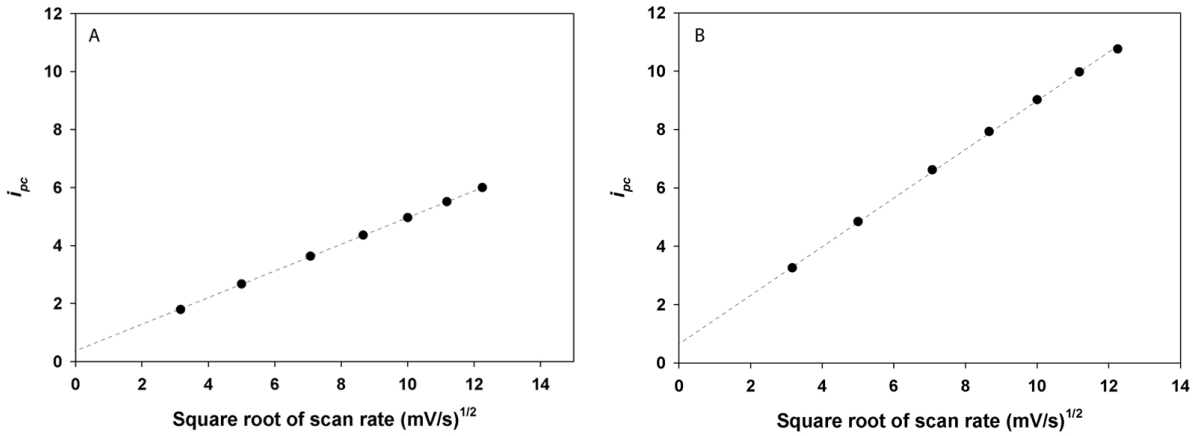

Figure 1.6: Peak current vs. square root of scan rate in CV (A) and CB (B) extracted from Figure 1.5.[14]

The Randles-Sevcik equation (below) is commonly used to describe the relationship between the peak currents in cyclic voltammetry and the applied scan rate.[27]

$$i_{pc} = (2.69 \times 10^8) n^{3/2} A C D^{1/2} \nu^{1/2} \tag{1.3}$$

In this equation, i_{pc} is the peak current, n is the number of electrons transferred in the redox reaction, A is the surface area of the working electrode, C is the concentration of the analyte in the bulk of the solution, D is the diffusion coefficient of the analyte, and ν is the applied potential scan rate. All the units are in SI.

When ferrocyanide is present in great excess, the peak currents in CB are proportional to the concentration of the limiting reactant, ferricyanide. Under these conditions, assuming equal surface areas for W_1 and W_2 electrodes, and identical diffusion coefficients for the reduced and the oxidized form, the peak currents in CB are approximately twice as large as those in CV. To clarify this point, one can consider the terms in Equation 1.3 together with the fact that in a biamperometric cell with a single reversible redox couple, the same reactions occur at W_1 and W_2 interfaces in the opposite directions.

Since the magnitudes of the currents flowing through the two electrode-solution interfaces are equal, the number of moles of ferrocyanide oxidized at one interface is equal to the number of moles of ferricyanide reduced at the other. For equal electrode areas and

equal diffusion coefficients, if ferrocyanide is present in great excess, then the magnitude of the current is dictated by the concentration of the other form, ferricyanide. When the limiting reactant is completely consumed at the surface of one electrode, the other reactant is incompletely consumed (in an equimolar amount) at the surface of the other electrode. Under biamperometric cyclic conditions, the limiting reaction will alternate between the two interfaces. Ferricyanide is produced at W_1 when the applied voltage is positive and the local increase in the quantity of ferricyanide equals the amount of ferrocyanide produced at W_2. Since the diffusion coefficients are similar the total surface areas of W_1 and W_2 is considered to be relevant in Equation 1.3. The experimentally observed deviation from an exact 2:1 ratio of the peak currents ($\sim$ 1.8:1) is believed to be due to the differences between the applied scan rates in CV and CB. Because the applied scan rate in CB will be distributed across both interfaces, the magnitude of the scan rate at the limiting interface in CB is smaller than the value at the working-electrode interface in CV. Further explanations of the interfacial reactions and the voltage distribution pattern in biamperometric cells will be discussed in Chapter 4.

A key feature in fixed-potential and cyclic biamperometry is that the ratio of the oxidized form of the analyte to its reduced form is not altered during the analysis as long as only one redox couple is used for both oxidation and reduction reactions. This allows multiple measurements on the same sample and may be of particular interest where only one form of the redox couple, in the presence of the other half, should be quantitated. Other applications of this method may be of interest to nanotechnologists where measurements on very small scales (e.g. microchips) are required, because the absence of a reference electrode greatly simplifies the miniaturization of the measurement apparatus.[28]

Details of the application of CB to the development of a viability/cytotoxicity assay for human corneal epithelial cell suspensions based on measurement of respiratory activity form a separate chapter in this thesis and are discussed in Chapter 2. Further developments of biamperometry are introduced in Chapter 4.

1.3.1 Application of Cyclic Biamperometry at Micro-Interdigitated Electrodes

Micro-interdigitated electrodes (μIDEs) are sets of closely spaced anodes and cathodes where the thickness of each set and distance between them are on the order of a few micrometers. These electrodes were introduced in modern electrochemistry to examine an alternative set-up to opposing planar electrodes in thin-layer cells. The purpose of employing μIDEs in this laboratory has been to generate steady-state currents at stationary solid electrodes.[29]

Micro-interdigitated electrodes have been used in several studies and applications including, but not limited to biosensors,[30] electrochemical sensors,[31] bioassays,[32] flow cell detectors,[33] batteries,[34] photodetectors,[35] electronic conduction measurements in polymers[36] and charge transport measurements in discotic liquid crystals.[37] Many of these applications use μIDEs in high frequency circuits, for impedance measurements.

Figure 1.7 illustrates a typical comb-like planar μIDE array with 5 μm gap and 5 μm band.[28] The proximity of anodes and cathodes in μIDEs allows the products of electrochemically reversible redox reactions to diffuse towards the differently-polarized electrodes nearby and react in the opposite manner. This phenomenon, which is known as redox cycling, can result in signal amplification factors of as high as 10^4 fold.[33]

Figure 1.7: A schematic illustration of a comb-like planar micro-interdigitated electrode array (left), a typical comb-like planar micro-interdigitated electrode array (middle) and a micrograph of the same electrodes showing the gaps and bands (right).[28]

Biamperometric cells can greatly benefit from redox cycling in miniaturized electrochemical cells. In addition, another advantage of biamperometry, when applied to μIDEs, immediately becomes noticeable. It has been recently shown that in miniaturized electrochemical cells where the auxiliary electrode cannot be positioned far away from the working electrode, the use of a conventional 3-electrode cell may not be a suitable approach. For amperometric detection of analyte, in a conventional 3-electrode cell, the reaction(s) occurring at the auxiliary electrode and possible interference by the product(s) at the working electrode are typically neglected.[38]

Cyclic biamperometry applied with μIDEs using the ferri-/ferrocyanide redox couple leads to the generation of a sigmoid current-voltage plot which is a characteristic of electrode reactions where no depletion of reactant(s) occurs at the electrode surface, as shown in Figure 1.8. In this case, redox cycling results in constant supply of reactants which consequently triggers the production of a limiting (or plateau) currents, instead of a peak currents.[28]

Interestingly, the limiting current at μIDEs is independent of the applied scan rate. This is due to the absence of a concentration gradient of reactants or products due to their regeneration at the opposing electrode(s) nearby.[28] This allows the experimenter to keep the scan rate at a very low value to minimize the charging current without affecting the faradaic current, therefore greatly improving the signal to background ratio.

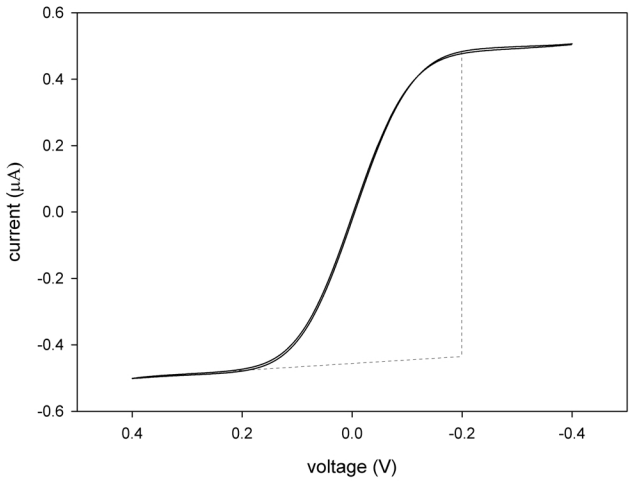

Figure 1.8: A plot of cyclic biamperometry at micro-interdigitated electrodes (25 pairs of 5 μm gap and 5 μm band, 2995 μm long) for a solution containing 0.200 mM ferricyanide, 0.200 mM ferrocyanide and 0.100 M KCl at 2 mV/s scan rate at room temperature.[28]

1.4 Selectivity, Interference and Limitations in Biamperometry and Conventional Three-Electrode Systems

In analytical chemistry, selectivity is defined as the ability to distinguish analyte from other species in the sample (interfering species).[27] However, to compare the selectivity between biamperometric and three-electrode cells it is necessary to define specifically what the experimenter is looking for.

As previously mentioned, the magnitude of the signal in biamperometric cells is proportional to the concentration of the limiting redox species when the other form of the redox species is present in great excess. For example, in a solution of Fe^{2+}/Fe^{3+}, it is possible to determine the concentration of either form in excess presence of the other form. However,

in conventional three-electrode amperometric methods that require a potential scan, e.g. cyclic or differential pulse voltammetry, the starting potential of the scan is often selected at a value where only one form of the redox species can be present in the vicinity of the electrode. So, it is the total concentration of the redox species that is quantitated and not the limiting form. In this example, biamperometry is more selective than the conventional three-electrode technique.

On the other hand, when more than one redox couple is present in the medium, biamperometric cells may generate non-specific current signal. For example, in a mixture containing Fe^{2+}, Fe^{3+}, quinone and hydroquinone, currently there is no way to identify the species that undergo the redox reactions at the two electrode-solution interfaces.

The generation of the biamperometric current does not necessarily require a redox couple. It has been shown than a biamperometric current can be produced when two irreversible redox reactions take place at the two electrode-solution interfaces.[39] For example, levodopa (3,4-dihydroxyphenylalanine) and permanganate can undergo oxidation and reduction at Pt electrodes, respectively, when the applied voltage across the two electrodes is ~ 100 mV.[39] This issue is more expressed when the signal is recorded for the blank solution in a medium containing other redox-active analytes. In such cases the signal from the blank solution[†], does not indicate the true blank signal. For example, when recording the current for a solution of 5.00 mM ferrocyanide in 0.100 M KCl (in absence of ferricyanide), trace elements present in KCl solution may result in generation of a biamperometric current.

Interfering species in three-electrode systems, however, have redox potentials which remain practically constant against the potential of the reference electrode within the course of an analysis. This allows the background signal to be measured and easily subtracted from the analyte response. Therefore, in this case, selectivity of biamperometric cells, compared to that of conventional three-electrode cells, is poor.

1.5 Electrochemical Measurement of Cell Viability

Electrochemical methods can be employed for assessment of cell viability. Such electrochemical assays often involve capturing of electrons from cell components and transferring them to a non-native electron acceptor, the reduced-form concentration of which is related to cell viability.[40–44]

[†]In our experiments with biamperometry, blank is the solution containing all components except the limiting electroactive species.

1.5.1 Identification of Bacteria Based on Amperometric Measurement of Respiratory Activity

Respiration is a series of electron transfer or redox reactions between several components of the electron-transport chain.[45] Aerobic respiration requires oxygen as the terminal electron acceptor, as opposed to anaerobic respiration, where the terminal electron acceptor is a species other than oxygen, for instance, NO_3^-, SO_4^{2-}, CO_2 or Fe^{3+}.[46]

In bacteria, the electron-transport chain resides in the cell membrane while in almost all eukaryotes the major electron-transport chain is embedded in the inner mitochondrial membrane.[46] Figure 1.9 shows the components of the electron-transport chain in a typical eukaryotic cell.[45] The respiratory complexes (numbered I - IV) consist of many of the embedded mitochondrial membrane proteins. These complexes are associated with various redox-active prosthetic groups where the reduction potential of each group successively increases. These complexes are mobile within the inner mitochondrial membrane. The first complex transfers electrons from NADH to coenzyme Q hence, it is known as coenzyme Q reductase. The iron-sulfur clusters in the complex are non-heme iron proteins that are mainly in the form of 2Fe-2S and 4Fe-4S clusters. For example, the 4Fe-4S cluster in the ferrodoxin protein (not shown) has one Fe^{2+} and three Fe^{3+} in its oxidized form and when the cluster is reduced one of the Fe^{3+} atoms is converted to Fe^{2+}. Complex I has two conenzymes including FMN and CoQ that each has three oxidation states and can accept or donate one or two electrons in a redox reaction. Complex II and III are succinate-CoQ reductase and CoQ-cytochrome C reductase, respectively. Cytochromes are heme proteins that function as electron transports by alternating the oxidation states of their iron atoms. Complex IV is a cytochrome C oxidase which transfers the electrons from cytochrome C to the terminal electron acceptor, oxygen.[45]

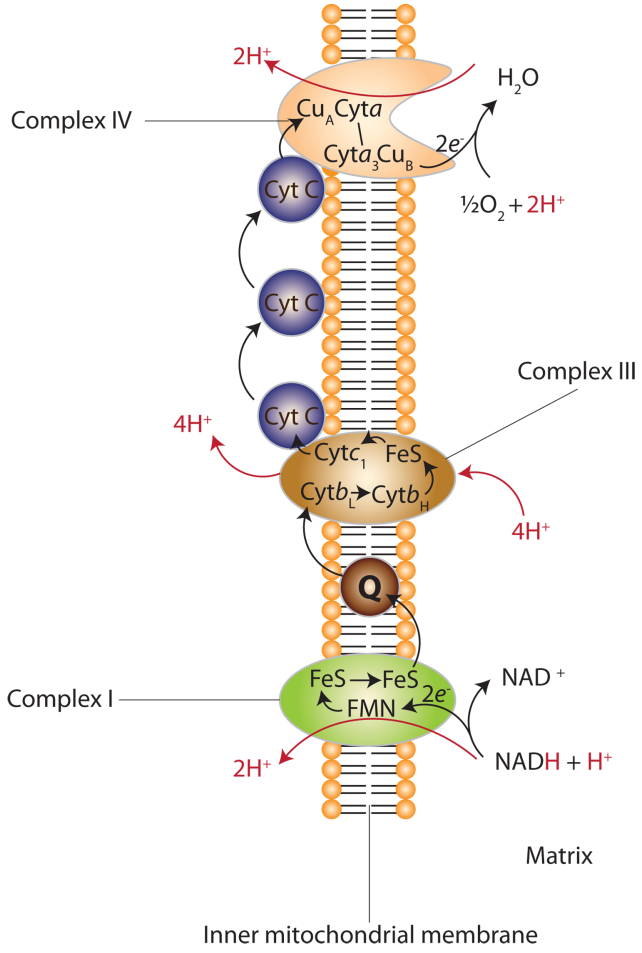

Figure 1.9: Schematic representation of a mitochondrial electron transport chain. Complexes I - IV include many of the proteins embedded in the inner mitochondrial membrane. Electrons are transferred from succinate to conenzyme Q by Complex II (not shown)[45] Complex I: NADH-coenzyme Q reductase, Complex II: succinate-coenzyme Q reductase, Complex III: coenzyme Q-cytochrome C reductase, complex IV: cytochrome C oxidase. "Q" in the figure represents coenzyme Q.

Respiratory activity of bacteria can be electrochemically monitored by measuring the consumption of the dissolved oxygen in the medium. For example, Karasinski *et al.* have reported the use of chronoamperometry for identification and differentiation of bacteria, based on patterns of oxygen consumption before and after exposure to antibiotics.[47]

Replacement of the terminal electron acceptor with a non-native oxidant having a

suitable reduction potential has also allowed scientists to monitor the respiratory activity of living cells.[40–42,48–51] Some of such respiratory-activity monitoring assays make use of redox dyes that, after reduction, are quantitated spectrophotometrically.[49–51] However, those that employ a conventional amperometric method use a 2- or 3-electrode cell, where the potential of the working electrode is controlled against a reference electrode.[40–42] Ertl *et al.*, in an earlier study in this laboratory, have reported the use of chronocoulometry for identification of bacteria in a biosensor array.[43] Their approach involves selective binding of microorganisms to the modified electrode surface based on lectin-lipopolysaccharide recognition and measurement of respiratory activity by replacing the terminal electron acceptor with $Fe(CN)_6^{3-}$, the reduced form of which, $Fe(CN)_6^{4-}$, can be quantitated in a coulometric cell.

This group has also reported the use of chronoamperometry for rapid antibiotic susceptibility testing.[41,44] This approach also relies on the reduction of ferricyanide by viable bacteria after exposure to the desired antibiotic. The concentration of ferrocyanide is then determined using a rotating disk electrode which is kept at 0.500 V vs. an Ag/AgCl reference electrode.

In both examples mentioned above, the concentration of one form of redox couple, i.e. ferrocyanide, has been determined in presence of a large excess of the other form, i.e. ferricyanide. This is a clear example of a situation where biamperometry would be more practical than conventional amperometry, due to the absence of a reference electrode, which simplifies the electrochemical cell.

1.5.2 Assessment of Metabolic Activity in Eukaryotic Cells Based on Amperometric Measurement of Respiratory Activity

Respiratory activity in eukaryotic cells can also be monitored electrochemically. However, because the electron-transport chain in eukaryotic cells resides in the inner mitochondrial membrane, a lipophilic or amphiphilic redox mediator is needed to cross the cell membrane.[48,52] These mediators can also be reduced by cytosolic dehydrogenases. Therefore, the measured activity is the sum of mitochondrial and cytosolic reduction.[53]

Figure 1.10 illustrates the structures of three lipophilic/amphiphilic redox mediators including menadione, dichlorophenolindophenol (DCIP) and N,N,N',N'-tetramethyl-p-phenylenediamine (TMPD) that can be used for electron shuttling across the cell membrane. Although, the redox reactions involving these mediators are pH-dependent; their use in the cell-containing solution does not alter the pH of the medium, because (i) the medium is buffered and (ii) both the oxidation and reduction of the mediator happen in the same solution.

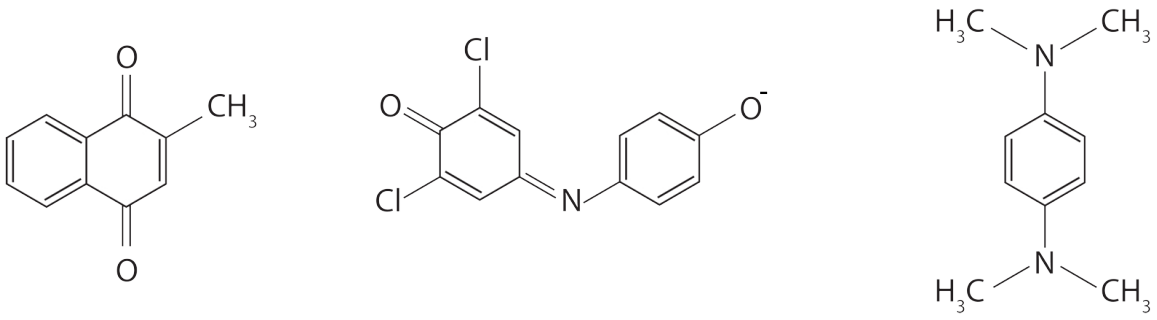

Figure 1.10: Structures of the lipophilic mediators. Menadione (left), DCIP (middle), TMPD (right)

Karube *et al.* have reported the use of ferricyanide along with menadione as the lipophilic redox mediator for chronoamperometric monitoring of biochemical oxygen demand in *Saccharomyces cerevisiae*.[48] Tsai *et al.* have used ferricyanide with menadione or succinate as the lipophilic mediator for assessment of cell viability of human MDA-MB-231 cell lines by chronoamperometrically monitoring the respiratory activity of the cells.[52] In addition to eukaryotic cells, Gram-positive bacteria and *S. cerevisiae* also require a lipophilic mediator such as dichlorophenolindophenol to shuttle the electrons from the electron-transport chain to the extracellular medium.[40,41]

In the studies mentioned above, biamperometry could be a convenient substitute for chronoamperometry, as the absence of a reference electrode would make the electrochemical cell simpler and one form of the redox couple can be readily quantitated in the presence of an excess of the other form. Because the current is proportional to the concentration of the limiting of the two redox forms, the experimenter must make sure that the analyte is the limiting reactant; otherwise, the other form of redox species will dictate the magnitude of the faradaic current.

1.6 Cell-Based Cytotoxicity Assays Used for Ocular Cytotoxicity Assessment

Several assays exist for the assessment of ocular irritants; however, no single assay has been approved by the regulatory agencies for complete replacement of the Draize test.[54]

In 1944 John H. Draize proposed an approach for cutaneous and ocular testing, which was soon adopted by FDA for safety evaluation of chemical compounds such as insecticides, sunscreens and antiseptics.[55] The original protocol of the Draize eye test was based

on determination of injuries to cornea, conjunctival and palpebral mucosae and the iris of rabbit models which used to be scored separately. After instilling 0.1 mL of liquids, solutions and/or ointments into one eye of 9 albino rabbits, readings were recorded after 1, 24 and 48 h, and if the residual injury was still present, another reading was made after 96 h. The evaluation was based on corneal opacity, scored 0-4, area of cornea involved, scored 0-4, reactivity of iris to light, scored 0-2, redness of conjunctiva, scored 0-3, swelling of conjunctival tissue, scored 0-4 and conjunctival discharge which was scored 0-4.[55]

Although the Draize test, after several modifications, is now considered a "very mild test"[56] experts have indicated several fallacies of the test. The Draize test does not offer a clear way of interspecies transfer of data from the rabbit model to the human experience and the large amount of the applied test material (in the original protocol) simply does not mimic the real-life accidental exposure situations. In addition, there are biological differences between the human eye and that of the rabbit which may lead to improper interpretation of data. For example, rabbits have a much slower blinking rate compared to that of humans and rabbits eyes produce relatively lower amount of tear in response to irritation. Other structural differences exist between the two. For instance, the ratio for the area of the conjunctiva relative to the cornea in humans is smaller than that in rabbits and rabbits have a nictitating membrane. The composition of the tear film is different among different genera. Also, rabbits have a thinner cornea without the Bowman's layer.[57,58]

Although the scores of the Draize test resemble linear continuous data, each single summed value is composed of several, often weighted, multi-parameter component. Therefore, numerically equal scores do not represent identical severity and often, the differences between units prevent logical comparison.[59] Due to variety of variables in the Draize test, reproducibility of the test is poor especially for moderately irritating compounds. Some of such variables include, type of animal, the rate of the chemical delivery, the tearing amount, time of post-exposure irritation and subjective grading of the examiner. Furthermore, different examiners often obtain nonidentical results for the same test substance.[60]

The two major parameters assessed in the Draize test are toxicity and inflammation. The judgment based on these external factors cannot ascertain the underlying mechanisms. Direct contact with the eye may also produce delayed allergy, structural alterations, other molecular changes and systemic effects. However, none of these parameters are evaluated in this test.[61]

The desire to find alternatives to animal testing led to initiation of new projects seeking to replace the Draize eye irritancy test. Some of these projects investigated modifications of the test which would results in less suffering of the animal, while some others seek to replace the test with *in vitro* substitutes.

Currently several *in vitro* alternative eye irritancy tests have been developed, some of

which have been accepted by the regulatory agencies. These are based on the evaluation of cytotoxicity at the organ-level, tissue-level or cellular level. Reviewing all of these methods is beyond the scope of this thesis; however, a brief review of cell-based ocular cytotoxicity assays is presented. These assays are based on the assessment of cell viability and form an important category of assays for the evaluation of ocular cytotoxicity, because eye irritants can trigger cytotoxicity of various types leading to cell death.[62] Due to the complexity of the irritation mechanism in the human eyes, contemporary ocular cytotoxicity assessment relies on a tiered-testing approach, which consists of a sequence of tests at different levels. Each level has a specific rank which is systematically determined. The first or primary levels have higher ranks and a positive result from such a test is enough to confirm that a positive result will occur at the subsequent levels. The sublevels for a test indicator are usually determined in order of complexity of effects. Cell-based cytotoxicity assays are usually performed at the initial levels for screening purposes, because they are relatively inexpensive and are able to readily distinguish highly irritant chemicals.[54,62,63]

1.6.1 The Neutral Red Uptake (NRU) Assay

The NRU assay is based on the cytotoxic effects of some chemicals that prevent the ability of viable cells to take up the neutral red dye, which is a marker of cell viability. Neutral red can penetrate through the cell membrane of healthy cells and accumulate in the lysosomes. Any modification to the cell membrane or the lysosomal structure may negatively affect the uptake of the dye, and this can be attributed to the cytotoxicity of the chemical.[64]

The test is performed on monolayer cell cultures (e.g. human epidermal keratinocytes) that have reached near-confluence. These monolayers are exposed to the test substance for 24 to 48 h after which the test substance is diluted away and the cells are incubated for 3 h with the growth medium containing the dye. After the incubation period, the cells are fixed (e.g. with 5% glutaraldehyde for 2 min), the extracellular dye is rinsed off and the optical density is measured at 540 nm. The results are compared to control samples that had not been exposed to the test substance and the concentration required for 50% inhibition is frequently reported as the expression of toxicity.[64] This assay is used for screening purposes by many pharmaceutical and cosmetic companies in a tiered-testing approach, in combination with other assays.[65]

1.6.2 The Neutral Red Release (NRR) Assay

The NRR assay was developed by Reader *et al.*[66] This assay is similar to NRU in its protocol in some aspects; however, the NRR assay has been designed for the evaluation

of relatively short-exposure toxicity resulting from damage to the cell membrane. In this assay the monolayer cell culture is first incubated with the medium containing the dye for 3 h, after which the cells are washed and briefly exposed to the test substance (for 1 to 5 min). After this step, the cells are fixed and the medium is replaced by an appropriate solvent to dissolve the dye from the interior of damaged cells. The optical density of the solution is then measured at 540 nm and compared to that of the control samples. The toxicological parameter is the concentration of the test substance causing a 50% decrease in the optical density.

1.6.3 The Red Blood Cell (RBC) Hemolysis Test

The RBC test relies on the cytotoxic potential of chemicals in disrupting the membrane of red blood cells. Upon exposure to cytotoxic substances, hemoglobin in red blood cells leaks through the compromised cell membrane, and is measured spectrophotometrically. In addition, denaturation of oxyhemoglobin can also be monitored.[67]

1.6.4 Fluorescein Leakage Test

The healthy corneal epithelium is impermeable to most potentially irritating chemicals. However, eye irritants can disrupt the integrity of the tissue by damaging the tight junctions between the cells, so that this impermeable barrier is impaired. The fluorescein leakage test is mostly conducted on mono- or multilayers of Madin-Darby canine kidney (MDCK) epithelial cells where the cell construct, after reaching confluence, separates a cell growth insert into two compartments. At this stage, the test substance is added to the upper compartment for a certain period of time. Then, the test substance is washed away and sodium fluorescein is added to the same compartment. After 30 min of incubation, the amount of fluorescein that has leaked into the lower compartment is measured spectrofluorometrically. The degree of leakage is then related to the extent of tissue disruption. The concentration of the test chemical triggering 20% or 50% leakage, relative to the controls, is then determined.[68,69]

1.6.5 The Silicon Microphysiometer (SM) or The Cytosensor Microphysiometer Assay

The silicon microphysiometer, also called the cytosensor microphysiometer assay, was developed by Burner *et al.*,[70] McConnel *et al.*,[71] and Catroux *et al.*[72] This assay relies on the

extent of acidic metabolite released by the cells to the surrounding medium in response to the toxic effect of irritants.

In this assay, the cells (e.g. normal human epidermal keratinocytes) are cultured on inserts and placed in a small flow-through chamber that has a stopped-flow capability. The pH-sensitive hydroxyl and amino groups form the coating of the silicon wall which is located in front of the cell culture. Upon the release of acidic metabolites, the change in the pH of the medium is sensed potentiometrically at the surface of the silicon wall. pH change is correlated with the metabolic state of the cells. Exposing the cells to incrementing concentrations of the test chemical for fixed periods, washing the test substance and measuring the pH in the medium are repeated until no acidic metabolites are secreted by the cells. The concentration of the test chemical causing 50% decrease in the amount of released acidic metabolites is then noted as the irritancy result.

1.7 Thesis Organization

In this thesis, an electrochemical assay for viability/cytotoxicity assessment of human corneal epithelial cells (HCECs) based on the biamperometric measurement of mediated cellular respiratory activity is presented. Chapter 2 concerns the measurement of respiratory activity and cytotoxicity/viability assessment of HCEC suspensions using cyclic biamperometry. Chapter 3 presents results from trans-epithelial resistance measurement using HCEC constructs as a corneal tissue model. This Chapter also deals with the issues of growing HCECs on cell inserts. In Chapter 4 a new biamperometric method, named differential pulse biamperometry, based on application of differential pulse waveforms in a biamperometric cell, is introduced. Chapter 5 presents a summary as well as suggestions for future research.

Chapter 2

Human Corneal Epithelial Cell Viability Assessment Using Cyclic Biamperometry

2.1 Viability Assessment of Human Corneal Epithelial Cells Based On Monitoring Metabolic Activities Using Cyclic Biamperometry

Electrochemical methods of cell viability assessment based on conventional three-electrode amperometry were discussed in Section 1.5. Other cell-based cytotoxicity assays that do not rely on redox reactions were briefly discussed in Section 1.6. Disparities are frequently observed among viability results obtained from different assays. For example, a cell incapable of DNA synthesis and reproduction is evaluated as dead if assayed based on the rate of DNA synthesis; but, the same cell is assessed as alive if a membrane-integrity-based assay is used.[73]

Although viability is an important criterion for the assessment of cytotoxicity, it is not the only criterion. Toxic chemicals may target different components in the cells affecting various functions without being lethal within the duration of the test. For example, a chemical hindering protein synthesis or the integrity of protein-making assemblies may not kill the cells; however, over a longer period, it may affect the rate of cell reproduction or trigger symptoms which are normally absent in healthy cells. Therefore, a battery of *in vitro* cytotoxicity/viability assays is now recommended in a tiered-testing approach for

proper identification and evaluation of toxic chemicals and/or for determination of safe usage doses.[74,75]

Two widely practiced assays for the assessment of cell viability are (i) the AlamarBlue® (resazurin) assay and (ii) the MTT (3-[4,5-dimethylthiazol-2-yl]-2,5-diphenyl tetrazolium bromide) assay. The AlamarBlue® assay relies on the ability of the intracellular enzymes to reduce the non-fluorescent blue dye to a highly fluorescent pink compound, resorufin. This allows the living cells to be spectrofluorimetrically quantitated.[76] The enzymes which are believed to reduce the dye include the mitochondrial enzymes such as flavin mononucleotide dehydrogenase, flavin adenine dinucleotide dehydrogenase, nicotinamide adenine dinucleotide dehydrogenase, nicotinamide adenine phosphate dehydrogenase and cytochromes.[77]

With the AlamarBlue® assay, as few as 80 cells in a single well (of a 96-well plate) can generate a reproducible and sensitive signal. AlamarBlue® is nontoxic to cells and does not require killing the cells; hence, the cells can be used for further investigation.[77]

The MTT assay is based on the ability of the intracellular enzymes to cleave the yellow tetrazolium salt to purple formazan crystals.[78] Because the formazan crystals are insoluble, a solubilization solution (usually either dimethyl sulfoxide, acidified ethanol, or sodium dodecyl sulfate in diluted hydrochloric acid) is required before reading the absorbance of the assay solution.[79]

To overcome the issue of solubilization of the formazan product in the MTT assay, other compounds, such as XTT (2,3-bis-(2-methoxy-4-nitro-5-sulfophenyl)-2H-tetrazolium-5-carboxanilide), MTS (3-(4,5-dimethylthiazol-2-yl)-5-(3-carboxymethoxyphenyl)-2-(4-sulfophenyl)-2H-tetrazolium) and other WSTs (water-soluble tetrazolium salts) have been introduced.

XTT yields a higher sensitivity and a wider dynamic range compared to MTT.[80] MTS, in the presence of phenazine methosulfate, produces a soluble formazan product with maximum absorption at 490-500 nm. MTS is a single-step assay and the absorbance measurements are performed after addition of the compound to the cell culture with no steps in between. However, it is susceptible to interference from other light-absorbing compounds.[81] WSTs are produced by addition of charged groups directly or indirectly to the phenyl ring of the MTT molecule. However, these compounds can easily be precipitated in the presence of anions such as carboxylate or phosphate.[82]

In all of these assays, the decrease in the intensity of fluorescence after exposure to the test chemicals is attributed to the damage to mitochondria or loss of cell viability.[83]

As previously explained, instead of colorimetric measurement of the endpoint, it is possible to electrochemically measure the amount of analyte reduced by the cell components.

In this chapter, the application of cyclic biamperometry (see Section 1.3) to the assessment of viability of human corneal epithelial cells is presented. In an attempt to construct a battery of tests aimed at the replacement of the Draize eye test, human corneal epithelial cell suspensions are used as the test model. The results presented in this chapter have recently been published.[83]

2.2 Materials and Methods

2.2.1 Chemicals and Instrumentation

Potassium ferricyanide, benzalkonium chloride, sodium dodecyl sulfate, hydrogen peroxide and D-(+)-glucose were purchased from Sigma-Aldrich and used as received. DMEM/F12 growth medium, fetal bovine serum (FBS), TrypLE^{TM} Express, Pen-Strep (Penicillin / Streptomycin) and sterilized 1X PBS (0.050 M phosphate buffer and 0.10 M NaCl) were obtained from Gibco Invitrogen and immortalized human corneal epithelial cells (HCECs) were purchased from RIKEN BioResource Center, Tsukuba, Japan (RCB #2280). A Sanyo incubator (model: MCO-18AIC) was used for cell incubation and a hemacytometer from Hausser Scientific (Horsham, PA, USA) was used for determination of cell concentration. Electrochemical tests were initially carried out using standard-size gold disk electrodes (1.6 mm in diameter gold disks, Bioanalytical Systems Inc.,West Lafayette IN, USA); however, further experiments were done using the microelectrodes (100 μm diameter, sealed in glass, see below). The electrochemical measurements were made using a CHI650A potentiostat (CH Instruments, TX, USA). Biamperometric measurements were made by connecting both the auxiliary and reference electrode leads to one of the gold electrodes and the working electrode lead to the other.

2.2.2 Methods

The gold disk microelectrodes used in this study (100 μm dia) were fabricated by placing a piece of gold wire ($\sim$ 5-6 cm-long, 100 μm dia) in a glass Pasteur pipette and melting the tip of the pipette on a Bunsen burner, so that the wire would be sealed inside the glass. After cooling down, the tip was broken to make a sharp edge. The edge was filed to make a right angle. Then, the other end of the wire was soldered to a copper wire which served as the electrode lead. Then, the body of the pipette was filled with silicone glue to fix the electrode lead in place. When the fabrication of the electrode was completed, the tip of the electrode was polished with 1 micron Buehler micropolish and the electrode was subjected

to 200 cycles of cyclic voltammetry in well-stirred 1.0 M sulfuric acid between +1.0 and −1.0 V.

HCECs were grown in 75-cm^2 culture flasks containing DMEM/F12 growth medium with 1% Pen-Strep and 10% FBS at 37°C with 5% CO_2. The growth medium was changed approximately every 48 h, and after reaching confluence (in 10-14 days), the cells were dislodged from the growth surface using TrypLE^{TM} Express and were suspended in 1X PBS. The cells were then centrifuged at 300 rcf for 7 min and washed with 1X PBS again to remove TrypLE^{TM} Express. After another centrifugation at 300 rcf for 7 min, the concentrated cell pellet was re-suspended in sterilized 1X PBS containing 5.00 mM glucose. In the final step, the cells were counted using a hemocytometer and were then subjected to the assay. Due to variation in transfer, diluting and washing the cells, the prepared stock solutions of cells had different concentrations. These cell stocks were used directly with no concentration adjustment. To measure the metabolic activity (total activity of mitochondrial and cytosolic dehydrogenases) of the cells, 65.0 μL cell suspension, 5.00 μL ferricyanide solution (200 mM unless otherwise indicated) and 20.0 μL lipophilic mediator solution (different concentrations for different mediators) were mixed together. The final concentration of ferricyanide was 10.0 mM. The mixture was kept at 37 °C for exactly 30 min, after which the samples were immediately flash frozen in liquid nitrogen to stop metabolic activity. Since the received TMPD was in the reduced form, after making the proper concentration of the solution, it was air-oxidized with bubbled filtered air using a microbial sterilization filter (0.22 micron dia.) for 72 h. For cytotoxicity evaluations, the same volumes of cells and ferricyanide were combined with 10.0 μL DCIP (0.900 mM stock, 100 μM final concentration in each sample) and 10.0 μL irritant solutions (different concentrations). For electrochemical analysis, the samples (5 replicates) were thawed, microfuged and the supernatant was examined by cyclic biamperometry for two complete cycles. The scans were performed at 25 mV/s between –0.400 and +0.400 V, beginning at –0.400 V, at room temperature.

2.3 Results and Discussion

Initial biamperometric measurements were performed using different growth media, i.e. +/– phenol red and +/– serum. However, preliminary results showed that one or more components in minimal essential growth medium (MEM) react(s) with ferricyanide. Therefore, further electrochemical tests were carried out in 1X PBS containing 5.00 mM glucose. Although glucose is a reducing sugar, at 37 °C and below, the rate of its reaction with ferricyanide is negligible, which makes it a non-interfering carbon source for the cells within

the duration of the test. Figure 2.1 shows a comparison of these two assay solutions (MEM and PBS-glucose) incubated with ferricyanide in the absence of cells.

Figure 2.2 represents a typical response from cyclic biamperometry in 1X PBS containing 5.00 mM glucose in the presence and absence of HCEC suspensions. Although initial results with standard-size gold disk electrodes were promising, the high volume of cell suspension required for each single test ($\sim$ 1.5 mL at $> 1.0 \times 10^6$ cells/mL) hindered the use of standard-size electrodes in further tests. Therefore, the fabricated microelectrodes were used in the rest of the experiments.

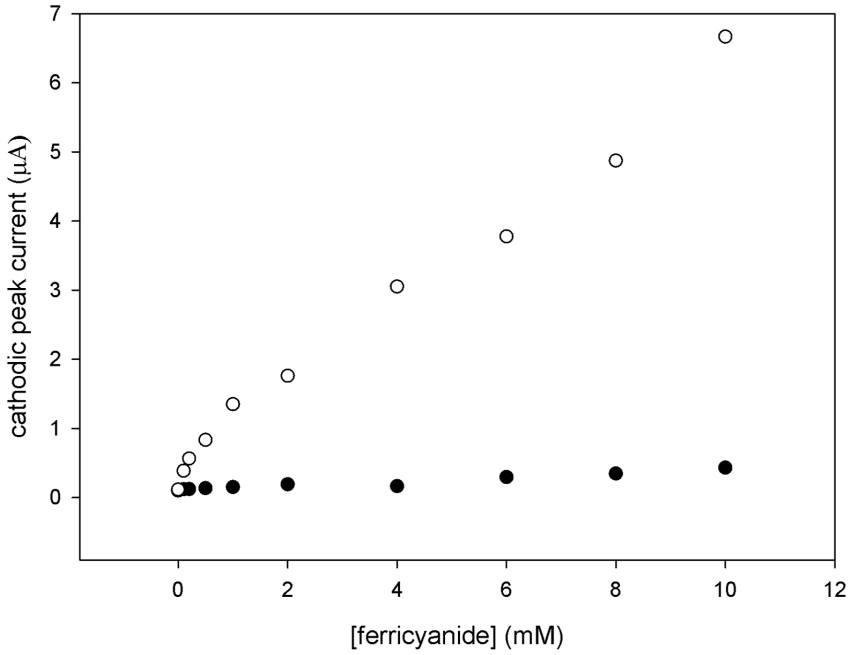

Figure 2.1: Cathodic peak current (i_{pc}) against concentration of ferricyanide after 30 min exposure at 37 °C. Solid circles represent 1X PBS containing 5.00 mM glucose and empty circles indicate MEM. Au standard gold disk electrodes (dia: 1.6 mm) were used for the measurements and there was no replicate.

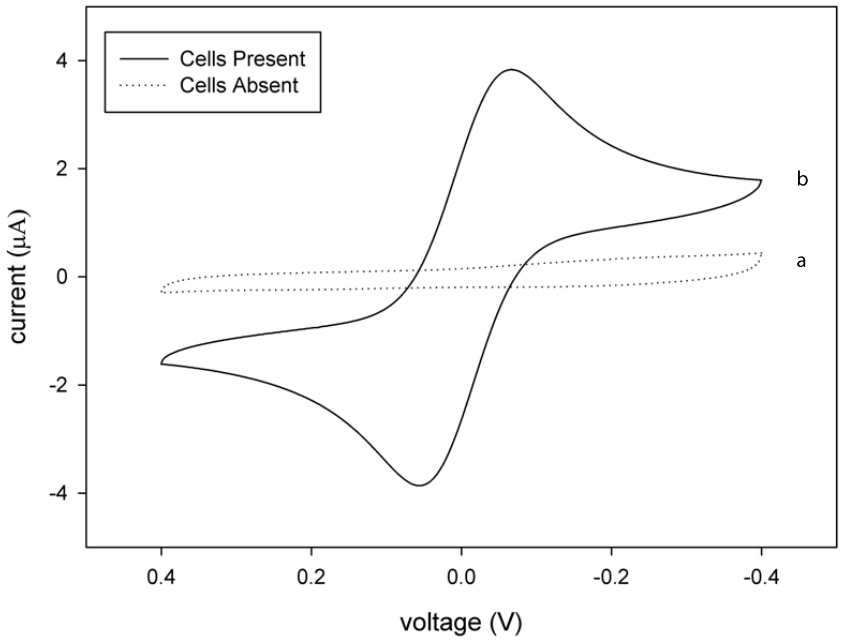

Figure 2.2: A typical representation of the signal in 1X PBS containing 5.00 mM glucose in (a) absence and (b) presence of 1 x 10^7 HCECs/mL after 30 min exposure. [ferricyanide] = 10.0 mM and [menadione] = 100 μM at 37 °C. Standard Au electrodes (1.6 mm dia)

Figure 2.3: Comparison of standard-size gold disk electrodes (left) and the microelectrodes (right). Approximately 40 μL cell suspension is sufficient for each electrochemical measurement when these microelectrodes are used.

Figure 2.3 illustrates the difference between the standard-size gold disk electrodes and the microelectrodes. The required volume for each electrochemical measurement can be reduced over 30-fold when these microelectrodes are used.

Optimization tests indicated that the highest peak current is obtained when approximately 10.0 mM ferricyanide is used in the extracellular medium. (Figure 2.4) Similar studies using *Saccharomyces cerevisiae* have been reported in the literature in which ferricyanide functions as the final electron acceptor.[84–87] The concentration of ferricyanide in these studies varies between 2 to 45 mM. This relatively large variation is due to differences in the incubation time (up to 2 h), cell concentration and the electrochemical method used (e.g. fixed potential amperometry without regeneration of ferricyanide or real-time regeneration of ferricyanide at a second electrode).

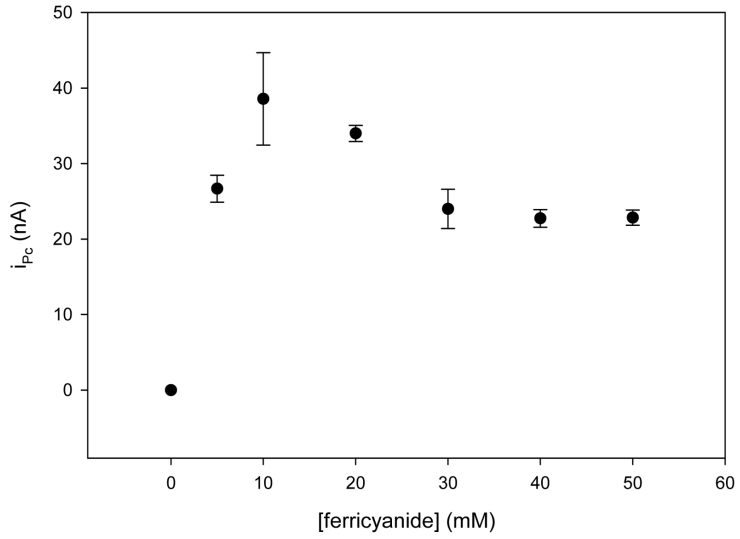

Figure 2.4: Cathodic peak current vs. concentration of ferricyanide in the presence of 1.0×10^7 cells/mL. Conditions: PBS/glucose (5.00 mM) containing 5.00 μM menadione, incubated 30 min at 37 °C prior to measurement with the microelectrodes. Error bars show one standard deviation of 5 replicates.

In this study, three lipophilic mediators, including dichlorophenol indophenol (DCIP), 2-methyl-1,4-naphthoquinone (also called menadione or vitamin K3) and N,N,N',N'-tetramethyl-p-phenylenediamine (TMPD) were evaluated for shuttling the electrons across the cell membrane. Figure 1.10 depicts the structures of these mediators. Initial studies were carried out using 100 μM menadione. However, the results showed that the optimal concentration of menadione varies slightly with the cell concentration. At a lower cell concen-

tration of 3.3×10^6 cells/mL, the optimal concentration of menadione is approximately 4.0 μM, but this optimal value increases to approximately 8.0 μM as the cell concentration increases to 1.0×10^7 cells/mL. (Figure 2.5) This slight variation may result from the hydrophobic nature of menadione, which partitions between the aqueous phase and the cell membrane/cytoplasm.

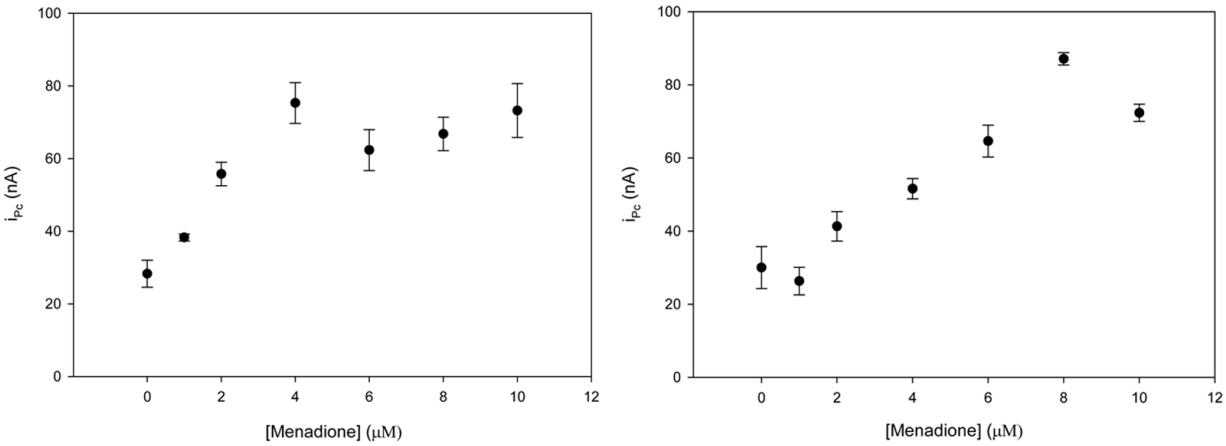

Figure 2.5: Cathodic peak current vs. concentration of menadione in the presence of 3.3×10^6 cells/mL (left) and 1.0×10^7 cells/mL (right) after 30 min exposure at 37 °C. Conditions: 1X PBS containing 5.00 mM glucose and 10.0 mM ferricyanide, Au microelectrodes 100 μm dia. Error bars represent 1 standard deviation of 5 replicates.

The optimal concentration of menadione in our studies appears to be far below those values reported in the literature for similar studies. In these reports, however, *Saccharomyces cerevisiae* has been used as the model, with the optimal concentration of menadione being mostly around 100 μM.[84–87] The very high concentrations of *S. cerevisiae* in these reports ($1.1 \times 10^8 - 1.3 \times 10^9$ cells/mL) may account for the relatively high optimal concentration of the mediator; however, it has also been shown that menadione is toxic to this species at 100 μM.[88] Menadione has lethal effects on *in vitro* cultured Hep G2 cells (a human liver carcinoma cell line) at 25-50 μM after an overnight incubation.[89] However, the toxic effects are not observed on bovine crystalline lenses at levels of up to 50 μM after 24 h incubation at 37 °C.[90]

Figure 2.6 shows the dependence of biamperometric peak current on DCIP concentration. With this mediator, the maximum signal is achieved when DCIP is present at 100 μM.

DCIP is more hydrophilic than menadione, and, although it is capable of crossing the

cell membrane, it is less likely to partition significantly into the membranes. For this reason, variation in the optimal DCIP concentration is less likely with DCIP than with menadione.

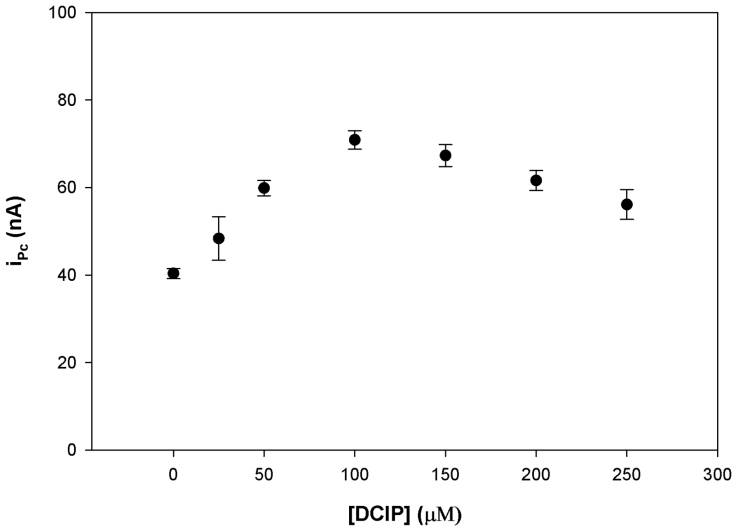

Figure 2.6: Cathodic peak current vs. concentration of DCIP in the presence of 9.9 $\times 10^6$ cells/mL after 30 min exposure at 37 °C. Conditions: 1X PBS containing 5.00 mM glucose and 10.0 mM ferricyanide, Au microelectrodes 100 μm dia. Error bars indicate 1 standard deviation of 5 replicates.

Similar studies have been reported using *S. cerevisiae* where the optimal concentration of DCIP has been 100 μM.[84–91]

TMPD was also investigated in this study. Similar to DCIP, TMPD is water-soluble, however, the reduced form of aqueous TMPD is not stable as its colour slowly changes from colourless to dark blue.[92] The commercially available TMPD is in its reduced form and must be air-oxidized prior to use. In this project the TMPD stock solution was bubbled with filtered air for 72 h at room temperature. This results in appearance of a stable deep blue colour which is the characteristic of the oxidized form of the mediator. Figure 2.7 shows cathodic peak current against concentration of TMPD corrected for the background signal (due to presence of slight amount of the reduced form of TMPD in the solution that electrochemically reacts with ferricyanide). The optimal concentration of TMPD appears to be around 200 μM.

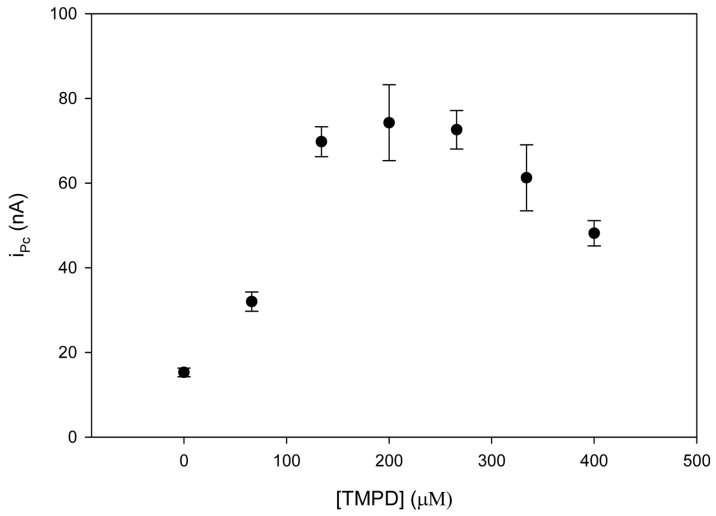

Figure 2.7: Cathodic peak current vs. concentration of TMPD in the presence of 9.6×10^6 cells/mL after 30 min exposure at 37 °C. Conditions: 1X PBS containing 5.00 mM glucose and 10.0 mM ferricyanide, Au microelectrodes 100 μm dia. Error bars indicate 1 standard deviation of 5 replicates.

Comparing Figures 2.5, 2.6 and 2.7, one can see that at zero concentration of the mediator , a small peak current is observed the magnitude of which varies with the concentration of the cells. This shows that ferricyanide can be reduced directly by the components of the respiratory chain of the cells.

Figure 2.8 represents the efficiency of each mediator at its optimal concentration. TMPD shows the best performance as an electron carrier; however, the tedious procedure of stock preparation and the large background signal excluded this mediator from further experimentation. Menadione, although providing the best signal to background ratio, was also excluded in further studies due to the dependence of its optimal concentration on cell density. In addition, menadione is sparingly soluble in water and its stock solution should be prepared in ethanol. Therefore, DCIP was chosen as the lipophilic mediator for the evaluation of the viability assay.

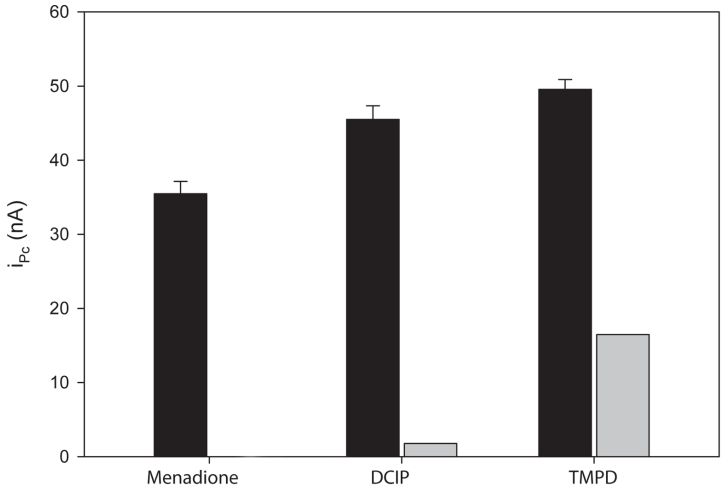

Figure 2.8: Cathodic peak current against the optimal concentrations of the mediators ([menadione] = 6.00 μM, [DCIP] = 100 μM and [TMPD] = 200 μM) in the presence (black bars, corrected for blank) and absence (grey bars) of 6.0×10^6 cells/mL. Conditions: PBS/glucose (5.00 mM) with 10.0 mM ferricyanide, incubated 30 min at 37 °C. Electrochemical measurements were done using the microelectrodes and error bars display 1 standard deviation of 5 replicates.

To evaluate the electrochemical cytotoxicity assay three well-characterized chemicals, including benzalkononium chloride (BAC), sodium dodecylsulfate (SDS) and hydrogen peroxide were used as the sample toxicants.

Benzalkonium chlorides are strong cationic surfactants that have been known for their superior protein denaturation function. BACs are widely used as disinfectants, germicides and preservatives in contact lens cleaning solutions.[93]

Figure 2.9 represents the cytotoxic effects of BAC assessed with this electrochemical assay. At lower concentrations, a statistically significant increase in the current response is observed (Student's t-test, p = 0.000729, 0.00299 and 0.0116 for 1.00 $\times 10^{-5}$, 1.00 $\times 10^{-4}$ and 1.00 $\times 10^{-3}$% BAC, respectively). This increase in metabolic activity at lower concentrations of BAC is believed to be an indicator for cells struggling to counteract the cytotoxic effects of BAC. Similar elevated metabolic activity or respiratory burst at lower administered concentrations of BAC has been observed when fresh-water prawns (*Macrobrachium rosenbergii*) were injected with 0.006% BAC.[94]

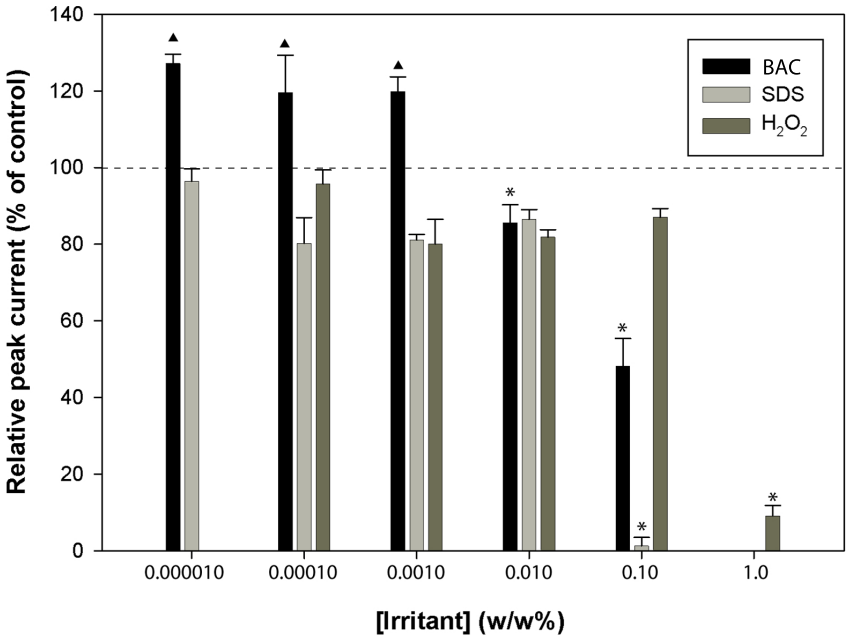

Figure 2.9: Cathodic peak current (relative to control) vs. concentration of the irritant. Cell concentrations were 4.9 $\times 10^6$, 9.4 $\times 10^6$ and 1.2 $\times 10^7$ cells/mL for BAC, SDS and H_2O_2, respectively. Solid triangle shows statistically significant increase ($p < 0.05$) relative to the control (dashed line) and asterisk shows statistically significant decrease ($p < 0.05$) in cell viability relative to the control (dashed line). The value at 0.0100% BAC is statistically significant ($p < 0.05$) when compared to the lower concentrations of BAC and not significant when compared to the control. The error bars indicate 1 standard deviation of 5 replicates and the exposure times were 15 min for BAC and 30 for SDS and H_2O_2.

Further increase in BAC concentration causes rapid decrease in cell viability after 15 min exposure. Ten-fold increments in BAC concentration from 0.00100 to 0.0100 and further to 0.100% trigger statistically significant losses (Student's t-test, $p = 2.08 \times 10^{-6}$ and 5.70 $\times 10^{-4}$, respectively) in the number of viable cells. These results are in agreement with those published in the literature using the water-soluble tetrazolium (WST-1) assay.[95]

SDS, another sample toxicant used in this study, is a strong anionic surfactant. It is well-characterized and widely used in ocular toxicology studies as a test toxicant.[96] Figure 2.9 also illustrates the cytotoxic effects of SDS on HCECs after 30 min exposure at 37 °C obtained with this electrochemical assay. According to these results, 0.10% SDS is lethal to cells within 30 min. The lethal dose (LD90) of SDS is expected to be between 0.01 and 0.10%; however, no further tests were conducted in this range. These results are also in

agreement with those previously reported in the literature in which WST-1 assay has been used for the assessment of SDS cytotoxicity.[97]

The last chemical evaluated by this electrochemical assay was H_2O_2. This strong oxidizing agent is naturally produced in various biochemical reactions within the cell; however, it is immediately decomposed to water and oxygen by the action of catalase, an enzyme present in virtually all aerobically respiring cells. The cytotoxic effects of H_2O_2 appear when the great excess mass of the substrate saturates the enzyme and a large ratio of the subsrate molecules remain unbound in the cytoplasm. Our results indicate that 1.00% H_2O_2 is lethal to cells within 30 min exposure at 37 °C. However, no further dilution between 0.100 and 1.00% was performed (Figure 2.9). Ubels *et al.* have recently reported similar results where human corneal epithelial cells have been exposed to 0.1 and 0.3% H_2O_2. According to their results, cell viability is minimally affected after 60 min exposure to 0.1% H_2O_2; however, viability greatly decreases after 60 min exposure to 0.3% H_2O_2.[98]

Taken together, these results demonstrate that cyclic biamperometry can be used for viability assessment of human corneal epithelial cells in PBS-glucose suspension. In an effort to minimize animal testing, this assay could be used in a tiered-testing strategy, together with other *in vitro* assays, for cytotoxicity assessment.

This new biamperometric assay does have limitations. For instance, redox activity of the substance to be tested must be considered, prior to the application of the electrochemical assay and, if necessary, control experiments should be performed. Some chemicals may be able to compete with ferricyanide for the oxidation of DCIP or for directly accepting electrons from cellular components. In that case, a lower apparent metabolic activity is registered. If the chemical directly reduces the ferricyanide a higher apparent metabolic activity would be observed. Not all redox-active compounds are of concern. The rate of electron transfer may be so low that under the experimental conditions this interference would be negligible. For example, the slow kinetics of electron transfer between glucose, a reducing sugar, and ferricyanide does not cause interference when glucose is present in the measurement medium.

Although the required cell concentration for this assay is higher than those needed for microscopy-based assays, the test volume, currently 90 μL, can be easily reduced if smaller electrodes are used. This, in principle, could facilitate the integration of this assay into high-throughput screening or lab-on-chip devices.

There are advantages of this assay over other metabolic assays. The turbidity of the sample suspension does not affect the electrochemical measurements as it would in optical assays. Also, biamperometric cells do not require any reference electrode and, consequently, miniaturization of the whole electrochemical cell is simpler. In addition, unlike

other amperometric assays, biamperometric measurements do not alter the composition of the medium as the ferrocyanide produced by the reduction reaction is accompanied by the production of ferricyanide at the second working electrode. This allows real-time monitoring of cell metabolic activity and, if combined with other complementary assays, the use of live animals for drug screening and cytotoxicity assessment could be reduced.

Chapter 3

Electrochemical Measurement of Trans-epithelial Resistance

3.1 Cultivation and Study of 3D Corneal Constructs

Several *in vitro*/*ex vivo* assays exist for the assessment of ocular toxicity, some of which have been accepted by the regulatory agencies. These assays, unlike those mentioned in Section 1.6, make use of the whole organ or a tissue segment to evaluate the integrity of the tissue. The assays include the bovine corneal opacity and permeability (BCOP) assay, the isolated rabbit eye (IRE) test, the isolated chicken eye (ICE) test, the ScanTox™ assay, the hen's egg test on the chorioallantoic membrane (HET-CAM), the chorioallantoic membrane vascular assay (CAMVA), the EpiOcular™ assay, the SkinEthic *in vitro* test on a reconstituted human corneal epithelial model, the Ocular Irritection® assay, the mucosal irritation model using slugs and the pollen tube growth assay. A detailed review of all of these assays is beyond the scope of this thesis and excellent in-depth review articles are available in the literature.[62] Here, a brief review of each of these methods is presented.

3.1.1 Bovine Corneal Opacity and Permeability (BCOP) Assay

The BCOP assay, which was developed by Gautheron *et al.*, uses a freshly isolated bovine cornea that is horizontally mounted onto a support and positioned in a temperature-controlled chamber so that the isolated cornea divides the chamber in two separate compartments. The apparatus is then placed inside an opacitometer and the chemical to be

tested is added to the upper compartment. After measuring the change in opacity, a fluorescent dye is also added to the upper compartment to measure permeability of the tissue. The measured opacity and permeability values are then used to classify the test substance accordingly.[99]

3.1.2 The Isolated Rabbit Eye (IRE) Test

The IRE test was introduced by Burton *et al.* and uses complete eyeballs obtained through dissection immediately after euthanizing laboratory rabbits. The eyeballs are vertically mounted into a chamber so that the cornea faces upward. To keep the cornea moist, pre-warmed phosphate buffer is periodically added. A visual check of the cornea before application of the test sample is necessary to make sure that the tissue is healthy. After application of the chemical to the surface of the cornea for a certain period of time, which varies depending on the level of the irritancy test, the opacity and thickness of the cornea is measured. Another check for the degree of fluorescent penetration is also carried out at 0.5, 1, 2, 3 and 4 h after exposure. In addition, for each test sample, the average swelling of three corneas is compared to the control. To improve the test performance, histological staining of the tissue may be conducted. Finally, the overall damage is quantified by a combined score from all the endpoints.[100]

3.1.3 The Isolated Chicken Eye (ICE) Test

The ICE test was developed by Prinsen and Koeter and is performed on the whole eyeballs of chicken right after slaughtering. Prior to application of the test chemical, the isolated non-damaged intact eyeballs are mounted into a chamber in which baseline corneal opacity and fluorescein retention are registered. Then, the eyeballs are exposed to the test substance for 10 s after which the test chemical is rinsed off and the cornea is examined for any change in thickness, opacity or fluorescein permeability. The assessment of corneal opacity and thickness is done after 30, 75, 120, 180 and 240 min; however, fluorescein permeability is only evaluated after 30 min. The mean change in each endpoint is recorded, based on which a score between 0 and 200 is assigned to the chemical as the ICE irritation index. One advantage of this assay is its ability to correlate irritancy to both cornea and conjunctiva.[101]

3.1.4 The ScanTox™ Assay

The ScanTox™ assay, developed by Sivak *et al.*, relies on measurement of the change in refractive characteristics of bovine or porcine lenses. In this method, the bovine or porcine eyes are obtained from a local abattoir from which the lenses are aseptically excised. The lenses are then examined for any damage and the healthy lenses are vertically mounted onto a support and are cultured in an appropriate transparent media for 24-48 h. The transparent culture containers are designed to allow periodic photography of laser beams which pass through the lens. The specifically designed laser scanner moves on a computer-controlled X-Y plane so that a number of beams can pass through different locations on the lens. This allows the lens spherical aberration to be determined and followed over time, or before and after exposure to chemicals. By passing several beams through different locations on the lens the focal length of the lens is measured from the intersection point of the principal plane and the optical axis of the lens.

Exposure of the lens to irritants may cause damage to the lens cells which invariably alters the balance of factors responsible for controlling spherical aberration. Therefore, the focal point of the lens is affected as a whole, and instead of a focal point, scattered points are observed. The time required to cause 100% increase in focal point variability is usually used as the endpoint of the test.[102,103]

3.1.5 The Hen's Egg Test on the Chorioallantoic Membrane (HET-CAM) Assay

The HET-CAM assay, which was developed by Luepke *et al.*, relies on the evaluation of three endpoints, including (i) haemorrhage, (ii) lysis and (iii) coagulation of the CAM in the 9^{th} day of embryonic development, when neither nerve tissue nor pain perception have developed. The most widely-used protocol involves the application of the test chemical onto the membrane and the measurement of the time required for the appearance of the endpoints. For scoring purposes, coagulation is often given a higher weight compared to haemorrhage and lysis.[104]

3.1.6 The Chorioallantoic Membrane Vascular Assay (CAMVA)

The CAMVA was developed by Leighton *et al.*[105] The assay relies on the assessment of the chorioallantoic membrane after exposure to the test substance. The test protocols dictate the removal of some of the albumen from the egg four days after fertilization, to

allow optimal development of the CAM. After resealing the cut on the membrane, the incubation continues for another six days prior to the application of the test substance. Exposing the CAM to the test substance may trigger haemorrhage, hyperaemia or the appearance of vessels devoid of blood. The concentration of the chemical required to cause such changes in 5 out of 10 treated eggs after 30 min is recorded as the endpoint.

3.1.7 The EpiOcular™ Assay

The EpiOcular™ assay is performed on a human-derived model made of epidermal keratinocytes. These cells differentiate to form a multilayer structure which resembles the human corneal epithelium. The assay was developed by MatTek Corporation (Ashland, MS, USA) and is usually conducted in combination with other cytotoxicity assays mainly with the methylthiazol tetrazolium (MTT) test. To be able to compare the EpiOcular™ assay results with those of *in vivo* assays, the effective exposure time needed to reduce the tissue viability to 50% is recorded. Using variable exposure time allows the evaluation of chemicals without dilutions. Consequently, both hydrophobic and hydrophilic substances can be tested. The very low thickness of the tissue construct enables it to mimic the behavior of both the cornea and the conjunctiva. Consequently, very mild to moderate irritancy can be predicted. The very short time required to lower the viability by 50% indicate that the test is capable of measuring moderate to severe eye irritation potential as well.[106]

3.1.8 The SkinEthic *in Vitro* Reconstituted Human Corneal Epithelium (HCE™) Model

The HCE™ assay was developed by SkinEthic Laboratories in Nice, France. The model uses an *in vitro* culture of immortalized human corneal epithelial cells. Usually the cells are grown on a polycarbonate support and are exposed to air from one side to form a 3D structure which morphologically resembles the cornea of the human eye.

The test endpoints can be cell viability using the MTT assay or lactate dehydrogenase (LDH) release, histology or gene expression. This assay can be used to demonstrate corneal repair and recovery *in vitro*. The other variation of this model utilizes transfected human corneal epithelial cell lines which, after exposure to air, form a multilayer construct. In this technique, the endpoints also include the decrease in the trans-epithelial electrical resistance.[107]

3.1.9 The Ocular Irritection® Assay

Another well-characterized non-animal ocular toxicity assay is the Ocular Irritection® assay formerly known as Eytex®. The method was developed from the idea of Gordon and Bergman[108] who were technicians at Avon laboratories, in the mid-1980s.

The first component of the Ocular Irritection® test consists of a membrane disc that allows controlled delivery of the test substance to a reagent solution. This mechanism mimics the cellular membrane. The other component of the test is the reagent solution which contains proteins, glycoproteins, carbohydrates, lipids, and low molecular weight chemicals that self-assemble into a macromolecular matrix. When rehydrated, this matrix behaves in a similar manner to the real transparent cornea, as it forms a highly ordered structure.

As observed in the Draize test, the cornea opacifies due to disruption of the ordered corneal proteins by the chemical irritant. It has been shown that corneal opacification also occurs due to denaturation of its proteins. Denaturation of the matrix proteins in the Ocular Irritection® test causes the formation of tiny insoluble particles which can be readily detected by measuring the extent of light scattering.[109,110]

3.2 Measurement of Trans-epithelial Resistance

A unique feature of epithelial cells is their ability to form formidable barriers between each other to tightly seal themselves together. Tight junctions, also called zonula occludens, are the protein structures that serve this function. This highly effective sealing of neighbouring cell membranes does not bring the cells in close contact over a broad region; however, tight junctions form sharp ridges at the seal point. The number of these ridges correlates well with tightness of the seal made by these proteins.[111]

Such barriers force molecules to cross the cell layer (e.g. an epithelial cell layer) by passing through the cells themselves. This prevents the movement of molecules between the cells and blocks the lateral movement of the proteins within the cell membranes.[111] The formation of membrane tight junctions changes the physical characteristics of the tissue. It has been shown that the appearance of tight junctions in a cell layer results in a dramatic increase in the electrical resistance across that layer, and the measurement of this trans-epithelial resistance (TER) provides information on the state of the tight junctions.[112]

The permeability of the tissue model to ions and electrons and the correlation of the extent of this permeability with the flux of small molecules across the tissue can be assessed

with TER measurements.[113,114] TER measurements have also been used for assessment of function and differentiation of tissue models.[112,115] In addition, such measurements provide information on the effect of physiological changes such as serum, and ATP depletion, on the integrity of an epithelial barrier.[116]

Changes in TER are considered to be indications of tissue integrity, rather than cell integrity, and for this reason, the measurement of TER can be employed as a sensitive assay for the assessment of damage caused by the test agents. It has been shown that a decline in TER, compared to changes in cell morphology or polarized insulin secretion, is a more sensitive indicator of tissue layer damage.[117,118]

In section 1.6 it was mentioned that viability is not the only parameter evaluated in cytotoxicity assessment because it is widely accepted that eye irritants, for example, may disturb the integrity of the cornea by damaging tight junctions but without an immediate impact on cell viability.[119,120] Therefore, assays involving TER measurements have been proposed for *in vitro* assessment of ocular toxicity.[121]

Miller *et al.* who first proposed using TER measurements for ocular cytotoxicity assessment, argued that TER is an especially appropriate parameter for the evaluation of ocular irritation, because the outer superficial cells of the corneal epithelium form extensive tight junctions; it has been shown that ocular irritants that result in swelling and opacification of cornea also cause an increase in epithelial permeability.[121]

TER measurements often accompany other assays, including the fluorescein permeability test, to reinforce the results. In addition, metabolic viability assays, such as tetrazolium salt or AlamarBlue® reduction assays, are also performed along with the TER measurements to exclude the possibility of cell death after a sharp decrease in TER. A sharp decline in TER, after exposure to the test substance, may also result from loss of cell viability and deterioration of the cell membranes.[112]

In our studies only the fork electrodes were used for measurement of TER; however, there is another type of TER measurement electrode set that theoretically results in more accurate measurements of the TER values. This electrode set uses a relatively long vertical chamber ($\sim$ 5 cm), at the bottom of which a large disk electrode and a reference electrode have been positioned. After addition of sufficient PBS buffer ($\sim$ 1.0 mL) the cell insert should be carefully dropped into the chamber and just enough buffer is added to cover the cell constructs. Then the cap of the tube, which also carries the other set of electrodes (one metallic disk and one reference electrodes), is positioned such that the disk electrode in the cap stays very close to the cells inside the construct. These electrodes, however, seem to disturb the cell constructs more dramatically. Also, sterilization of the whole apparatus is more difficult and the possibility of cross contamination is higher.

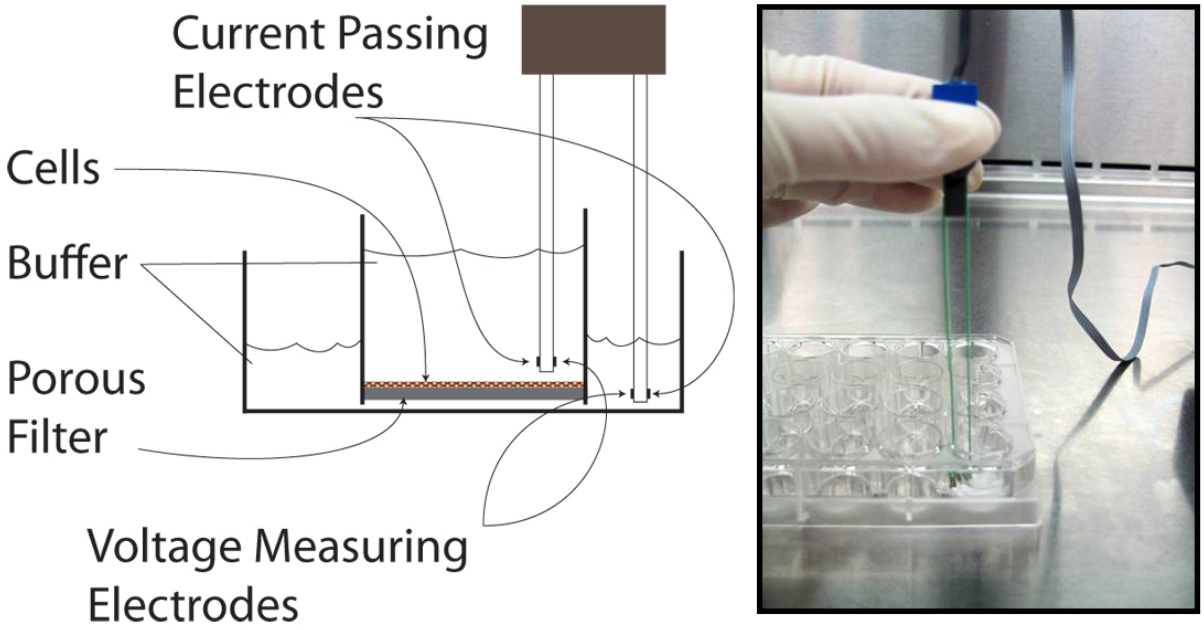

Figure 3.1: EVOM^2 fork electrodes for measurement of trans-epithelial resistance.

To normalize size differences across which resistance is measured experimental values for resistance are multiplied by the area of the barrier, since resistance is inversely proportional to area. This allows comparison of measured values between differently-sized samples in different laboratories. A commonly practiced approach for preparation of the 3D corneal constructs is to remove the growth medium from the inside of the cell inserts after a few days of incubation (depending on the initial concentration of seeded cells).[122–124] This approach, which is known as air-lifting, will result in exposure of the cells to the air from one side and unidirectional diffusion of the nutrients from the other side through the lower layer(s) of the cells. It is known that epidermal cells at an air-liquid interface can undergo organized stratification and morphologically resemble real tissues compared to those submerged under the growth medium.[125] It is believed that this resemblance is due to similarities between the unidirectional nutrient diffusion patterns in the culture and that *in vivo*.[126]

In this chapter, TER measurements are reported for human corneal epithelial cells cultured into 3D corneal tissue constructs. In addition, staining conditions were optimized to view tight junctions by confocal microscopy. Preliminary results for biamperometric respiratory activity of the constructs are also presented. Current issues and future directions for improvement of this assay to be used in a tiered-testing strategy are also discussed.

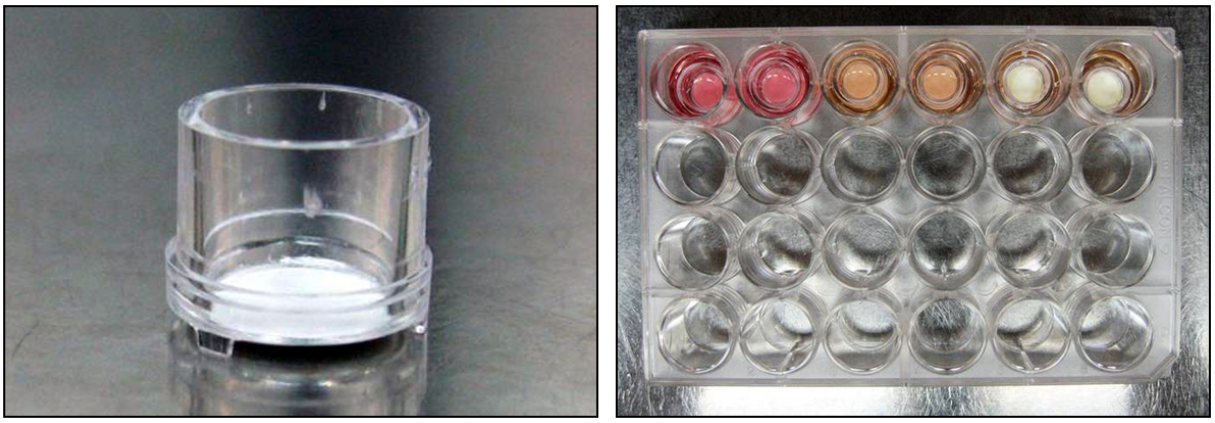

Figure 3.2: Polystyrene cell culture inserts (0.45 μm pores, 12 mm diameter, mixed cellulose esters filter)(left) and seeded cells (right) Unseeded control samples are seen in dark pink, seeded non-airlifted in orange and seeded air-lifted in white.

3.3 Materials and Methods

3.3.1 Chemicals and Instrumentation

Sterile polystyrene culture inserts (0.45 μm pore size, 12 mm dia., mixed cellulose esters filter, Figure 3.2) were purchased from Millipore Corp. Billerica, MA, USA. Culture plates (6- and 24-well) were bought from Becton Dickinson Labware, Franklin Lakes, NJ, USA. DMEM/F12 growth medium, fetal bovine serum (FBS), Pen-Strep (Penicillin/Streptomycin) and sterilized phosphate-buffered saline (1X PBS) were obtained from Gibco Invitrogen and immortalized human corneal epithelial cells (HCECs) were purchased from RIKEN BioResource Center, Tsukuba, Japan (RCB #2280). A Sanyo incubator (model: MCO-18AIC) was used for cell incubation and a hemacytometer from Hausser Scientific (Horsham, PA, USA) was used for determination of cell concentration. Trans-epithelial resistance measurements were carried out using an EVOM^2 epithelial voltmeter/ohmmeter with fork electrodes. (World Precision Instruments, Sarasota, FL, USA) Electrochemical respiratory activity measurements were carried out with two microelectrodes (100 μm dia.) sealed in glass using a CHI650A potentiostat (CH Instruments, TX, USA). Confocal microscopy studies were performed using the LSCM 510 Meta, Carl Zeiss Inc.

3.3.2 Methods

HCECs were grown according to the method reported by Youn *et al.*[127] Briefly, the inocula were prepared in 75-cm^2 culture flasks (see section 2.2.2) and were suspended in 1X PBS. After counting the cells the inserts were seeded with $\sim 8.4 \times 10^3$ cells (equivalent to 9.5×10^3 cell/cm^2) and were put into 24-well plates containing 1.0 mL of DMEM/F12 (+10% FBS, +1% Pen-Strep) in each well. Then an aliquot of the same medium (0.50 mL) was dispensed into each insert. At the beginning the medium in each well was changed every 48 h; however, as the cells grew this interval was reduced to every 24 h. The first TER measurements were carried out after 48 h in 1X PBS. For this purpose, the inserts were washed with 1X PBS and then put in a sterile 24-well plate containing 0.90 mL 1X PBS in each well; then, 0.45 mL of the same buffer was added to the inside of the inserts. After the TER measurements, the inserts were taken out of the PBS buffer and put back into the medium as before and incubated at 37 °C. When the first sudden increase in the TER value ($\sim$ 10 days) became evident, the test samples were air-lifted and the constructed tissue models were exposed to humidified air (by putting a large water container inside the incubator). The constructs were kept in the air-lifted state for different durations (up to 78 days) before being used for cytotoxicity assessment.

3.4 Results and Discussion

The first trial for construction of the 3D corneal tissue constructs involved growth of the HCECs on the inserts for 21 days, during which TER was measured every 48 h. Figure 3.3 illustrates TER results during construct growth over this period of time.

The results of TER values in the first trial (497 ± 36 $\Omega.cm^2$) were in agreement with those reported in the literature, in that the TER values of air-lifted samples were higher than those of non-air-lifted ones.[124,128] Toropainen *et al.* have reported TER values in the range of 100 – 350 $\Omega.cm^2$ after 22 days of cell growth on the air-lifted inserts, which are still higher than the TER values of their own non air-lifted samples. Their report also compares various adhesion proteins, including collagen gel coating, collagen gel coating with fibroblast cells and collagen gel coating with laminin. The highest TER values ($\sim$ 600 $\Omega.cm^2$ after 30 days) have been observed using collagen gel coating with fibroblast cells.[124] Very similar results (468 ± 89 $\Omega.cm^2$ after 20 days) have been also reported by Ward *et al.*[128]

After the TER measurements on day 21 the air-lifted inserts were used for preliminary cytotoxicity assessment. Benzalkonium chloride (BAC), sodium dodecylsulfate (SDS) and

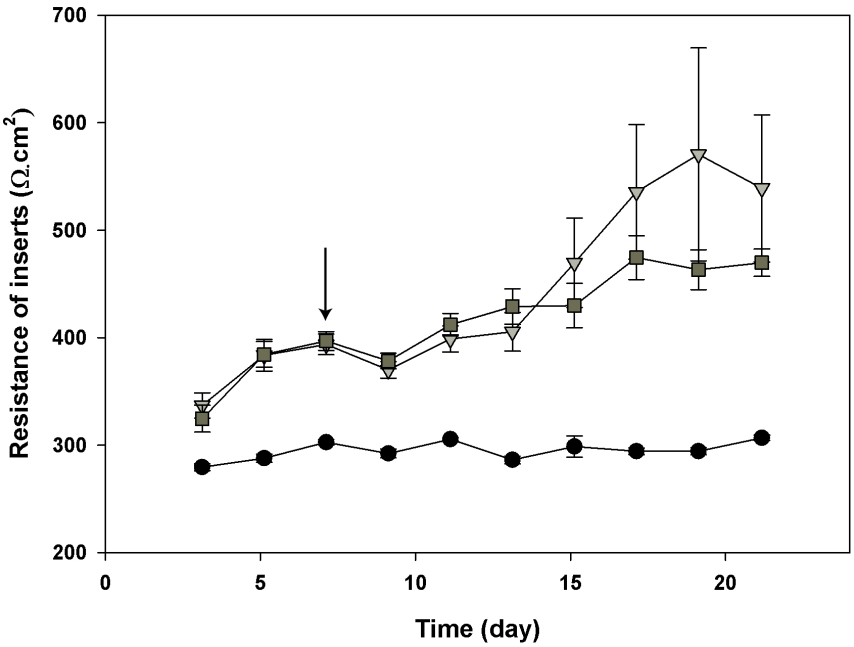

Figure 3.3: Resistance of inserts vs. time; (circles) 5 unseeded controls, (squares) 3 seeded non-air-lifted controls, (triangles) 25 seeded air-lifted test samples. The arrow shows the time of air-lifting after the measurements were made on that day. The error bars indicate 1 standard deviation.

hydrogen peroxide were used as the sample toxicants, for each of which a low (0.00100%) and a high (0.100%) concentration were studied.

Figure 3.4 and Figure 3.5 depict the cytotoxic effects of BAC and SDS assessed through measurement of TER, respectively. In all cases, a sharper drop in the average relative resistance is observed after the first 5 min. At high concentration of BAC (0.100%) the resistance seems not to vary after the first 5 min. However, a more consistent decline in the TER value is observed with 0.00100% BAC (Figure 3.4). Unfortunately, in these preliminary studies, no parallel control tests during the cytotoxicity assessment were performed. As a result, no quantitative conclusion or solid explanation for the decrease in the TER can be provided.

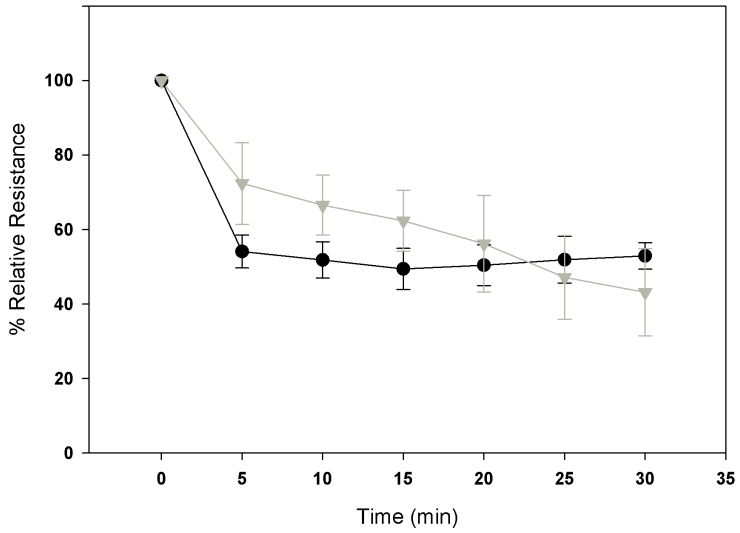

Figure 3.4: Relative TER values (corrected for unseeded control) after exposure to 0.00100% (triangles) and 0.100% BAC (circles). Error bars represent 1 standard deviation for 3 replicates.

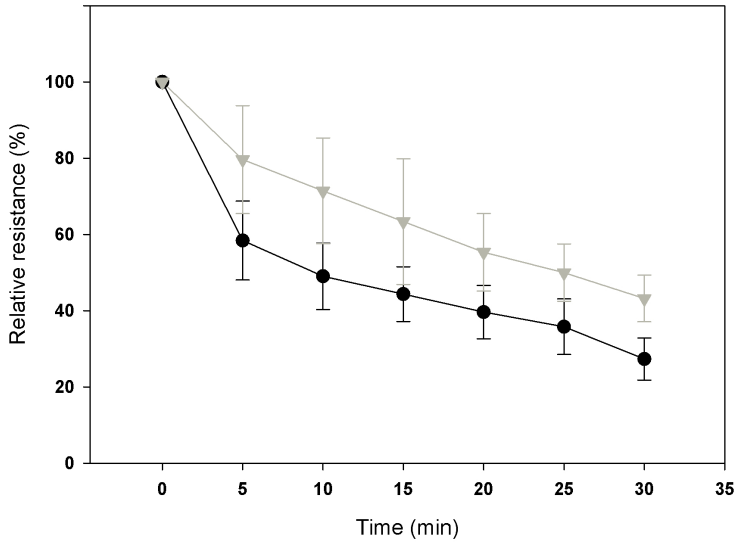

Figure 3.5: Relative TER values (corrected for unseeded control) after exposure to 0.00100% (triangles) and 0.100% SDS (circles). Error bars represent 1 standard deviation for 3 replicates.

In the case of SDS-treated samples, a more gradual decrease is observed over time. Based on the results obtained from the respiratory measurement assay in the previous chapter, BAC and SDS, at 0.00100%, should not affect cell viability within the duration of the test; therefore, the decrease in the TER at the lower concentration of these surfactants may imply disturbance of tight junctions. It has been reported that surfactants such as BAC and SDS, at low concentrations, can be incorporated into and adversely affect the physical properties of the cell membrane.[129] It has been suggested that incorporation of these surfactants into the cell membrane results in (i) formation of mixed micelles, (ii) removal of phospholipids from the cell membrane and (iii) solubilization of the cell membrane when it is saturated with the surfactant. These surfactants are also known for affecting the tight junctions.[129] Sasaki *et al.* have reported that BAC at 0.002% affects the tight junction integrity leading to an increase in the permeability of rabbit cornea. In addition, treating rabbits cornea with 0.05% BAC decreases the corresponding TER to an analytically unmeasurable value.[130]

Figure 3.6 shows the influence of hydrogen peroxide on the TER. Both tested concentrations of H_2O_2, 0.00100 and 0.100%, seem to have similar effects on the TER. Although at these levels hydrogen peroxide is not lethal to cells (see section 2.3) due to action of intracellular catalase, it appears that H_2O_2 may affect the integrity of tight junctions.

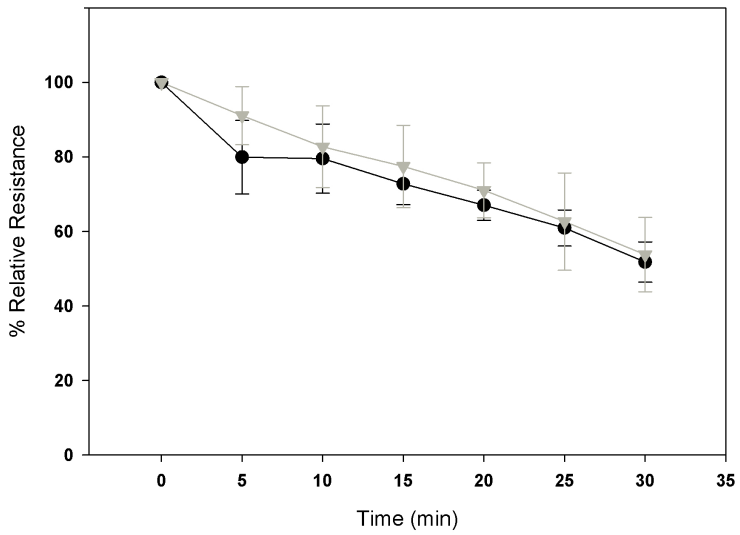

Figure 3.6: Relative TER values (corrected for unseeded control) after exposure to 0.00100% (triangles) and 0.100% H_2O_2 (circles). Error bars represent 1 standard deviation for 3 replicates.

All inserts, after exposure to the sample toxicant, were rinsed with 1X PBS and were

returned to the growth medium. The samples were kept at 37 °C for 24 h to examine the extent of recovery. Figure 3.7 depicts the change in the TER value of the treated inserts before and after a 24-h recovery. The inserts treated with 0.100% BAC and 0.100% SDS exhibit no recovery because, as seen in section 2.3, at this concentration these surfactants are lethal to the cells within 30 min. The only statistically significant sign of recovery was observed with the inserts that had been treated with 0.00100% SDS. In the other cases no statistically significant increase in the resistance was observed.

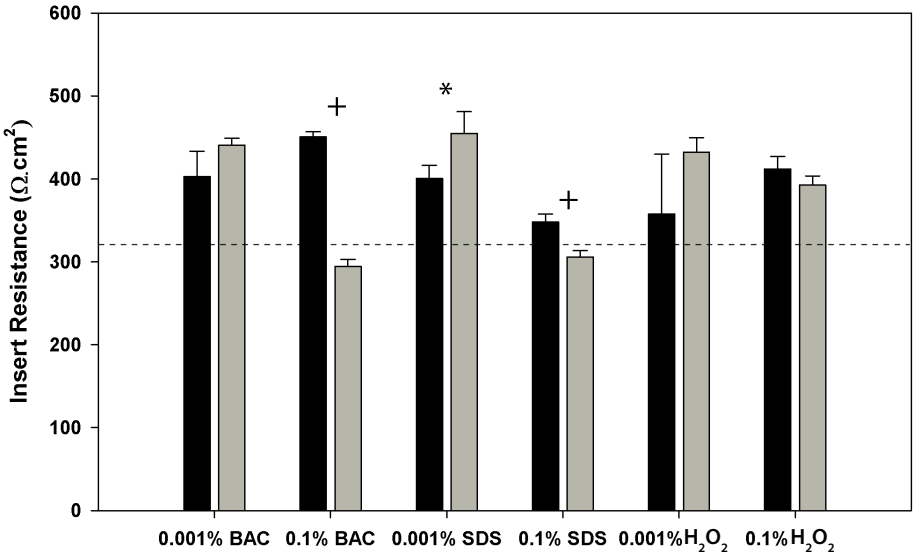

Figure 3.7: Resistance of treated inserts before (black) and after (grey) a 24-h recovery. The horizontal dashed line represents the average resistance of the unseeded inserts and the error bars show 1 standard deviation of 3 replicates. $*$ and $+$ indicate statistically significant ($p < 0.5$) increase and decrease in TER, respectively.

A few of the inserts, which were subjected to the TER measurements for the cytotoxicity assessment, were also subjected to cyclic biamperometry for assessment of respiratory activities. For this purpose, the same optimal conditions as those for cell suspensions, discussed in the previous chapter, were applied. A cyclic biamperogram was recorded every 15 min right after the TER measurement for each insert. Figure 3.8 shows the respiratory activity of the stratified cell constructs over the course of TER measurement. The proportional time-dependent increase in the biamperometric peak current, which is proportional to ferrocyanide concentration, indicates that the cells are alive. A plateau or concave-down curvature would have indicated cell death. However, the corresponding TER values, shown

in Figure 3.9, exhibit a sharp decline. Taken together, these results clearly illustrate the disruption of the cell layers and probable damage to the tight junctions. Although control tests (measurements of resistance over time in the solution containing ferricyanide and DCIP excluding the irritants) were not carried out during the TER measurements, the results illustrate that combination of these two assays can potentially be employed for assessment of tight junctions in a tiered-testing strategy for cytotoxicity assessment.

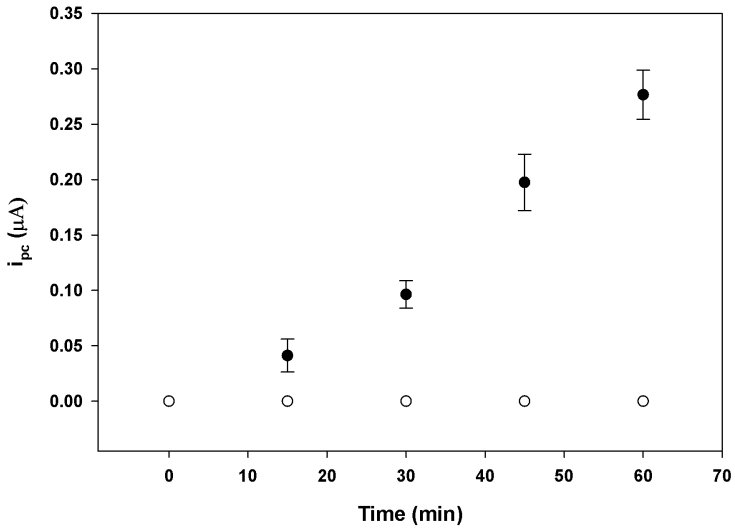

Figure 3.8: Respiratory activity of stratified cell constructs (solid circles) and unseeded controls (empty circles) measured with cyclic biamperometry. Scan rate = 25 mV/s, Au disk electrodes (100 μm dia.) The medium contains 10.0 mM ferricyanide and 100 μM DCIP. Error bars indicate 1 standard deviation of 3 replicates. Only one unseeded control sample was subjected to the measurements.

Despite the fact that the TER values in our preliminary results were in agreement with those in the literature, they are far below the TER values of excised rabbit corneal tissue, which are around 3000 – 8000 Ωcm^2.[131] Considering that rabbits have a thinner cornea, without the Bowman's layer, the difference between the TER values in the preliminary tests and the TER from human cornea is even larger. The large difference between our preliminary cytotoxicity data and those published by Sasaki *et al.*[130] also encouraged a more comprehensive assessment of 3D cell constructs and the TER assay.

A second trial of stratified cell culture was prepared, which consisted of 2 unseeded controls, 3 seeded non-airlifted controls and 18 seeded air-lifted test samples. The samples were cultured for 78 days under the same conditions as before. However, to prevent disturbing the cultures during the TER measurements and growth medium renewal, the

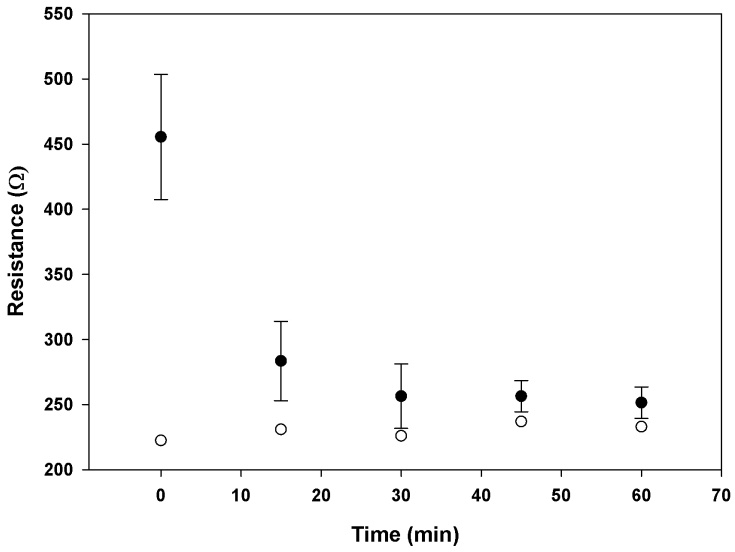

Figure 3.9: TER measurement for ferricyanide-exposed stratified cell constructs (solid circles) and unseeded controls (empty circles). The error bars indicate 1 standard deviation of 3 replicates. Only one unseeded control sample was subjected to the measurements. Conditions are as indicated in Figure 3.8.

samples were put into 6-well plates carrying a larger volume of medium for each sample. This allowed the medium renewal frequency to drop to once every 72 h as opposed to once a day. In addition, in this trial, 4 TER measurements at 90-degree angles to each other were made for each insert and the average value was recorded as the resistance on that day. Figure 3.10 illustrates the TER results from this trial of culture preparation. It is clear that the standard deviation in TER values of air-lifted inserts increases very rapidly as the average TER increases. The standard deviations in the air-lifted samples in Figure 3.10 have been calculated without excluding the outliers which in some cases include $\sim$ 30% of the population. The reason to do this was to demonstrate the overal instability of the inserts, although this may imply that trans-epithelial resistance measurement is not a sensitive method. To prevent such an implication, the raw data for daily measurements have been shown in Appendix A.

To understand the reasons for such large standard deviations, a few of the inserts were selected for study using confocal microscopy. The stratified multilayer cell cultures were stained using Hoechst 33258, a dye for staining the DNA in the cell nucleus. Figure 3.11 (A and B) show the stained multilayer cells. Obviously, the cells do not hold onto each other as clusters of the cells were detached during the rinse steps and some were floating on

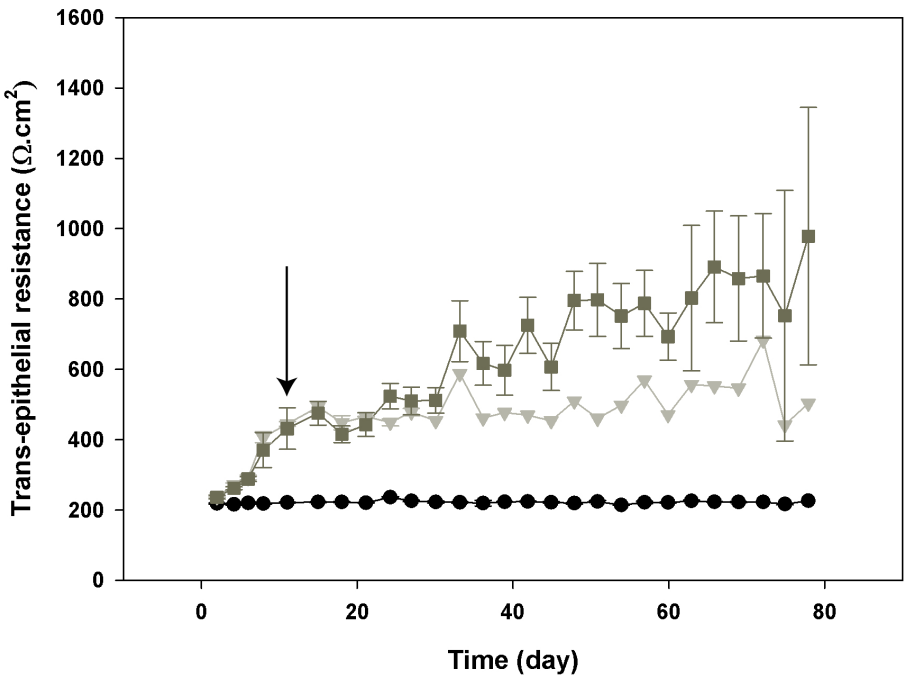

Figure 3.10: Resistance of stratified constructs vs. time; (circles) 2 unseeded controls, (triangles) 3 seeded non-airlifted controls, (squares) 18 seeded air-lifted tests. The arrow shows the time of air-lifting after the measurements were made on that day. The error bars indicate 1 standard deviation.

the slide under the microscope. The interaction between the cells and the growth surface was even weaker because in some cases the whole cell structure was floating in the inserts during the rinse steps. In addition, the cells in the multilayer construct do not seem to form any defined vertical pattern similar to those seen in a real human cornea. (Figure 3.12)

The cell line used in this study is known to be capable of forming membrane tight-junctions.[132] However, in view of the unusually weak cell-cell adhesion observed in this study, proof for the presence of tight-junction proteins was required; therefore, a few of the inserts were selected for staining with ZO-1 dye, a fluorescent-tagged monoclonal antibody which specifically binds to tight-junction proteins. Unfortunately, because the cells could not be fixed onto the support, all ZO-1-staining trials with the stratified multilayer constructs were unsuccessful.

To examine the presence of membrane tight-junctions in the cell line, a monolayer cell culture was prepared. After reaching confluence, the culture support was cut into several pieces and these were subjected to the ZO-1 staining protocol. (See Appendix B) Figure 3.13 shows the HCEC monolayers stained with ZO-1 which were also counterstained with Hoechst 33258. Evidently, the cells are capable of forming tight junctions which are seen in green around the blue nuclei. In addition, the cells are not as compact as those in the multilayer constructs.

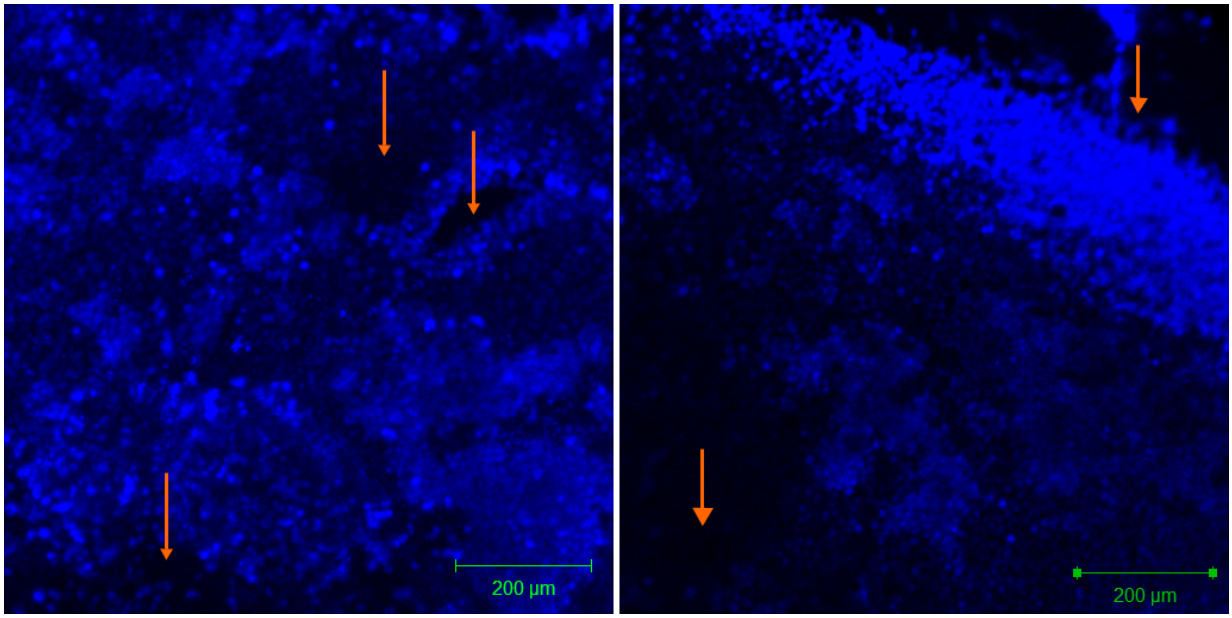

Figure 3.11: Micrographs of the stratified multilayer HCECs grown on the inserts. The cells were stained with Hoechst 33258. (See Appendix B) The red arrows show the holes or crevices formed by detachment of cell clusters. (Magnification: 10X)

Additional test samples from this cultivation were used for a few cytotoxicity experiments to examine the effects of sample toxicants (e.g. BAC) on tight-junctions under the microscope. The result of these experiments could serve as visual controls for cytotoxicity assessments using the stratified cell constructs. A decline in TER after exposure to toxicants could be attributed to disruption of membrane tight-junctions but could also be a result of cell lysis. For this reason, visual confirmation is required. Hence, during verification of the results obtained with the TER assay, the multilayer constructs were also stained after exposure to the toxicant for visual purposes. Figure 3.14 illustrates the effect of BAC on the membrane tight-junctions after 30 min exposure at 37 °C. Deterioration of tight-junctions is evident as the concentration of BAC increases. At the highest tested

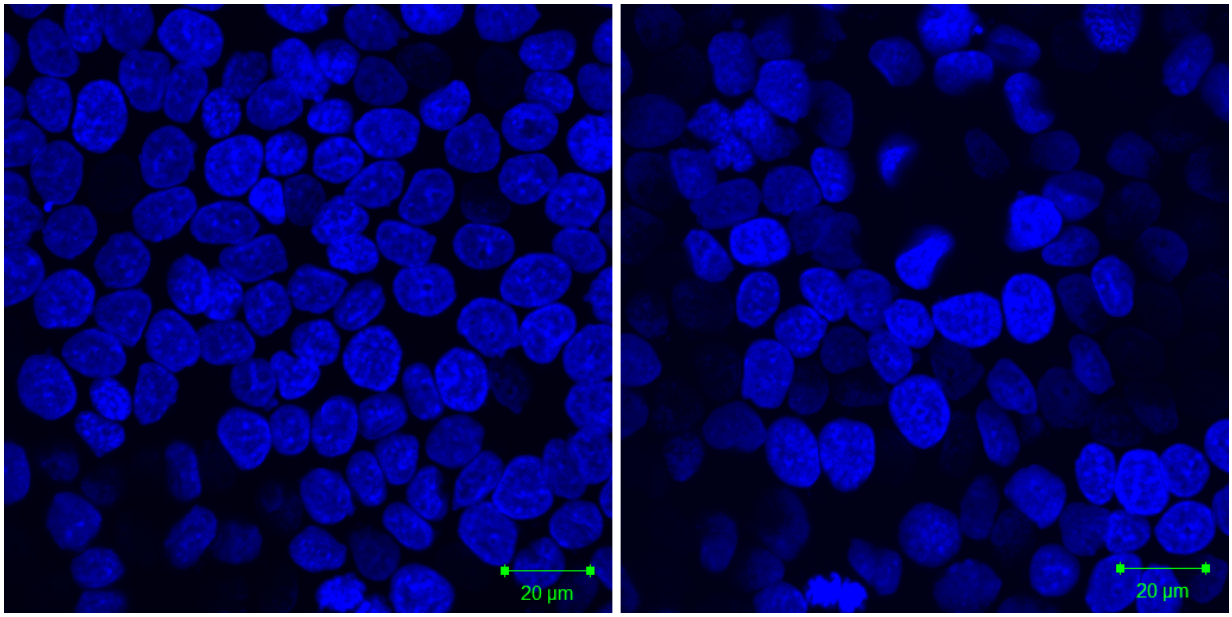

Figure 3.12: Micrographs of the stratified multilayer HCECs grown on cell inserts. The cells were stained with Hoechst 33258. (See Appendix B) (Magnification: 63X)

concentration of BAC (0.100%), nothing could be observed under the microscope, i.e. the screen was completely black in all tested slides (data not shown).

Although formation of tight-junctions between neighbour cells holds the multilayer cell construct together, tension forces during wash steps may be high enough to break the tissue in the weak areas resulting in detachment of cell clusters. These forces might also easily dislodge the cells which are even more weakly bound to the support. Therefore, during the last week of multilayer cell growth, only the cell media were routinely changed with no TER measurement. The rationale was to prevent any further disruption of the tissue before the final TER measurement and the cytotoxicity assessment. Unfortunately, after addition of the buffer onto the inserts for the TER measurements in all cases the multilayer constructs were completely detached from the inserts and clumped together, floating in the buffer. Further studies with multilayer cell constructs were ceased for financial reasons.

In future work, various adhesion proteins/polymers should be tested to find a suitable adhesion layer for this cell line. Secondly, a lower frequency of TER measurement after air-lifting (e.g. once a week) will possibly lead to the construction of more rigid multilayers with less standard deviation among the replicates. Thirdly, the humidity inside the incubator does not seem to be high enough to prevent the air-lifted samples from dryness because, in some cases a small dry area at the centre of the inserts was visible. In addition, if the

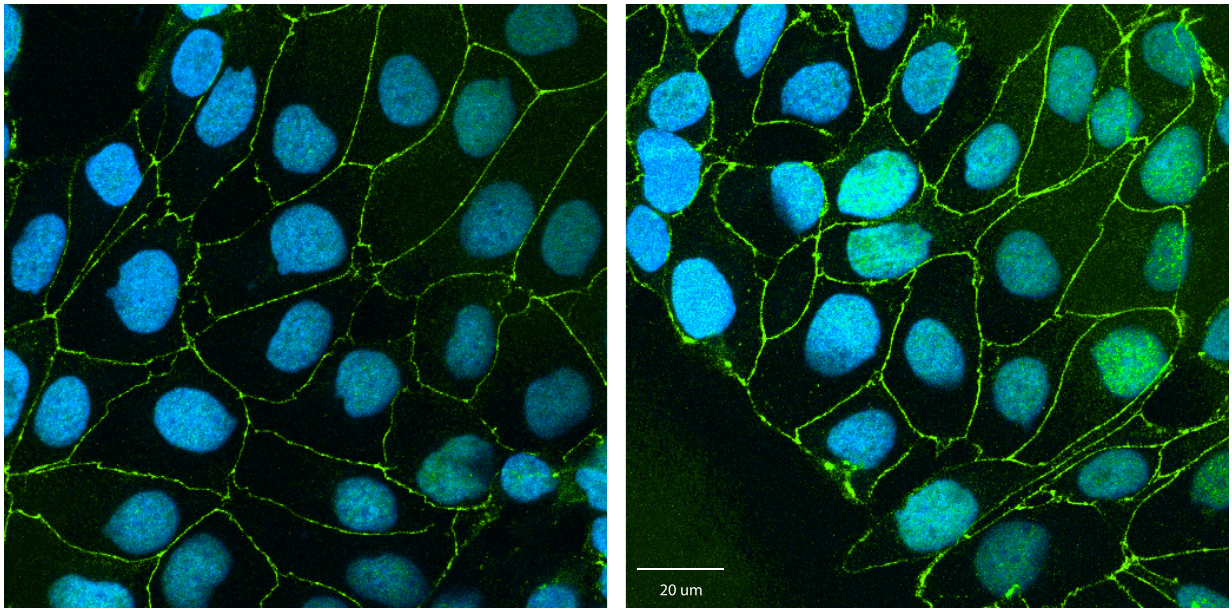

Figure 3.13: HCEC monolayers stained with Hoechst 33258 (blue nuclei) and ZO-1 (green membrane tight-junctions). (Magnification: 63X)

idea of air-lifting is to mimic the unidirectional diffusion of nutrients to the outer layers of cells in a real cornea, the cells should not be left in contact with the insufficiently-humid air, because in real cornea the cells are covered by the tear film, although this film is very thin.

Taken together, the combination of the respiratory activity monitoring assay and the TER measurement assay can potentially be employed for prescreening of chemicals at large scales for evaluation of ocular cytotoxicity. However, further studies should be conducted to optimize the experimental conditions for the production of stable and consistent 3D stratified constructs. Also, the endpoint signal of these assays should be tabulated to be able to categorize the chemicals accordingly.

Monitoring the respiratory activity and measurement of TER at the same time enables the experimenter to distinguish between chemicals that lethally affect the cells within the duration of exposure and those that affect the integrity of the tissue but without immediate effect on the cell viability. If the tested substance is lethal to cells, both the respiratory activity and TER should decrease over time; however, if the chemical damages the tissue integrity without immediate impact on cell viability, only the TER values should decline over time, while the integrated response from the respiratory activity should keep increasing over time.

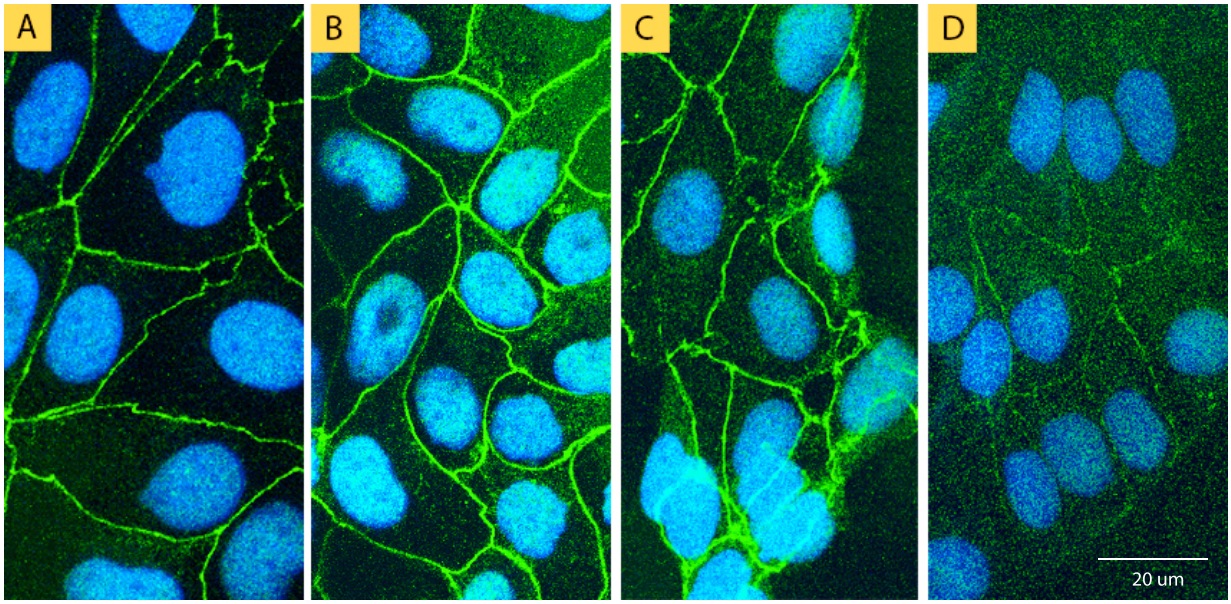

Figure 3.14: Effect of BAC on membrane tight-junctions of HCECs after 30 min exposure. (A) Control, (B) 0.000100%, (C) 0.00100%, (D) 0.0100% BAC. In (D) the green dye is very faint. (Magnification: 63X)

The most commonly used assays for ocular irritancy tests are assays based on isolated organs such as the bovine corneal opacity and permeability assay (BCOP), isolated rabbit eye (IRE) test and the isolated chicken eye (ICE) test. The test endpoints in these assays are the degree of opacity and permeability after exposure to the test substance. Substantial loss of opacity or permeability is enough to put the chemical in the severely irritant category; however, when the loss of permeability or opacity is not noticeable to the naked eye, histological tests are performed to rule out possible damages that do not trigger the endpoints because it has been shown that some severely irritant chemicals such as parafluoranalin, quinacrine and sodium oxylate fail to alter corneal opacity or permeability.[62] Yet, these assays have been approved and validated by the European Centre for the Validation of Alternative Methods (ECVAM) only for identification of severe irritants/ocular corrosives, and have also been accepted by the EU and the US regulatory agencies (June 2008) for the same purpose.[63,133]

It is recommended to combine these assays with assays that are suitable for other endpoints (e.g. cytotoxicity assays) to be able to detect milder irritants,[134,135] when the *in vitro* cell-based assays are performed. TER and respiratory activity measurements can potentially be used at this level in a tiered-testing strategy for assessment of ocular irritants.

Finally, the level of confidence in all alternative tests, including TER and respiratory activity measurements, depends on the availability of a suitable benchmark, technical expertise, historical data on similar chemicals and understanding the limitations of each assay. Hence, the use of *in vitro* alternative tests is company-specific and is limited to the type of material to be tested.[62] Overall, this has enabled many companies to eliminate or minimize the use of animals in the context of eye irritation assessment.

In conclusion, the *in vitro* alternative assays presented in this and the previous chapter cannot be viewed as stand-alone assays for evaluation of eye irritants, because they cannot assess some of the parameters used in the evaluation of ocular cytotoxicity, including the immune response of the host, and the extent of recovery after exposure to the test substance. However, as mentioned before, after optimization of experimental condtions, the combination of the respiratory and the TER assays can potentially form a separate tier for pre-screening of chemicals during ocular cytotoxicity evaluations.

Chapter 4

Differential Pulse Biamperometry

4.1 Introduction

The introduction of potential pulse methods in electroanalytical voltammetry allowed significant progress in the quantitation of trace levels of redox-active analytes.[136] Pulse methods originated within the context of classical polarography, i.e. voltammetry using a dropping mercury electrode, and the initial impetus for the development of pulse methods was to suppress the charging current arising from the expansion of the mercury drop* and the changing applied potential. However, since 1980, these methods have been used with solid electrodes as well.[2] The commonly-used potential waveforms in voltammetry and the

* As the mercury drop expands at a fixed potential, the increase in the surface area results in an increase in the amount of total charges at the surface of the electrode. This phenomenon accompanies the flow of electrons in the connecting leads, which is known as the charging current.

shapes of the corresponding current responses at solid electrodes are illustrated in Figure 4.1.

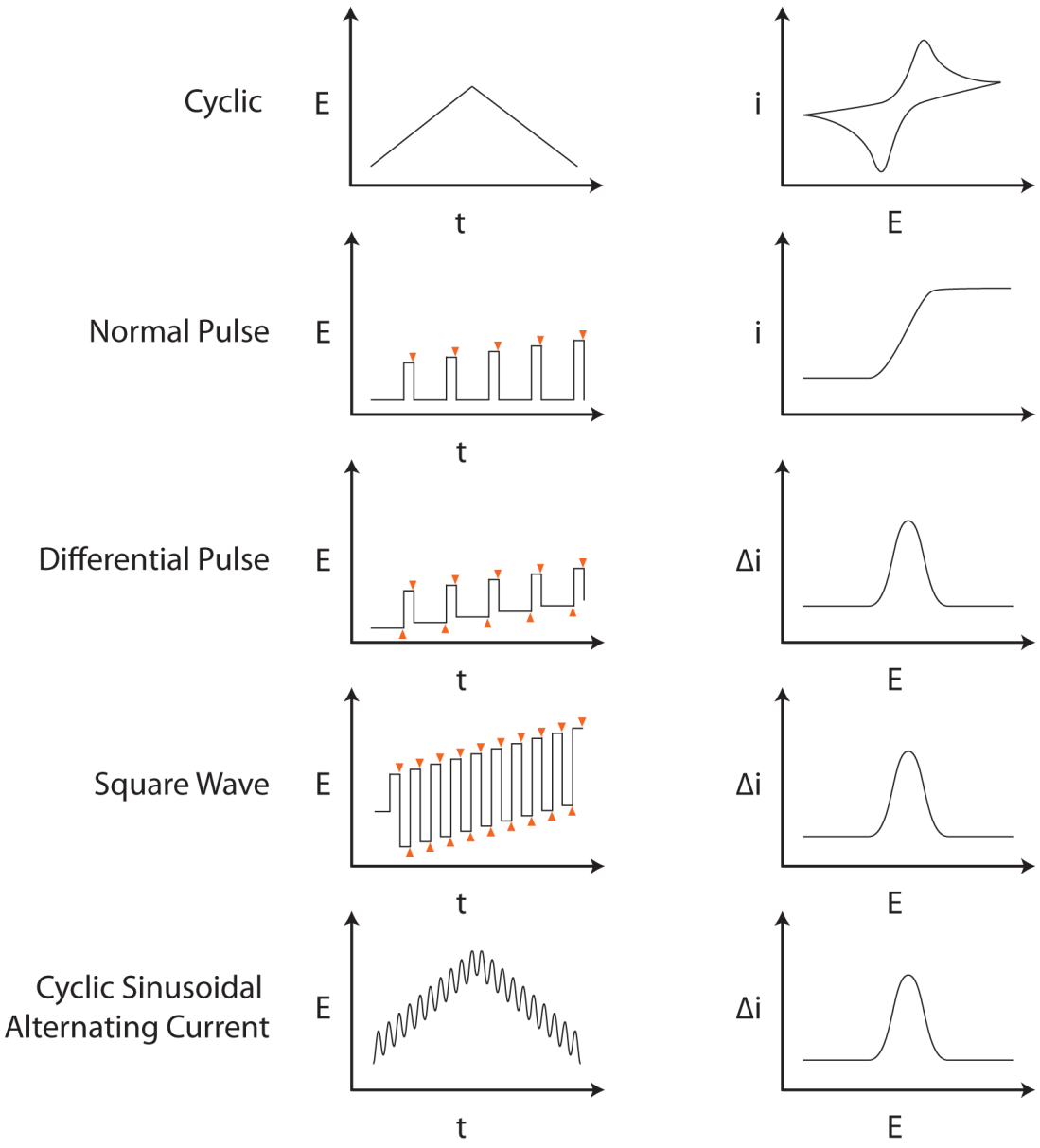

Figure 4.1: Commonly-used potential waveforms in voltammetric analysis. The tiny triangles in normal pulse, differential pulse and squarewave waveforms indicate the moment for current sampling.

In principle, the background current at solid electrodes of all types is dominated by the charging current. In practice, however, the undesirable faradaic processes[†] involving electrode material, solvent or electrolyte impurities can contribute significantly to the background signal.

Although the higher background current in differential pulse voltammetry (DPV), compared to that in differential pulse polarography (DPP), i.e. voltammetry at mercury drop electrode, negatively affects the sensitivity of the former method, the freedom to choose shorter pulse widths in DPV is an advantage of DPV over the DPP.[2]

The applied potential waveforms in DPV, using analog instruments, are generated by superimposition of a slow-changing voltage ramp and square-shaped pulses as shown in Figure 4.2. The current is sampled twice for each pulse, once just before the application of the pulse and again, at the end of that pulse. The difference between the two is then reported as the response current (Figure 4.2).

As previously mentioned in Section 1.1, upon application of a potential difference, the electrode-solution interface behaves similar to a capacitor in that a transient current flows through the electrode lead which is known as the charging current. Eq. 4.2 shows the relationship between charging current, $I(t)$, and time t across a capacitor with the capacitance C after application of a voltage V_0. R represents the resistance of the circuit.[137]

$$I(t) = \frac{V_0}{R} e^{-t/RC} \tag{4.1}$$

Figure 4.3 illustrates this relationship.

Because the linear voltage sweep in Figure 4.2 is changing very slowly, it is assumed that the voltage is practically constant during the time of the pulse application. In addition, modern digital instruments for application of differential pulse waveforms produce perfectly rectangular pulses; hence, the potential does not change during the pulse application at all. Consequently, it should be clear that sampling the current twice for each pulse and taking the difference between the two allow the experimenter to practically eliminate the charging component (background) of the signal response.

The double layer capacitance, C_{dl}, is variable with electrode material, type of electrolyte and the applied potential. Table 4.1 shows some examples of the double layer capacitance values for different electrode materials and different electrolytes.[138–141]

[†] Faradaic processes are the electrochemical redox reactions occurring at the surface of electrode that result in transfer of electrons to/from the electrode.

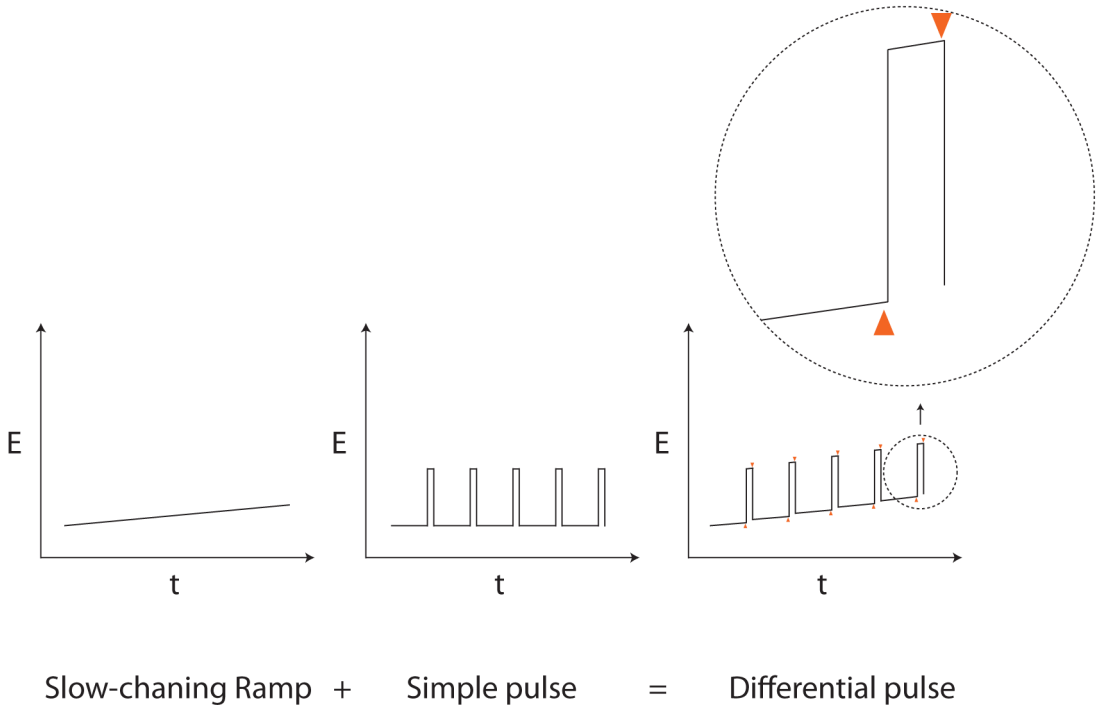

Figure 4.2: Differential pulse waveforms are obtained by superimposition of a slow-changing voltage ramp and simple pulses. The orange solid triangles show the locations of current sampling.

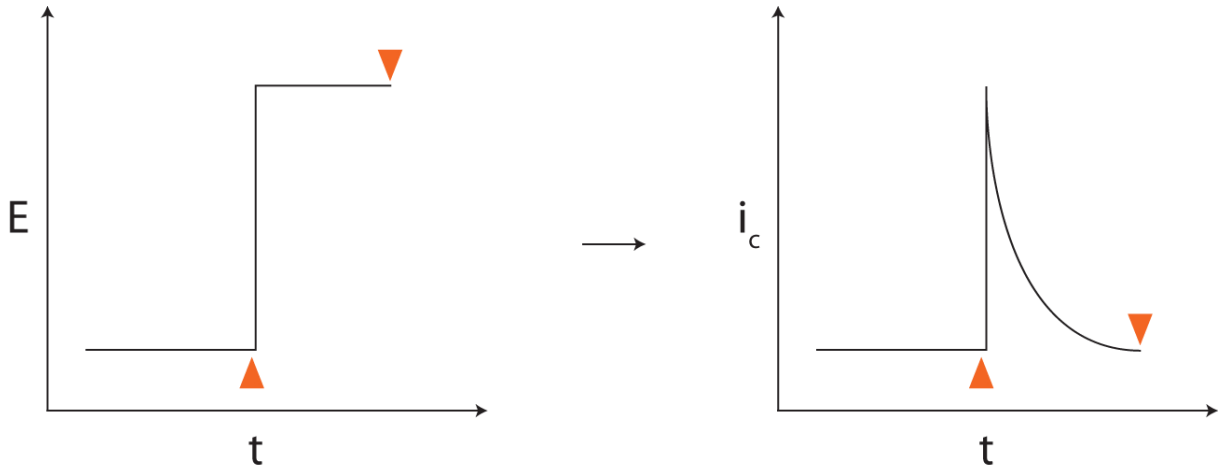

Figure 4.3: Decay of charging current with time (right) after application of a potential difference (left).

Table 4.1: Examples of double layer capacitance values for different electrode materials, different electrolytes and at different applied potentials.[138–141]

Electrode Material	Electrolyte	Potential range vs. SCE (V)	C_{dl} ($\mu F/cm^2$)
Zn	30% KOH	(–1.34, –1.5)	180 – 420
Hg	0.001 mM NaF	(–0.8, –1.6)	5 – 25
Hg	0.1 M NaF	(–0.7, –1.2)	16 – 32
Ag	0.01 M NaF	(–1.5, 0)	25 – 80
Ag	0.01 M KPF_6	(–1.5, 0)	25 – 50
Au	0.01 M $HClO_4$	(–0.4, +0.6)	20 – 58

It is important to note that a chemical system may behave reversibly under conventional DC-voltammetric conditions (e.g. linear sweep voltammetry) but quasi-reversibly or irreversibly under conditions of differential pulse voltammetry. For instance, systems with sluggish electron transfer generate skewed peak shapes under conditions of differential pulse voltammetry.[2]

For a reversible system, the peak height in differential pulse polarography is given by

$$i_{max} = \frac{nFAD^{1/2}C}{\pi^{1/2}(\tau - \tau')^{1/2}} \left(\frac{1-\sigma}{1+\sigma}\right) \qquad \text{where} \qquad \sigma = e^{\left(\frac{nF\Delta E}{2RT}\right)} \tag{4.2}$$

where n, F, A, D and C have their usual meanings; ΔE is the pulse height, τ' and τ are time points for the current measurements right before application of the pulse and at the end of the pulse, respectively. From the equation, it is clear that larger pulse heights trigger larger peak currents. The quotient $(1-\sigma)/(1+\sigma)$ reaches its maximal value of unity when large pulse heights are used;[142] however, pulse heights of larger than 100 mV result in deterioration of the resolution and should be avoided. Shorter pulse widths also enhance the faradaic response, but the higher sensitivity of DPV over older pulse methods, e.g. normal pulse voltammetry, is due to more efficient elimination of the background signal and not because of faradaic response improvement.[2]

The superior sensitivity of pulse methods (e.g. DPV) and their enhanced detection limits (up to 3 orders of magnitude) over traditional sweep-based voltammetric methods have encouraged their use in electrochemical sensing devices.[142] For example, very recently, differential pulse voltammetry has been employed for the detection of dengue virus on compact disk chips,[143] the simultaneous detection of nucleic acids, proteins and small molecules on a sensor array chip,[144] and the detection of carcinoembryonic antigen, using miniaturized immunosensing probes.[145]

In this Chapter, differential pulse waveforms have been examined in biamperometric cells. To understand the resulting data, a brief summary the voltage distribution profile in cyclic biamperometry is presented.

We have previously shown that the distribution of the applied voltage between the two electrode-solution interfaces during application of a linear voltage sweep in biamperometric cells is a function of the concentration ratio of the oxidized to the reduced form of the redox couple at the surfaces of the electrodes.[14] This distribution at any moment occurs such that more of the applied voltage occurs at the interface where the limiting reaction is taking place. Figure 4.4 shows the potential profiles at W_1 during the application of a voltage ramp for a series of constant total concentration of $Fe(CN)_6^{3-}/Fe(CN)_6^{4-}$ at different ratios.

In Figure 4.4, the slope of the line at any point indicates the fraction of the applied scan rate sensed at the electrode-solution interface at that particular voltage.

Table 4.2 shows the values of the slopes for the linear segments of each curve multiplied by the applied scan rate (2 for each curve) which give the predicted scan rates at the electrode-solution interface.[14]

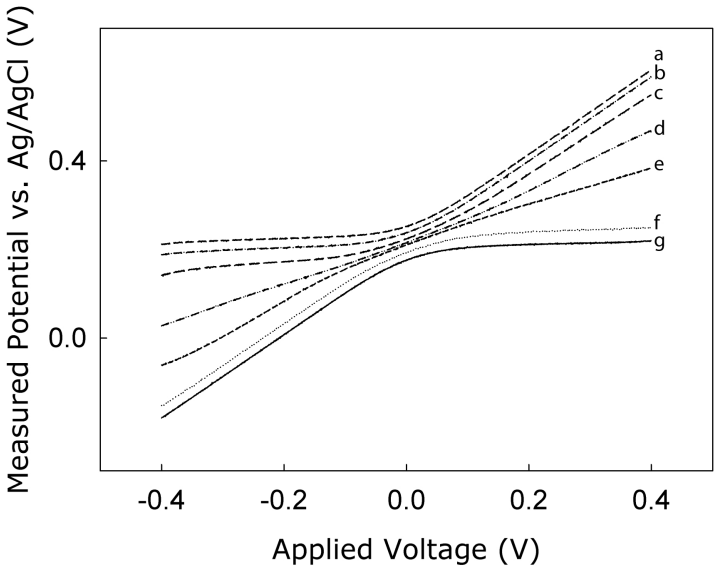

Figure 4.4: Plots of measured potential at W_1 (vs. an Ag/AgCl reference electrode) against the applied voltage for a constant total $Fe(CN)_6^{3-}/Fe(CN)_6^{4-}$ of 2.00 mM with 25 mV/s scan rate. The concentration ratios ([ferricyanide]:[ferrocyanide]) are (a) 4:1 (b) 2.33:1 (c) 1.5:1 (d) 1:1 (e) 1:1.5 (f) 1:2.33 (g) 1:4. The solutions also contain 0.100 M KCl and the measurements were carried out at 25 °C with standard-size gold disk electrodes of 0.0240-cm^2 (W_1) and 0.0239-cm^2 (W_2) areas.[144]

A complete biamperometric cell can be represented by an equivalent circuit such as that shown in Figure 4.5.[14] Since the magnitudes of the currents passing through the interfaces are equal but opposite, one can determine the ratio of the impedance values at the two interfaces; however, it is necessary to make a few assumptions beforehand.

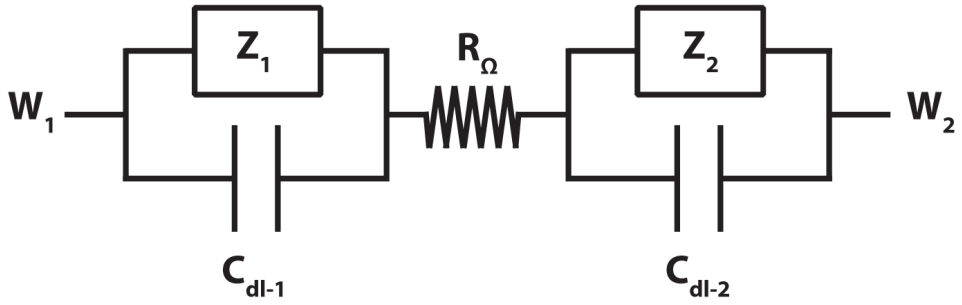

Figure 4.5: An equivalent circuit for a biamperometric cell. W_1 and W_2 represent the working electrodes with double layer capacitances of C_{dl-1} and C_{dl-2} and electrochemical impedances of Z_1 and Z_2. R_Ω represents the resistance of the bulk solution.

At the low frequency limit, the impedance at an electrode-solution interface for small sinusoidal perturbations has been described as:

$$Z = R_\Omega + R_{ct} + C_{dl}(RT/n^2F^2A)((1/D_O^{1/2}C_O^*) + (1/D_R^{1/2}C_R^*))^2 \tag{4.3}$$

where R_Ω, R_{ct} and C_{dl} represent the solution resistance, the charge transfer resistance and the double layer capacitance, respectively and F, A, D, C and n have their usual meanings. For simplicity, at any moment during the scan, we assume the CB waveform as two unidirectional perturbations of small amplitude. Therefore, Equation 4.3 can be broken into two equations

$$Z_1 = R_\Omega + R_{ct} + C_{dl}(RT/n^2F^2A)(1/D_O^{1/2}C_O^*)^2 \tag{4.4}$$

$$Z_2 = R_\Omega + R_{ct} + C_{dl}(RT/n^2F^2A)(1/D_R^{1/2}C_R^*)^2 \tag{4.5}$$

Further simplification occurs when R_Ω and R_{ct} are negligible compared to the third term (the mass-transfer based term). This assumption should be valid for a diffusion-limited reaction in an electrolyte of high ionic strength and for a redox couple with rapid kinetics of electron transfer.

Therefore, the Z_1/Z_2 and Z_2/Z_1 ratios can be written as

Table 4.2: Comparison of experimental and predicted voltage scan rates at W_1.[14]

				Predicted ν mV/s	Measured ν mV/s	Predicted ν mV/s	Measured ν mV/s
$[Fe(CN)_6^{4-}]/[Fe(CN)_6^{3-}]$	(Z_1/Z_2) ox, Eq. 4.7	(Z_1/Z_2) red, Eq. 4.6	Applied scan rate, mV/s	ox	ox	red	red
0.0200	292×10^1	0.000340	50	50.0	48.9	0.0200	1.30
0.0500	468	0.00210	50	50.0	49.0	0.110	1.50
0.100	117	0.00850	50	49.6	49.0	0.420	1.60
0.200	29.2	0.0340	50	48.3	48.9	1.60	1.90
0.250	18.7	0.0530	25	23.7	23.8	1.30	1.20
0.429	6.36	0.156	25	21.6	23.7	3.40	1.50
0.500	4.68	0.212	50	41.2	46.1	8.70	3.70
0.556	3.79	0.262	50	39.6	44.7	10.4	4.60
0.625	2.99	0.331	50	37.5	43.9	12.4	5.10
0.667	2.63	0.377	25	18.1	22.5	6.80	2.70
0.714	2.29	0.433	50	34.8	41.1	15.1	6.90
0.833	1.68	0.589	50	31.4	34.9	18.5	10.4
0.909	1.41	0.701	50	29.3	30.5	20.6	14.3
1.00	1.17	0.848	25	13.5	17.4	11.5	11.4
1.00	1.17	0.848	50	26.9	25.7	22.9	20.7
1.10	0.966	1.03	50	24.6	19.7	25.3	28.3
1.20	0.812	1.22	50	22.4	15.7	27.5	32.5
1.40	0.596	1.66	50	18.7	14.1	31.2	33.7
1.50	0.520	1.91	25	8.50	10.1	16.4	19.8
1.60	0.457	2.17	50	15.7	8.70	34.2	40.0
1.80	0.361	2.75	50	13.3	5.80	36.7	42.7
2.00	0.292	3.39	50	11.3	5.10	38.6	43.4
2.33	0.215	4.62	25	4.40	1.30	20.6	23.6
4.00	0.0730	13.6	25	1.70	0.900	23.3	23.6
5.00	0.0470	21.2	50	2.20	1.300	47.7	46.8
10.0	0.0117	84.8	50	0.580	0.900	49.4	47.9
20.0	0.00290	339	50	0.150	0.600	49.9	48.2
50.0	0.000470	212×10^1	50	0.020	0.800	50.0	48.8

$$Z_1/Z_2 = D_R C_R^{*2}/D_O C_O^{*2} \tag{4.6}$$

$$Z_2/Z_1 = D_O C_O^{*2}/D_R C_R^{*2} \tag{4.7}$$

Here we assumed that C_{dl}/A values are the same for both electrodes. These assumptions allow us to compare the experimental and the theoretical values of impedance ratios. Figure 4.6 represents the comparison of calculated fractional impedance values $(Z_1/Z_2)/(Z_1/Z_2{+}1)$ with the experimental values determined from the slopes of the linear portions of the curves in Figure 4.7.[14] This figure shows that the calculated impedance ratios based on the assumptions made earlier can correctly predict the direction of change in impedance ratios during a voltage scan. Therefore, during a diffusion-controlled reaction the impedance at the interface where the limiting reaction occurs is much larger than the impedance at the other interface.

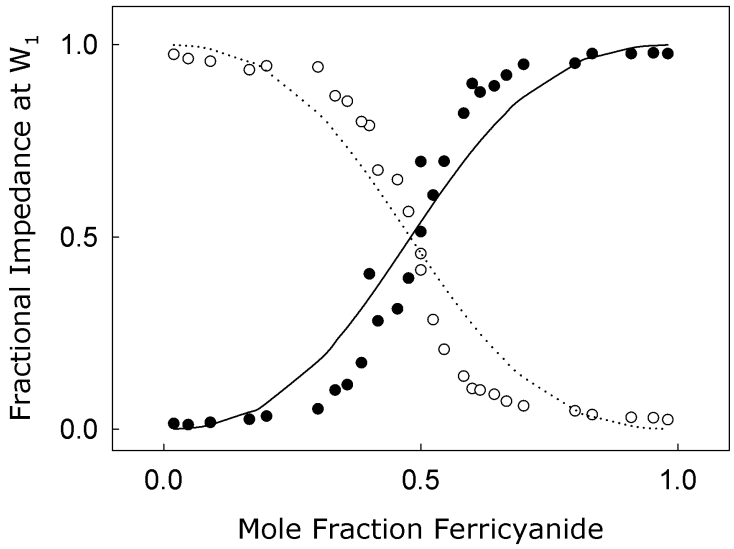

Figure 4.6: Calculated $(Z_1/Z_2)/(Z_1/Z_2+1)$ from Eq. 4.6 and Eq. 4.7 (lines) and the corresponding experimental values from Table 4.2.

One major issue with the application of differential pulse voltammetry to miniaturized devices is the difficulty of manufacturing a proper reference electrode at the same scale on that of the working electrode. In Chapter 1 and in this section, traditional biamperometry and the recently-introduced cyclic biamperometry were reviewed. The hallmark of these electrochemical cells, compared to traditional three-electrode cells, is the lack of

a reference electrode in the circuitry. This greatly facilitates miniaturization of biamperometric cells and their incorporation into small-scale sensing devices. The application of the differential pulse waveforms in biamperometric cells could enhance the sensitivity and lower the detection limit of the electrochemical cell. In the following sections, the application of differential pulse waveforms in biamperometric cells is investigated. To study the distribution of the applied voltage pulses between the two electrode-solution interfaces, independent measurements of pulse shapes were undertaken using a commercial reference electrode.

4.2 Materials and Methods

4.2.1 Chemicals and Instrumentation

Potassium ferricyanide, potassium ferrocyanide, and potassium chloride were purchased from Sigma-Aldrich in the highest available quality and were used as received. Buehler Micropolish II (1 μm) was purchased from Tech-Met Canada. Standard gold disk working (d = 1.6 mm, unless otherwise stated) and Ag/AgCl reference electrodes were obtained from Bioanalytical Systems Inc. (West Lafayette, IN). However, most experiments were carried out with the microelectrodes (100 μm dia.) sealed in glass unless otherwise stated. All solutions were prepared in distilled, deionized water (Barnstead NanoPure) and the experiments were carried out at ambient temperature 22 $\pm$ 1 °C. Electrochemical measurements were made using a CHI650A potentiostat (CH Instruments) having a rise time of less than 1 μs. Typically, scans were initiated at the most positive applied potential (DPV) or voltage (DPB). A data acquisition board NI-USB-6251 was used to monitor the working-to-reference electrode potential during differential pulse experiments, and this was connected to a PC running a small program (written by myself) in LabView software (National Instruments).

4.2.2 Methods

The electrode preparations and determination of the electroactive surface area of the electrode have been described elsewhere.[14] Briefly, the electrodes are polished using 1 micron Buehler micropolish, rinsed and put in a sonicator for 30 s. Then the solution in the sonicator is changed and the electrodes are sonicated for another 30 s. In the final step the electrodes were also sonicated in 4 M HNO_3 and again rinsed with deionized water. To

calculate the electroactive surface area of the standard-size electrodes, 1-step chronoamperometry is applied in a solution with a known concentration of ferricyanide for which the diffusion coefficient in 0.10 M KCl solution is known. The slope of the plot of $i(t).t^{1/2}$ against t is a constant value from which, using the Cottrel equation (see below), the electroactive surface area of the electrode is calculated.

$$i(t) = \frac{nFACD^{1/2)}}{\pi^{1/2}t^{1/2}} \qquad \Longrightarrow \qquad i(t).t^{1/2} = \frac{nFACD^{1/2}}{\pi^{1/2}} \tag{4.8}$$

To apply the biamperometric waveforms, the working electrode lead was connected to one of the metallic electrodes (W_1), while the reference and auxiliary electrodes leads together were connected to the other gold electrode (W_2).

Potential profiles were monitored using two channels of the NI data acquisition system. One channel monitored the applied differential pulse voltage waveform, while the other channel measured the time-dependent potential difference between W_1 and an Ag/AgCl reference electrode. The data acquisition frequency on each channel was set to 1000 Hz.

4.3 Results and Discussion

Application of the differential pulse waveforms to the biamperometric electrochemical cells containing an electrochemically reversible redox couple results in generation of voltage-dependent current profiles similar to those observed in differential pulse voltammetry as shown in Figure 4.7.

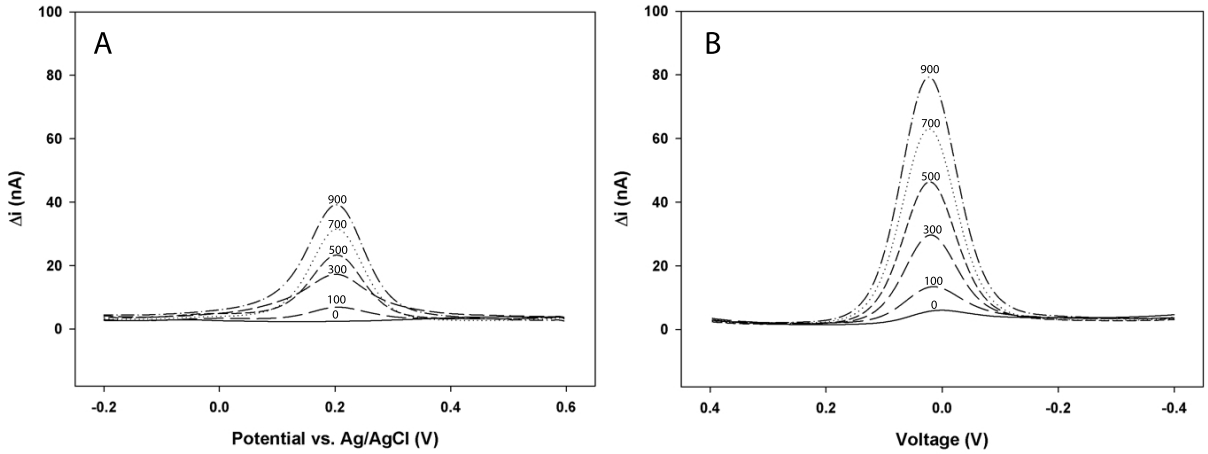

Figure 4.7: DPV (A) and DPB (B) for a series of ferricyanide concentrations, shown on the same scale. The numbers on the curves show [ferricyanide] in μM. In both cases the solutions contain 0.100 M KNO_3; however, DPB solutions also contain 10.0 mM of ferrocyanide. Pulse amplitude: 50 mV, pulse width: 100 ms, pulse period: 200 ms, pulse increment: 4 mV using the microelectrodes (dia: 100 μm)

In both cases the peaks correspond to the current difference between the current sampling points (Figure 4.1). A clear difference between the two methods is that the absence of the reference electrode in DPB results in formation of the peak voltages near 50 mV. However, the peak potentials in DPV are observed near the formal redox potential of the ferri/ferrocyanide redox couple (0.227 $\pm$ 0.001 V vs. Ag/AgCl in 0.100 M KNO_3) in the electrolyte solution.[14] In addition, the peak heights in DPB are considerably larger than those in DPV when one form of the redox species is present in great excess.

In an attempt to understand the behavior of the biamperometric cell, the potentials of each metallic electrode were measured against an external Ag/AgCl reference electrode during the application of differential pulse waveforms from +0.400 to –0.400 V. Figure 4.8 shows the distribution of the applied voltage between the two electrode-solution interfaces for a 0.100 M solution of KNO_3 containing 0.100 mM ferrocyanide and 0.900 mM

ferricyanide.

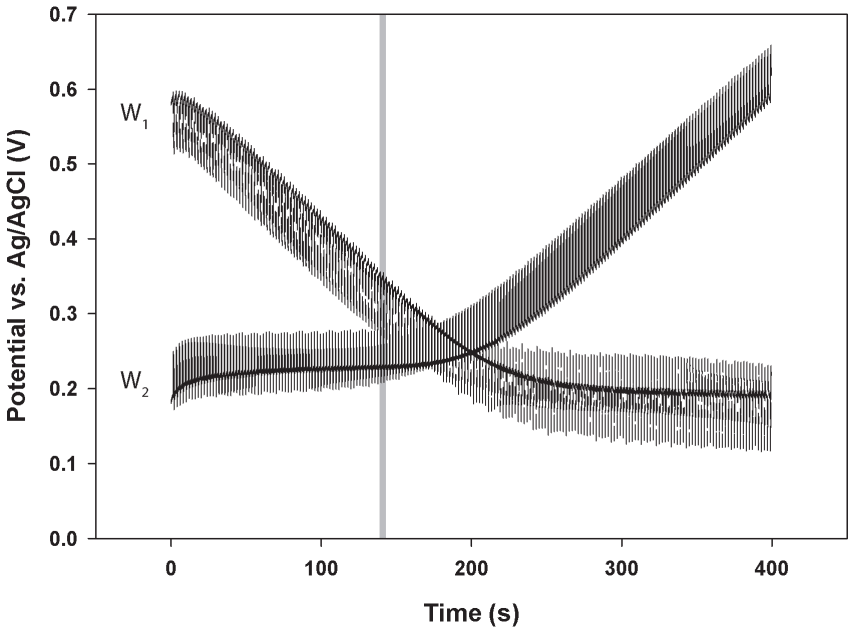

Figure 4.8: Typical potential profiles at W_1 and W_2 measured against an external Ag/AgCl reference electrode during a scan from +400 to –400 mV. The medium contains 0.900 mM ferricyanide and 0.100 mM ferrocyanide in presence of 0.100 M KNO_3. Pulse height, increment, pulse width and pulse period are 50 mV, 4 mV, 500 ms and 2000 ms, respectively. Two identical standard-size gold disk electrodes (d = 1.6 mm) have been used for W_1 and W_2. The grey bar represents the region at which the anode and the cathode switch after application of the pulses.

The general trend of the voltage distribution profiles in this figure mimics the pattern observed for cyclic biamperometry shown in Figure 4.4. This can be easily explained by referring to Figure 4.2, where the components of the differential pulse waveform have been illustrated. A closer look at Figure 4.8, however, reveals the differences between the pulse shapes at different base voltages as shown in Figure 4.9. In this figure, at any given point during the scan, the sum of the voltages at each interface ([B + (-A)] because the pulses at the interface are applied at opposing directions) is equal to the applied voltage by the potentiostat (C). This can serve as a test for proper functioning of the potentiostat. The apparent pulse height at the limiting interface, m, is much larger than that at the other interface, n. Also at the limiting interface the pulse shape has the characteristics of a charging capacitor (top left and the middle right pulses in Figure 4.9). To understand why

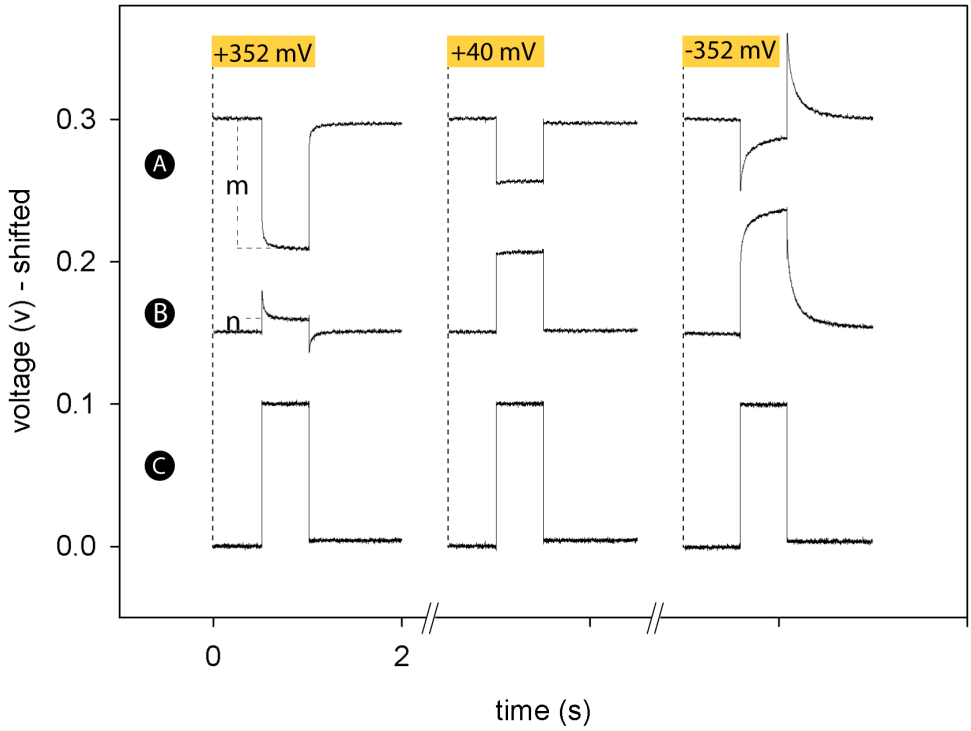

Figure 4.9: Typical potential profiles for DPB pulses measured against an external Ag/AgCl reference electrode during a scan from +400 to –400 mV. (A) Potential profile at W_1, (B) potential profile at W_2 and (C) sum of the potential values at W_1 and W_2. The medium contains 0.900 mM ferricyanide, 0.100 mM ferrocyanide in presence of 0.100 M KNO_3. Pulse height, increment, pulse width and pulse period are 100 mV, 4 mV, 500 ms and 2000 ms, respectively. For the sake of comparison, the potential values have been shifted along the x- and the y-axes. Two identical standard-size gold disk electrodes (d = 1.6 mm) have been used for W_1 and W_2.

the pulse curvatures have different orientations, we consider each interface in Figure 4.5 where an impedance is parallel to a capacitor.

In Section 4.1 and in previous work,[14] it was shown that in a biamperometric cell the impedance at the limiting interface is much larger than that at the other interface when the reaction is diffusion-limited, i.e. at extreme voltages. Although the frequency of the pulses in Figure 4.8 and Figure 4.9 is very low (0.5 Hz because pulse period = 2 s), the rapid rise time of the potentiostat ($< 1\mu s$) implies a very high "instantaneous frequency" ($> 5 \times 10^5$ Hz) at the moment of pulse application. Upon application of the

pulse, the limiting interface in Figure 4.5 behaves in a similar way to a pure capacitor because the impedance is much larger than $2\pi fC$ where $2\pi f$ is the angular frequency and C is the capacitance (the double layer capacitance in this case).[137] Consequently, the voltage profile at this interface shows a capacitor charging effect. Also, because the total voltage is strictly controlled by the potentiostat, the voltage-time curve at the other interface shows a complementary voltage profile. In addition, when the reaction is not diffusion-limited, i.e. when the voltage at the top of the pulse is around 0 V, the pulse heights are of similar size and are rectangular in shape as shown in the middle section of Figure 4.9.

Although it is widely accepted that an electrode-solution interface can behave in a similar way to a capacitor, unlike a real capacitor, the double layer's RC value (time constant) varies depending on the applied voltage and electrolyte concentration. In an attempt to understand how the double layer time constant changes during a differential pulse biamperometry scan, the limiting interface has been modeled as a capacitor. This assumption led to the estimation of the RC values at the limiting interface by a curve fitting approach.

The voltage across a real capacitor in series with a resistor, upon application of a potential difference, has the following relationship with time:

$$V(t) = V_0(1 - e^{-t/RC}) \tag{4.9}$$

where V_0 is the applied potential difference and RC is the time constant of the RC circuit. Using this equation, it is possible to find the best-fitting curve (by varying the RC value using Microsoft Excel) to the voltage profile at the limiting interface during application of a differential pulse biamperometry scan (see Appendix C). Briefly, by changing the RC value, the curve that produces the least sum of squared differences between the experimental and the mathematically obtained curve is selected. Then, the RC value of this curve is selected as the estimate for time constant at that voltage. The estimated RC values using this approach, as a function of the base voltage are shown in Figure 4.10.

Figure 4.10 shows that the time constant at the limiting electrode-solution interface drops dramatically when the applied voltage at the interface is around zero (corrected for pulse amplitude). On the plot this decline is observed where the base voltage is approaching +50 mV from both sides and this is because the potentiostat records the base voltage instead of the voltage at the top of the pulse. This rapid decline in RC occurs because of a rapid drop in the magnitude of the impedance at the interface, which, in turn, happens due to transition from a primarily large mass-transfer based resistance (in a diffusion-controlled reaction) to a voltage region where very limited electrochemical reactions take place.

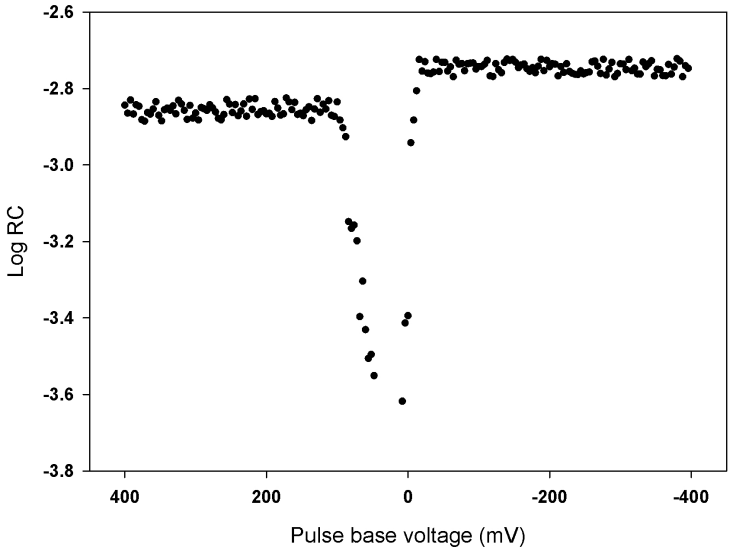

Figure 4.10: Log RC vs. the base voltage for each pulse during a scan from +400 to –400 mV. The conditions are the same as those in Figure 4.9.

Since the rise-time of the potentiostat is smaller than 1 μs (the exact time is not known), RC time-constants calculated using this approach cannot be smaller than 1 μs; hence, those data points in Figure 4.10 with Log RC values smaller than –6 have been removed from the figure. Using this model for the electrode-solution interfaces during differential pulse biamperometry, it is possible to explain the differences in the peak heights for DPB and DPV in Figure 4.7.

Before closing the circuit, the surface concentrations of ferri/ferrocyanide are equal to those in the bulk of the solution. When the switch is closed, a much larger electrode-solution potential difference occurs at the interface where the limiting reaction occurs, i.e. at W_1 electrode-solution interface where ferrocyanide is reacting. As ferrocyanide is rapidly consumed at the surface of W_1, an equal amount of ferrocyanide is generated at the surface of W_2. Since the reaction at W_1 is diffusion-limited, the surface concentration of ferrocyanide should decrease from the initial bulk concentration (e.g. 50.0 μM) to zero. At the same time the same amount of ferrocyanide is generated at the surface of W_2. Therefore, the surface concentration of ferrocyanide at W_2 approximately equals the sum of that in the bulk solution (50.0 μM) and the electrochemically generated amount (i.e. 50.0 μM) or simply twice as much as its concentration in the bulk of the solution. As the base voltage approaches the origin from left hand side in Figure 4.8, the peak shoulders in Figure 4.7 appear. This is due to the fact that less and less electrochemical reactions occur

after application of the pulses, because, the magnitude of the applied voltage window at the top of the pulses gets smaller and smaller. When the voltage values at the top of the pulses cross each other, (this region has been shaded in Figure 4.8) the position of the anode and the cathode momentarily switches during the pulse application; however, the applied voltage window at the top of the pulses is still not large enough for the redox reactions to take place. As the base voltage shifts more to the right (positive values), the applied voltage window at the top of the pulses gets larger and larger and eventually becomes large enough for the redox reactions to occur. At the same time the applied voltage window at the base of the pulses shrink. Since the positions of the anode and cathode, after the pulse application, have already been switched, the surface concentration of ferrocyanide at W_2 is twice, in principle (with electrodes of equal area), that in the bulk of the solution and a much larger peak current is observed. Generation of faradaic currents in DPB require the presence of both halves of the reversible redox couple which is not the case for DPV. In fact, peak currents in DPV are proportional to the total concentration of both halves of the redox couple. Figure 4.11 shows the peak current vs. the concentration of ferricyanide for a series of solutions containing a *constant total concentration* of ferri/ferrocyanide.

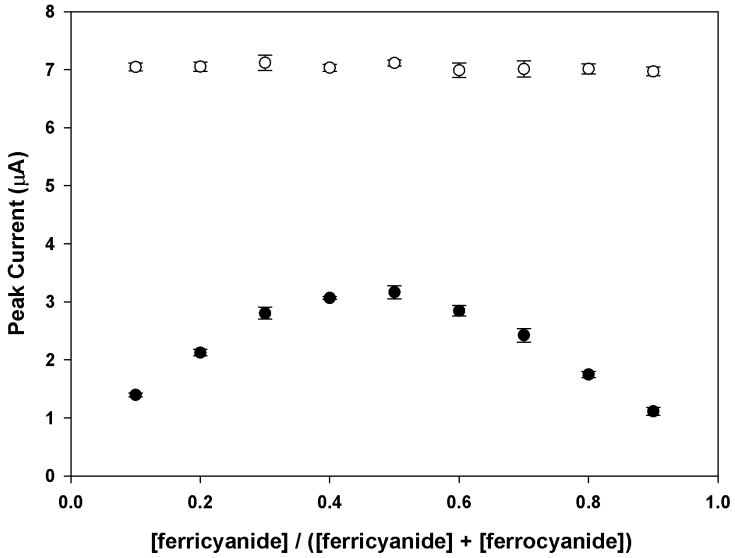

Figure 4.11: Peak current vs. mole fraction of ferricyanide for a series of solutions with a constant 1.00 mM total [ferricyanide] + [ferrocyanide] in 0.100 M KNO_3 for DPV (empty circles) and DPB (solid circles). Pulse amplitude: 50 mV, pulse width: 50 ms, pulse period: 200 ms and pulse increment: 4 mV. Two standard-size gold disk electrodes (1.6 mm dia.) with electroactive surface area of (W_1 : 2.40×10^{-2} and W_2: 2.39×10^{-2} cm^2) were used for the measurements

DPB peak currents depend on the concentration of the limiting of the two redox species because the applied voltage window is adjusted so that both redox reactions can take place or otherwise no faradaic current flows. For a constant total concentration of ferri/ferrocyanide, the peak current reaches its maximal value when the redox species are present in 1:1 ratio. (It is assumed that identical electrodes are used for W_1 and W_2 and the diffusion coefficient of ferricyanide is equal to that of ferrocyanide; in reality, the diffusion coefficient of ferricyanide, 7.63 $\times 10^{-6}$ cm^2/s, is slightly larger than that of ferrocyanide, 6.50 $\times 10^{-6}$ cm^2/s, in 0.100 M KCl[146]). DPV peak currents, however, are proportional to the total concentration of the redox couple, because the starting potential for the scan is selected where only one form of the redox analyte can exist in the vicinity of the electrode; consequently, while approaching the formal redox potential of the couple, only one form of redox species is accumulated at the surface of the electrode.

Figure 4.12 shows plots of peak current against the concentration of ferricyanide for DPB and DPV on the same scale. A linear relationship between the peak current and concentration of ferricyanide is observed in both cases. The coefficients of determination (R^2) for all plots were greater than 0.98. In addition, at the tested concentrations, the average y-intercepts and their standard deviations are on the same order of magnitude for DPV and DPB as shown in Table 4.3.

Table 4.3: y-intercepts (b) and the corresponding standard deviations (s_b) for DPB and DPV.

Pulse Height (mV)	10		30		50		70		90	
	b	s_b	b	s_b	b	s_b	b	s_b	b	s_b
DPB ($\times 10^9$)	-0.161	0.219	1.351	1.595	-0.764	0.389	-2.886	1.055	-1.089	1.518
DPV ($\times 10^9$)	0.444	0.085	0.028	0.341	0.54	0.392	0.834	0.604	3.481	0.604

The difference between the conditions in this figure and those in Figure 4.11 is that in the latter the total concentration of ferri- and ferrocyanide is constant, hence, the magnitudes of the peak currents in Figure 4.11 are dictated by the concentration of the limiting species, which is always smaller than the total concentration of the two species. However, it is the total concentration of the two species that determines the magnitude of peak currents in DPV. In Figure 4.12, the concentration of the limiting species, in the presence of great excess of the other form, is equal to the concentration of the analyte reacting under DPV conditions.

The peak currents in DPB are also inversely proportional to the square root of pulse width similar to that observed in DPV (see Eq. 4-2). Figure 4.13 depicts this relationship for DPB and DPV. In both cases the coefficients of determination are greater than 0.99.

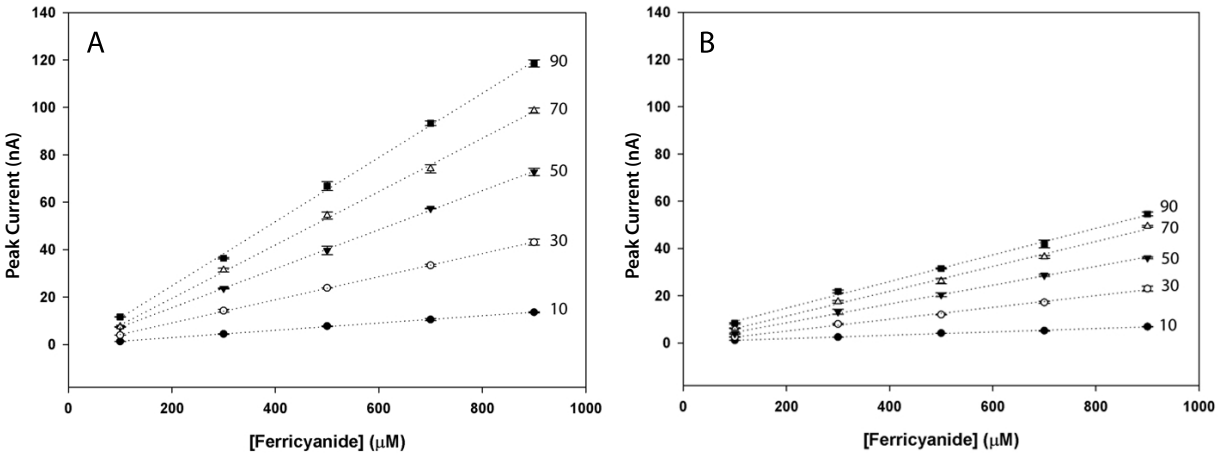

Figure 4.12: Peak current vs. [ferricyanide] for DPB (A) and DPV (B). The media also contain 0.100 M KNO_3 and 10.0 mM ferrocyanide (for DPB only). The numbers beside the plots indicate the applied pulse amplitude in mV. Pulse period: 200 ms, pulse width: 100 ms, pulse increment 4 mV. The microelectrodes (100 μm dia.) were used for the measurements.

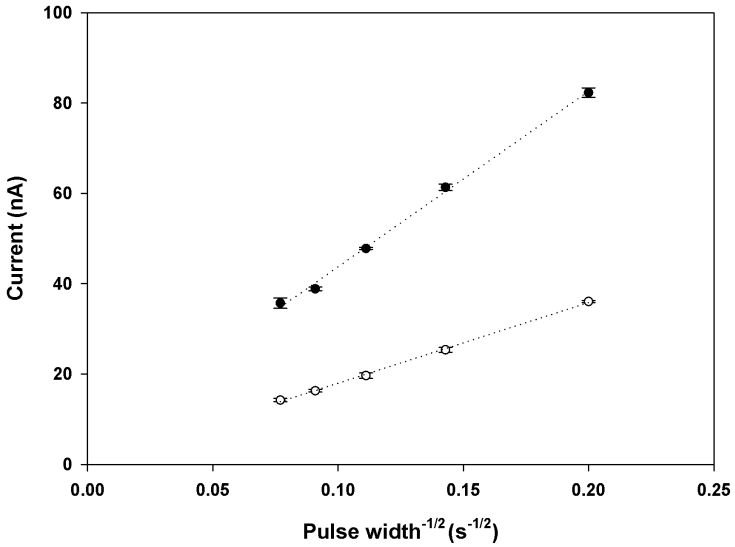

Figure 4.13: Peak current vs. inverse square root of pulse width for DPB (solid circles) and DPV (empty circles). The media contain 50.0 μM ferricyanide and 10.0 mM ferrocyanide (for DPB only) in 0.100 M KNO_3. Pulse amplitude: 50 mV, pulse period: 200 ms, pulse increment: 4 mV. The gold disk microelectrodes (100 μm dia.) were used for the measurements.

The peak currents in DPB are also proportional to $(1-\sigma)/(1+\sigma)$ (see Eq. 4-1) Figure 4.14 shows the peak current in DPB and DPV for various concentrations of ferricyanide on the same scale. In all plots the coefficients of determination, R^2, are greater than 0.98.

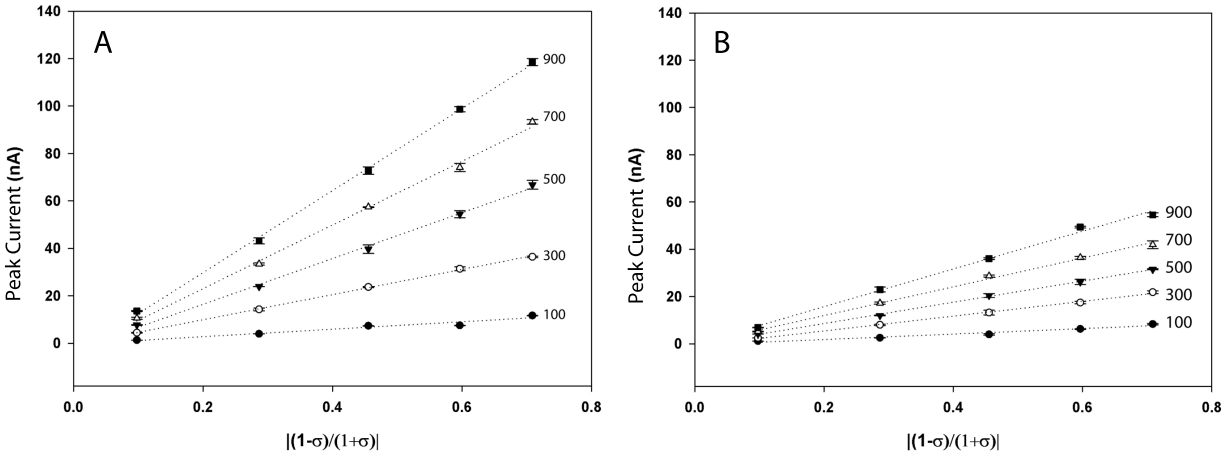

Figure 4.14: Peak current versus $(1-\sigma)/(1+\sigma)$ for DPB (A) and DPV (B). The numbers beside the plots indicate the concentration of ferricyanide in the solution. Pulse period: 200 ms, pulse width: 100 ms, pulse increment 4 mV. The microelectrodes (100 μm dia.) were used for the measurements.

Simplicity and high sensitivity of differential pulse biamperometry allow this method to be used for quantitation of various electrochemically reversible compounds in the presence of an excess of their opposing form. When only one form of the redox active analyte is present, another redox active molecule can be added to the medium to undergo the opposing redox reaction, i.e. the presence of a redox couple is not mandatory for generation of a biamperometric signal.

Although differential pulse biamperometry can be more sensitive than differential pulse voltammetry, its area of application is more limited and the experimenter should be aware of these limitations. One major limitation, as previously mentioned, is that when both forms of the electroactive redox couple are present in the medium the form present in great excess should be known.

When in contact with ambient air, several electroactive redox species may be present in an equilibrium state with their opposing form. In the blank solution, the species that is present in great excess must be present or added to the solution. This enables quantitation of the relative concentration of the opposing form present in the stock solution and subsequent subtraction of this signal from the signal obtained from test solutions. The presence of a small percentage of the limiting form in the stock solution also dictates the limit of detection that can be achieved with differential pulse biamperometry. Therefore, to achieve lower detection limits one must make sure that the form present in great excess

is as pure as possible. Another major limitation is the selectivity of DPB when more than one redox couple is present in the medium. Because the position of the applied voltage window is not fixed on the potential axis, the redox couple that can produce higher currents will undergo the redox reactions. For example, TMPD (see Figure 1.10) is a redox mediator, the oxidized form of which exists in an equilibrium with its reduced form when it is dissolved in water due to air-oxidation. This mediator undergoes two one-electron oxidation reactions, both of which are electrochemically reversible. However, only one of the two peaks is observed during a DPB scan as shown in Figure 4.15.

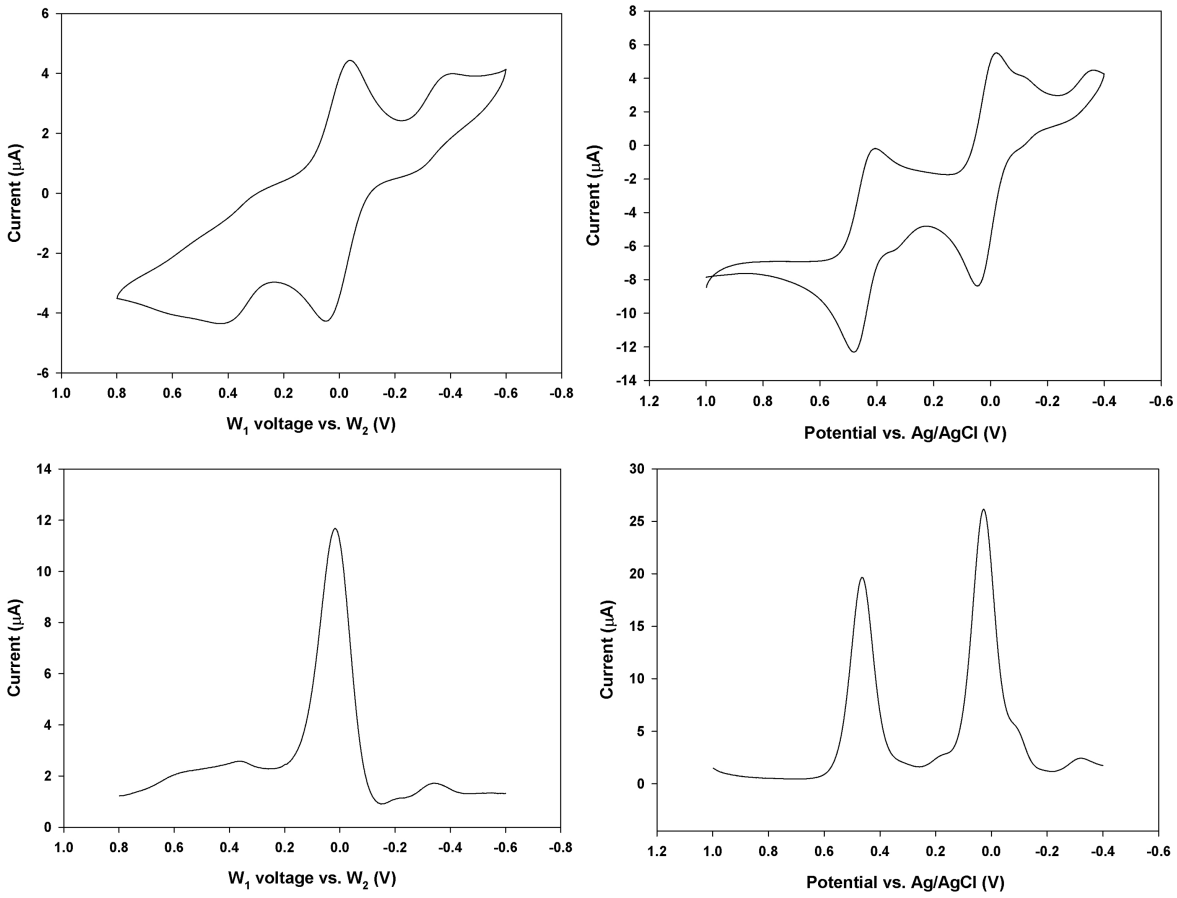

Figure 4.15: CB (top left) and CV (top right) with 4 mV/s scan rate, and DPB (bottom left) and DPV (bottom right) for a 1.00 mM solution of TMPD in 0.10 M KNO_3. The conditions for differential pulse waveforms are: pulse amplitude = 30 mV, pulse width = 50 mV, pulse period = 200 ms and pulse increment = 2 mV. Commercially-available standard-size gold disk electrodes (dia = 1.6 mm) were used.

Looking at the biamperometric graphs in Figure 4.15, one may assume that the W_1 electrode has swept 1.4 volts (from +0.8 to –0.6 V). In reality, however, the magnitude of the swept voltage is far less than 1.4 volts as shown in Figure 4.16. In this case, W_1 sweeps only 773 mV.

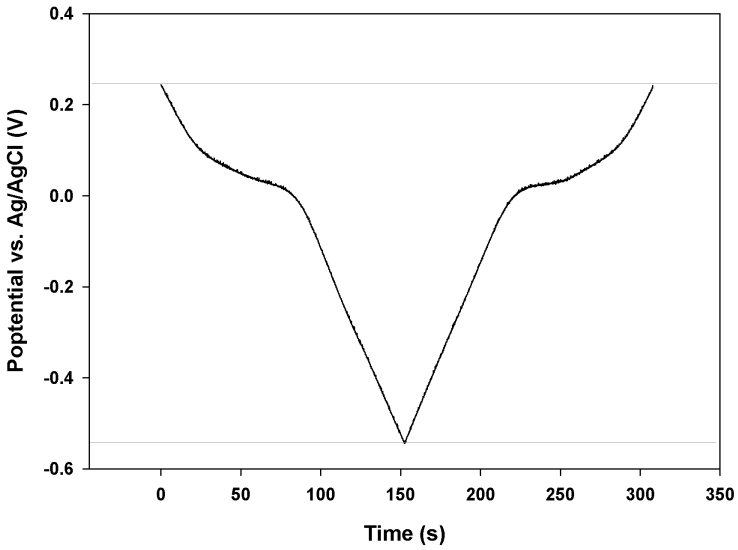

Figure 4.16: Potential of W_1 vs. an external Ag/AgCl electrode during the CB scan in Figure 4.15.

To summarize, it was shown that differential pulse waveforms can be applied in biamperometric cells and when one form of the redox couple is present in great excess, the peak current is proportional to the concentration of the limiting species. Under these conditions, the peak currents are twice as large in DPB compared to the peak currents observed in DPV, provided that an equal amount of the limiting species is present in the solution without the excess presence of the other form. It was also observed that under these conditions, the peak currents in DPB are linearly proportional to the fraction $(1-\sigma)/(1+\sigma)$ (see Eq. 4.2) and to the inverse square root of the pulse width. In addition, it was demonstrated that biamperometric cells cannot distinguish between the redox couples when more than one redox couple is present in the solution; hence, these cells may not be a suitable choice when multiple redox couples are present in the medium.

Based on these results biamperometry cannot currently be used for diagnostic purposes. However, DPB can serve as an analytical tool where identity of the electroactive species which is to be quantitated in the solution, is known. It is necessary to perform the diagnostic tests and control experiments before application of DPB. Under right conditions,

DPB can be used as a favourable method of analysis. For example, DPB can be used with disposable electrochemical cells where inexpensive screen-printed carbon electrodes are used. In Section 5.2 a few applications are presented for future studies involving DPB.

Chapter 5

Summary and Suggestions for Future Research

5.1 Summary of Original Contributions

In this thesis, recent advances in biamperometry together with applications of the recently introduced cyclic biamperometry, in *in vitro* ocular cytotoxicity assessment have been presented. For the cytotoxicity/ viability assessment, cultured human corneal epithelial cells have been used as a model. The assay presented relies on the electrochemical measurement of the respiratory activity of the cells. This measurement is done by capturing electrons from the components of the respiratory chain and transferring these electrons to a non-native terminal recipient.

In practice, a lipophilic reversible redox mediator, capable of crossing the cell membrane, is used to capture the electrons from the components of the respiratory chain and the cytosolic dehydrogenases. The reduced form of the mediator shuttles the electrons to the extracellular medium where ferricyanide, the terminal electron recipient, is present. Reduction of ferricyanide by the lipophilic mediator regenerates the oxidized form of the mediator and prepares the molecule for another cycle. The generated ferrocyanide is then quantitated using cyclic biamperometry and its amount is related to the extent of cell respiration.

In this study, three lipophilic redox mediators including 2,6-dichlorophenolindophenol, menadione (vitamin K3) and N,N,N',N'-tetramethyl-p-phenylenediamine were evaluated. The mediators were compared with each other under their optimal conditions and 2,6-dichlorophenolindophenol was selected for further studies.

To demonstrate the cytotoxicity assessment, three well-characterized toxicants including benzalkonium chloride, sodium dodecylsulfate and hydrogen peroxide were used and it has been shown that the electrochemical assay is able to detect the cytotoxicity of the test chemicals near their cytotoxicity thresholds reported in the literature.

Although conceptually similar assays using spectrophotometric or fixed potential techniques have been used for the measurement of respiratory activity of prokaryotes and eukaryotes, quantitating the extent of respiratory activity in mammalian cells using non-fixed-voltage biamperometry for cytotoxicity/viability assessment purposes is exclusive to this study.

In Chapter 3, culturing human corneal epithelial cells on growth inserts, in an attempt to construct 3D corneal tissues, was discussed. The culture growth was monitored by electrochemical measurement of the trans-epithelial resistance. Although in some cases very high trans-epithelial resistance values (up to 2260 $\Omega.\text{cm}^2$) were obtained after 78 days of culture growth, the stratified cell layers were very unstable and consequently cytotoxicity studies could not be performed on these constructs. Preliminary data, however, have shown that the combination of the respiratory assay and the TER measurements can provide useful information on the state of tight junctions after exposure to test chemicals. Any decrease in both the extent of respiratory activities and TER indicates the loss of viability; however, a decrease in TER without an accompanying decline in respiratory activities can be attributed to disruption of tight junctions, provided that control experiments are performed to exclude other possible interfering factors. TER measurements have been used for over two decades for evaluation of the integrity of various tissues. To deduce useful information, the TER measurements are commonly combined with other cytotoxicity/viability assays (e.g. fluorescein permeability test and MTT). In this thesis, however, combination of two electrochemical assays for ocular cytotoxicity assessment has been introduced which can form a separate testing level in a tiered-testing approach for cytotoxicity assessment. As it stands, the presented electrochemical approach is not complete; however, the measures required to improve the TER assay in future studies are discussed in the next section.

In Chapter 4, differential pulse biamperometry was introduced. This electrochemical method involves application of the differential pulse waveforms to the biamperometric electrochemical cells. It has been shown that the analytical response of this method displays linear relationships with various experimental parameters including concentration of the limiting reactant, inverse square root of the pulse width and the fraction $(1-\sigma)/(1+\sigma)$ (see Equation 4.2). It has been also shown that in a solution containing only one reversible redox couple where one form is present in great excess, the method is more sensitive than differential pulse voltammetry. In addition, the absence of a reference electrode in the electrochemical cell will facilitate miniaturization of the electrochemical cell and

reduces the manufacturing costs. Therefore, the method can potentially be employed in construction of single-use measurement chips.

In conclusion, the work presented in this thesis, when combined with other currently-available tests, could benefit industry by lowering the expenses of ocular cytotoxicity assessment. In addition, development of *in vitro* alternative tests such as the one presented in this thesis, would result in the laboratory tests becoming more ethically acceptable by reducing the number of animal tests and their harshness.

5.2 Suggestions for Future Research

To improve the performance of the electrochemical cytotoxicity assay, differential pulse biamperometry, instead of cyclic biamperometry, can be used for the measurement of respiratory activity. The higher sensitivity offered by DPB can, in principle, reduce the time required for the assay, because any change in the concentration of ferrocyanide can be determined more accurately.

Regarding the TER measurement assay, since the constructed corneal tissues are not destined to undergo permeability tests (e.g. the fluorescein permeability test), they should firmly adhere to the support. To achieve this, various adhesion proteins should be tested. In addition, during the growth period, the least number of TER measurements should be made to minimize the disruption induced by the measurement procedure. Furthermore, control tests must be performed to make sure that the respiratory assay substances (i.e. ferricyanide, ferrocyanide and the mediator) do not damage the tight junctions at the concentrations used in the assay. This way, the two assays can be combined to obtain complementary data regarding the cytotoxicity assessment.

After construction of proper 3D corneal tissues and combining the results from the two assays, a wide variety of chemicals must be tested and the results should be compared with the those obtained from the currently-available assays. Based on these results, the response from this method should be classified so that new test chemicals can be categorized based on their cytotoxicity.

New applications for differential pulse biamperometry can be defined. For example, the method can be employed in an enzyme-linked immunoassay when the product(s) of the enzymatic reaction is quantitated.

While searching in the literature, one quickly notices that there are numerous electrochemical amperometric immunoassays that use an amplification method (e.g. enzymatic amplification) to either detect a single electroactive analyte or use a redox couple to further

amplify the signal with redox cycling. The electroanalytical methods of detection in the former cases are often one of the pulse-based methods (e.g. differential pulse or square wave) and in the latter cases are fixed-voltage methods. For example, Pei *et al.* (2013) have used cyclic voltammetry to detect the free prostate-specic antigen using electroactive silver-mediated poly(amidoamine) dendrimer nanostructures as molecular tags.[147] Or, Tang *et al.* (2013) have used differential pulse voltammetry for detection of low-abundance proteins coupling with nanocatalyst-based redox cycling.[148]

In principle, DPB can be employed to enhance the performance of these assays. If a redox couple is used in the assay together with a fixed-voltage amperometric detection method, DPB can be directly applied to the assay with no modification to the assay. However, when only one redox active analyte exists, an external redox active molecule can be added to the assay medium to undergo the opposing reaction. For example, levodopa (3,4-dihydroxyphenylalanine) and permanganate, can generate biamperometric signal where the former reacts at the surface of the cathode and the latter at the anode. The advantage of employing DPB is that absence of the reference electrode allows low-cost electrodes (e.g. single-use carbon screen-printed) to be used for detection of the analyte without impairing the quantitation limit.

Appendix A

Daily Raw Data for Trans-epithelial Resistance Measurement

During the growth of corneal inserts, the average trans-epithelial resistance in the air-lifted samples exhibited a large standard deviation mainly due to instability of the constructs. In some cases the whole or a portion of the corneal construct was floating in the solution, after addition of the phosphate buffer. This resulted in a large decline in the trans-epithelial resistance for the tested insert in that particular day. The following table displays the unmodified trans-epithelial resistance values measured during the growth of the inserts. To obtain the normalized resistance (in $\Omega.cm^2$ unit) the values must be multiplied by 1.131.

Table A.1: Unmodified trans-epithelial resistance of the corneal constructs (in Ω) in the second trial

Measurement time after seeding (h)	48	100	144	191	264.5	359.5	433	507	582
Non-seeded insert	167	164	167	168	169	170	170	170	180
Non-seeded insert	169	168	171	167	171	172	172	169	183
Seeded non-airlifted	182	215	218	325	335	364	332	359	335
Seeded non-airlifted	185	204	225	295	349	394	368	357	346
Seeded non-airlifted	181	208	231	318	342	380	334	358	355
Seeded airlifted # 1	182	200	230	245	262	372	352	311	375
Seeded airlifted # 2	180	205	227	293	345	370	310	307	391
Seeded airlifted # 3	180	200	219	378	401	377	275	345	512
Seeded airlifted # 4	185	208	221	332	375	381	356	311	410
Seeded airlifted # 5	184	203	222	292	376	390	323	344	408
Seeded airlifted # 6	174	198	230	370	415	408	325	330	436
Seeded airlifted # 7	177	200	228	250	358	409	297	313	402
Seeded airlifted # 8	178	196	212	212	249	341	349	363	355
Seeded airlifted # 9	176	206	230	320	396	410	328	342	405
Seeded airlifted # 10	178	200	219	320	353	347	298	309	418
Seeded airlifted # 11	190	210	227	329	409	357	298	404	442
Seeded airlifted # 12	189	197	220	311	365	402	310	318	422
Seeded airlifted # 13	193	200	224	242	264	333	328	320	370
Seeded airlifted # 14	180	196	219	260	301	378	299	328	380
Seeded airlifted # 15	177	199	208	246	297	331	340	397	371
Seeded airlifted # 16	192	206	221	240	282	371	319	309	381
Seeded airlifted # 17	178	198	223	238	270	312	351	401	375
Seeded airlifted # 18	183	202	205	238	252	294	295	375	391
Seeded airlifted # 19	181	197	230	235	255	368	329	304	358

Table A.1: Continue

Measurement time after seeding (h)	647	722	796	868	934	1005.5	1077.5	1148.5	1220.5
Non-seeded insert	172	169	169	163	171	171	169	170	170
Non-seeded insert	175	173	172	174	172	173	172	167	174
Seeded non-airlifted	368	349	452	355	367	361	349	392	354
Seeded non-airlifted	358	C	–	–	–	–	–	–	–
Seeded non-airlifted	378	C	–	–	–	–	–	–	–
Seeded airlifted # 1	373	395	469	465	537	638	465	559	493
Seeded airlifted # 2	383	378	608	528	542	632	459	537	603
Seeded airlifted # 3	415	385	584	505	520	678	576	770	660
Seeded airlifted # 4	404	382	552	509	483	622	570	672	618
Seeded airlifted # 5	373	390	528	476	544	575	484	628	538
Seeded airlifted # 6	442	385	570	490	499	642	554	670	663
Seeded airlifted # 7	407	415	505	546	460	586	478	581	535
Seeded airlifted # 8	344	338	430	461	449	508	428	542	642
Seeded airlifted # 9	407	405	773	418	533	533	496	563	602
Seeded airlifted # 10	452	445	595	533	497	605	503	645	683
Seeded airlifted # 11	418	387	608	494	501	595	361	688	684
Seeded airlifted # 12	432	414	599	484	400	542	463	712	880
Seeded airlifted # 13	340	331	445	403	392	442	390	535	562
Seeded airlifted # 14	397	381	505	599	338	418	401	513	523
Seeded airlifted # 15	328	402	421	333	380	435	407	498	510
Seeded airlifted # 16	369	370	459	418	361	504	465	564	535
Seeded airlifted # 17	334	494	548	412	373	470	360	585	518
Seeded airlifted # 18	444	388	612	466	420	618	542	753	795
Seeded airlifted # 19	C	–	–	–	–	–	–	–	–

C: Contaminated

Table A.1: Continue

Measurement time after seeding (h)	1293.5	1365	1437.5	1509.5	1580.5	1654.5	1730.5	1797.5	1869.5	
Non-seeded insert	165	173	169	175	171	172	171	165	173	
Non-seeded insert	164	168	171	172	172	170	171	168	175	C
Seeded non-airlifted	383	438	362	428	425	420	525	340	387	
Seeded non-airlifted	–	–	–	–	–	–	–	–	–	
Seeded non-airlifted	–	–	–	–	–	–	–	–	–	
Seeded airlifted # 1	M	–	–	–	–	–	–	–	–	
Seeded airlifted # 2	565	565	479	690	592	742	842	429	420	
Seeded airlifted # 3	624	612	570	600	827	688	730	499	772	
Seeded airlifted # 4	581	605	556	674	784	657	720	47	678	
Seeded airlifted # 5	501	522	530	601	670	651	718	452	501	
Seeded airlifted # 6	620	620	573	630	611	678	C	–	–	
Seeded airlifted # 7	480	585	475	576	628	560	C	–	–	
Seeded airlifted # 8	523	658	470	679	546	630	575	449	520	
Seeded airlifted # 9	563	654	525	607	728	637	576	507	570	
Seeded airlifted # 10	M	–	–	–	–	–	–	–	–	
Seeded airlifted # 11	551	556	595	625	730	684	512	596	740	
Seeded airlifted # 12	680	772	660	1120	1130	1140	1054	1112	1625	
Seeded airlifted # 13	597	585	599	865	807	900	780	1432	1365	M
Seeded airlifted # 14	498	490	478	280	520	400	448	454	700	
Seeded airlifted # 15	550	579	605	384	598	554	C	–	–	
Seeded airlifted # 16	501	556	433	300	538	486	454	491	550	
Seeded airlifted # 17	555	490	450	630	573	498	580	478	592	
Seeded airlifted # 18	860	845	C	–	–	–	–	–	–	
Seeded airlifted # 19	–	–	–	–	–	–	–	–	–	

C: Contaminated
M: The insert was taken for confocal microscopy analysis.

Appendix B

Staining HCECs with ZO-1 and Counter Staining with Hoechst

To be able to get a visual proof for formation of tight junctions in human corneal epithelial cell line a monolayer culture of the corresponding cell line was prepared in a culture flask. After reaching the confluence the bottom of the flask was gridded in 5-mm square shapes and cut with a glass cutter (Figure B.1).

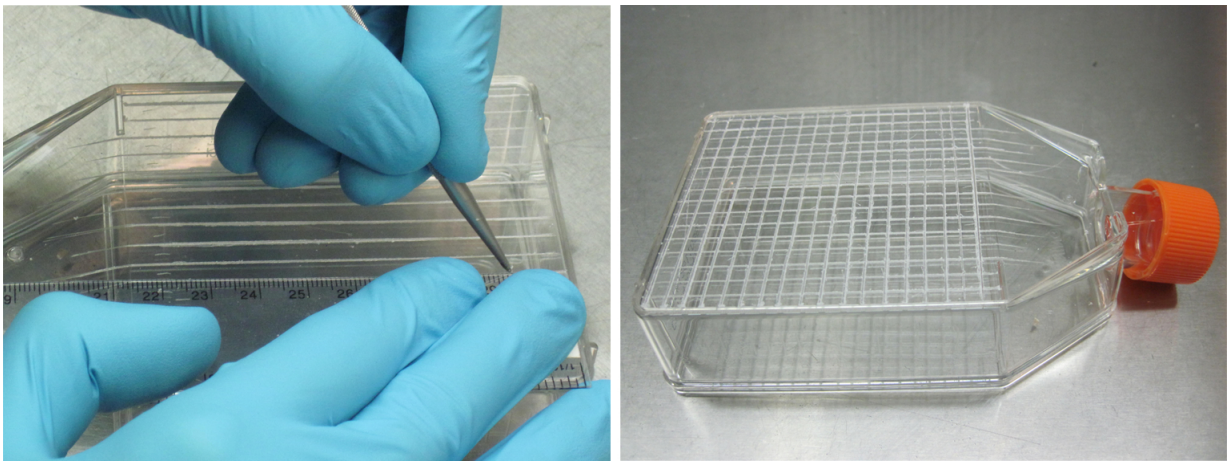

Figure B.1: Making gridlines and cutting the culture flask with a glass cutter.

After cutting the pieces out, the squares (> 160 pieces) were placed in 96-well plates containing the original growth medium for 2 h. (Figure B.2) Then, the cells were rinsed in 1X PBS three times and were exposed to various concentrations of BAC (0, 0.000100,

0.00100, 0.0100 and 0.100%) in 1X PBS for 30 min after which the samples were rinsed three times with 1X PBS and were exposed to various fixatives at different temperatures for 30 min as shown below:

(1) Pure ethanol at –20 °C
(2) Pure ethanol at RT
(3) 50% ethanol / 50% acetone at – 20 °C
(4) 50% ethanol / 50% acetone at RT
(5) 0.50% formaldehyde at RT
(6) 0.50% formaldehyde at +4 °C
(7) 4.0% formaldehyde at RT
(8) 4.0% formaldehyde at +4 °C

After fixation, the cells samples were rinsed three times with 1X PBS and incubated in 1X PBS containing 2% BSA for 15 min at room temperature. Then, without rinsing, the medium was replaced with 1X PBS containing 5 μg/mL ZO-1 and then, the samples were incubated at 37 °C for an hour. (Figure B.2) After this incubation the samples were rinsed with 1X PBS and counter stained with 0.50 μg/mL of Hoechst 33258 for 10 min at room temperature. Finally the cell samples were rinsed three times with PBS and were placed in 1X PBS ready for investigation under confocal microscopy. Figure B.3 shows the results.

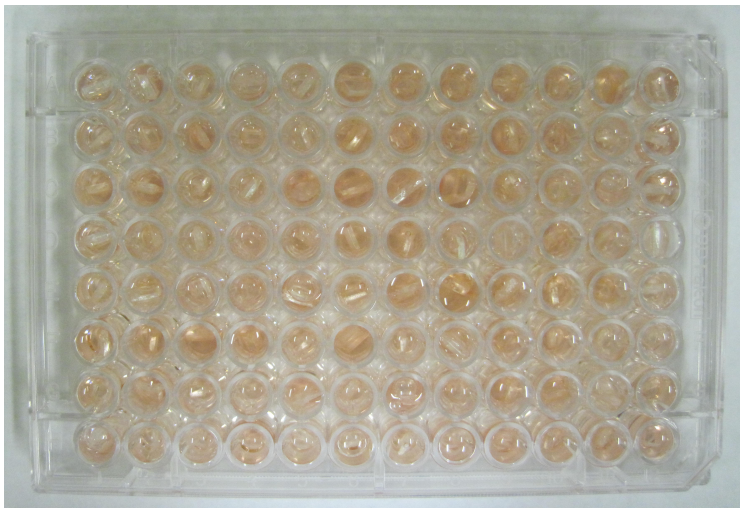

Figure B.2: Placement of the cell-carrying squares in 96-well plates for staining.

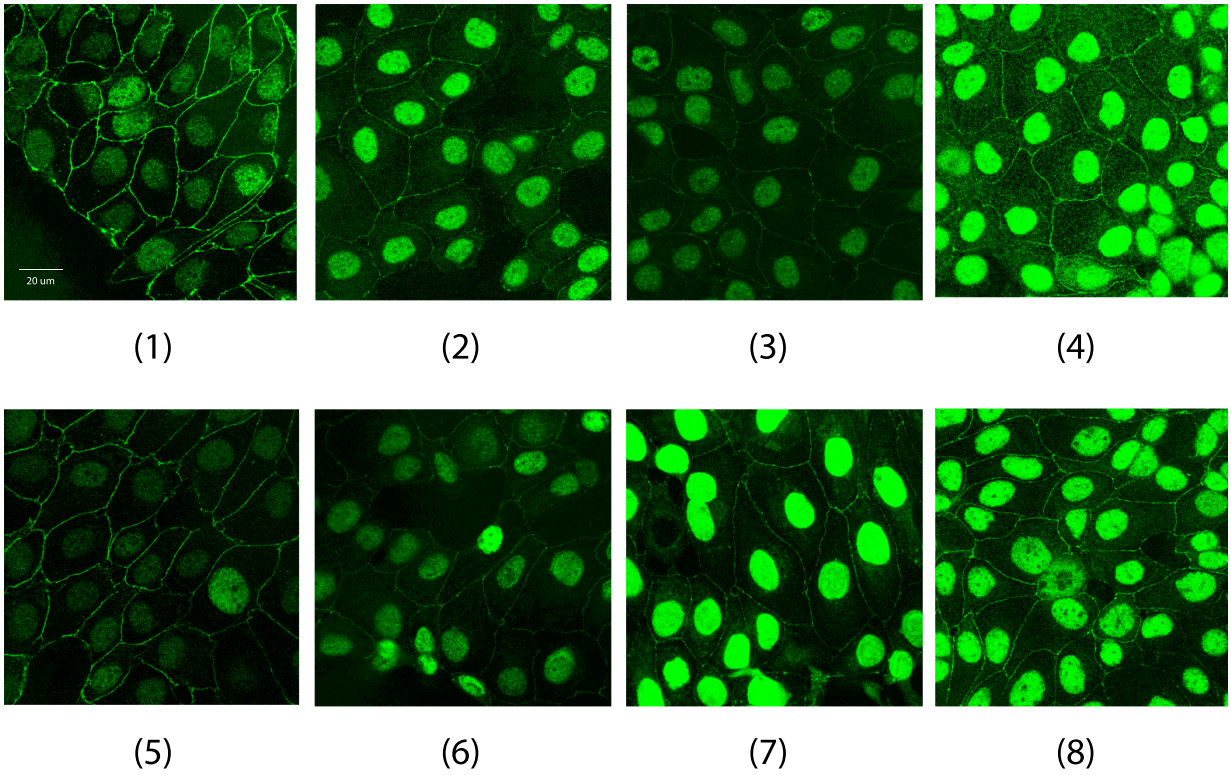

Figure B.3: Using various fixatives HCEC monolayers were stained ZO-1 and Hoechst. Numbers 1 to 8 indicate the corresponding numbers for the fixatives tabulated on page 90. To facilitate comparison of the results, the channel for blue light passage has been turned off so only the green fluorescent emitted light is observed.

The results showed that the best fixative for this cell line is 0.50% formaldehyde at room temperature or pure methanol at –20 °C.

Appendix C

Time Constant Calculations of Differential Pulse Biamperometry in Microsoft Excel 2010

To approximately calculate the time constant, RC, of the electrode-solution interface after application of a pulse in differential pulse biamperometry the "Solver" add-in for Microsoft Excel 2010 was used. Since the pulse width had been set to 500 ms and the voltage reading frequency of the data acquisition board was 1000 Hz, for every single pulse within the scan range (+ 400 to – 400 mV) 500 data points were cut and pasted onto a spreadsheet starting from the very last value before application of the pulse. (Figure C.1)

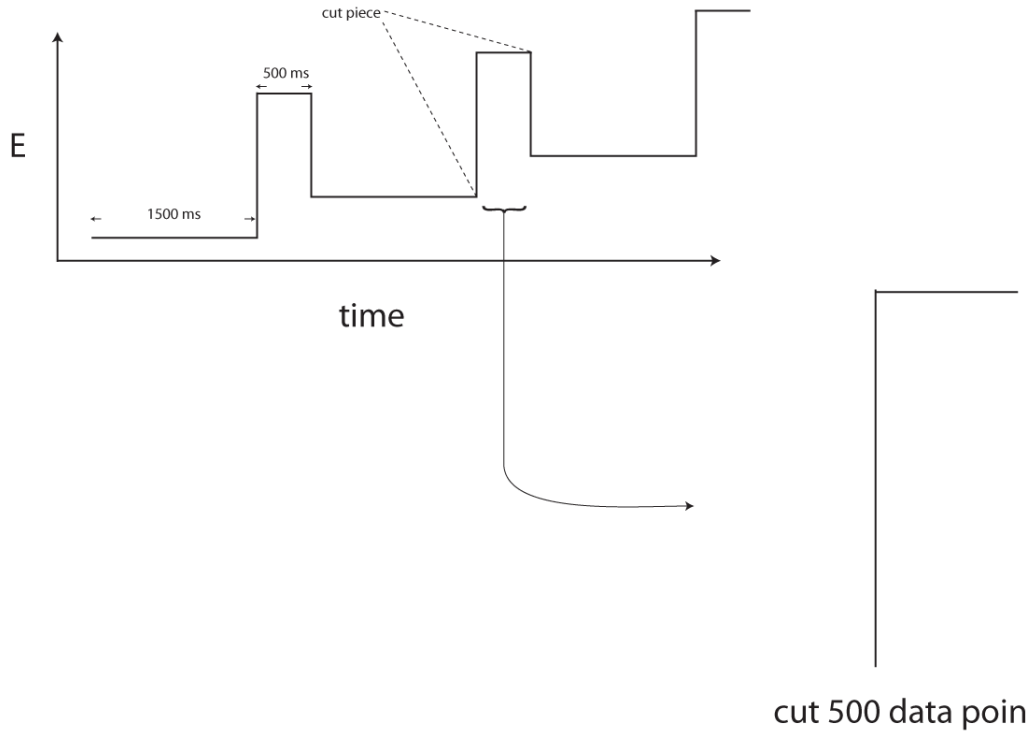

Figure C.1: 500 data points were cut for each pulse starting from the value just before application of the pulse.

In the next step, the absolute value of the difference between the voltage values and the base voltage was taken and the resulting series was normalized between 0 and 1 so that the base voltage was assigned the value of 0 and the maximal value of the voltage during the pulse was set to 1. In the next column the theoretical voltage based on different RC values were calculated using the following equation.

$$V_c = V_0(1 - e^{-t/RC}) \tag{C.1}$$

where V_0 is the applied voltage, V_c is the voltage across the capacitor and t is the time after application of the pulse. The RC value that results in the least sum of squared difference between the theoretical and experimental values was recorded as the RC for the electrode-solution interface at that base voltage. (Figure C.1)

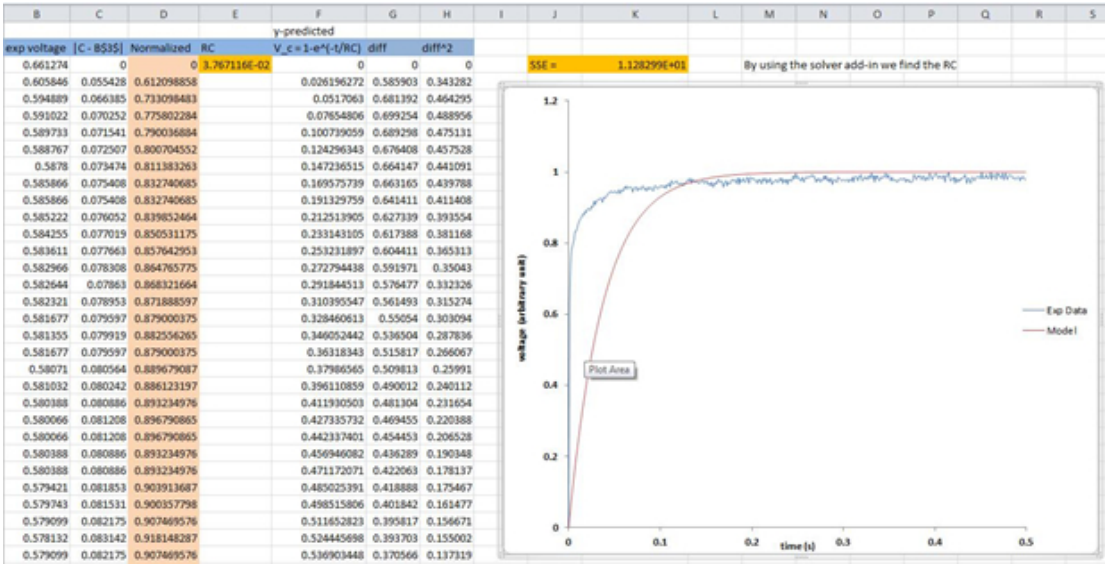

	B	C	D	E	F	G	H	I	J	K	L	M	N	O	P	Q	R	S
					y-predicted													
	exp voltage	|C - B3|	Normalized	RC	V_c = 1-e^(-t/RC)	diff	diff^2											
	0.661274	0	0	3.767116E-02	0	0	0		SSE =	1.128299E+01		By using the solver add-in we find the RC						
	0.605846	0.055428	0.612098858		0.026196272	0.585903	0.343282											
	0.594889	0.066385	0.733098483		0.0517063	0.681392	0.464295											
	0.591022	0.070252	0.775802284		0.07654806	0.699254	0.488956											
	0.589733	0.071541	0.790036884		0.100739059	0.689298	0.475131											
	0.588767	0.072507	0.800704552		0.124296343	0.676408	0.457528											
	0.5878	0.073474	0.811383263		0.147236515	0.664147	0.441091											
	0.585866	0.075408	0.832740685		0.169575739	0.663165	0.439788											
	0.585866	0.075408	0.832740685		0.191329759	0.641411	0.411408											
	0.585222	0.076052	0.839852464		0.212513905	0.627339	0.393554											
	0.584255	0.077019	0.850531175		0.233143105	0.617388	0.381168											
	0.583611	0.077663	0.857642953		0.253231897	0.604411	0.365313											
	0.582966	0.078308	0.864765775		0.272794438	0.591971	0.35043											
	0.582644	0.07863	0.868321664		0.291844513	0.576477	0.332326											
	0.582321	0.078953	0.871888597		0.310395547	0.561493	0.315274											
	0.581677	0.079597	0.879000375		0.328460613	0.55054	0.303094											
	0.581355	0.079919	0.882556265		0.346052442	0.536504	0.287836											
	0.581677	0.079597	0.879000375		0.36318343	0.515817	0.266067											
	0.58071	0.080564	0.889679087		0.37986565	0.509813	0.25991											
	0.581032	0.080242	0.886123197		0.396110859	0.490012	0.240112											
	0.580388	0.080886	0.893234976		0.411930503	0.481304	0.231654											
	0.580066	0.081208	0.896790865		0.427335732	0.469455	0.220388											
	0.580066	0.081208	0.896790865		0.442337401	0.454453	0.206528											
	0.580388	0.080886	0.893234976		0.456946082	0.436289	0.190348											
	0.580388	0.080886	0.893234976		0.471172071	0.422063	0.178137											
	0.579421	0.081853	0.903913687		0.485025391	0.418888	0.175467											
	0.579743	0.081531	0.900357798		0.498515806	0.401842	0.161477											
	0.579099	0.082175	0.907469576		0.511652823	0.395817	0.156671											
	0.578132	0.083142	0.918148287		0.524445698	0.393703	0.155002											
	0.579099	0.082175	0.907469576		0.536903448	0.370566	0.137319											

Figure C.2: Rearrangement and normalizing voltage values in a single pulse.

After rearrangement and normalizing the voltage values on the spreadsheet we use the Solver Add-in to find the optimal RC. To do this, in the "Solver Parameter" dialogue box the cell in which sum of squared difference (in this case K3) is calculated is set to Min by changing the variable of RC (in this case cell E3) between 0.0000001 and 0.01. Before pressing the OK button we make sure that "Evolutionary" option is selected in the"Select a Solving Method" dropbox. This option takes a longer time to calculate the Min value but gives a more accurate result. (Figure C.1)

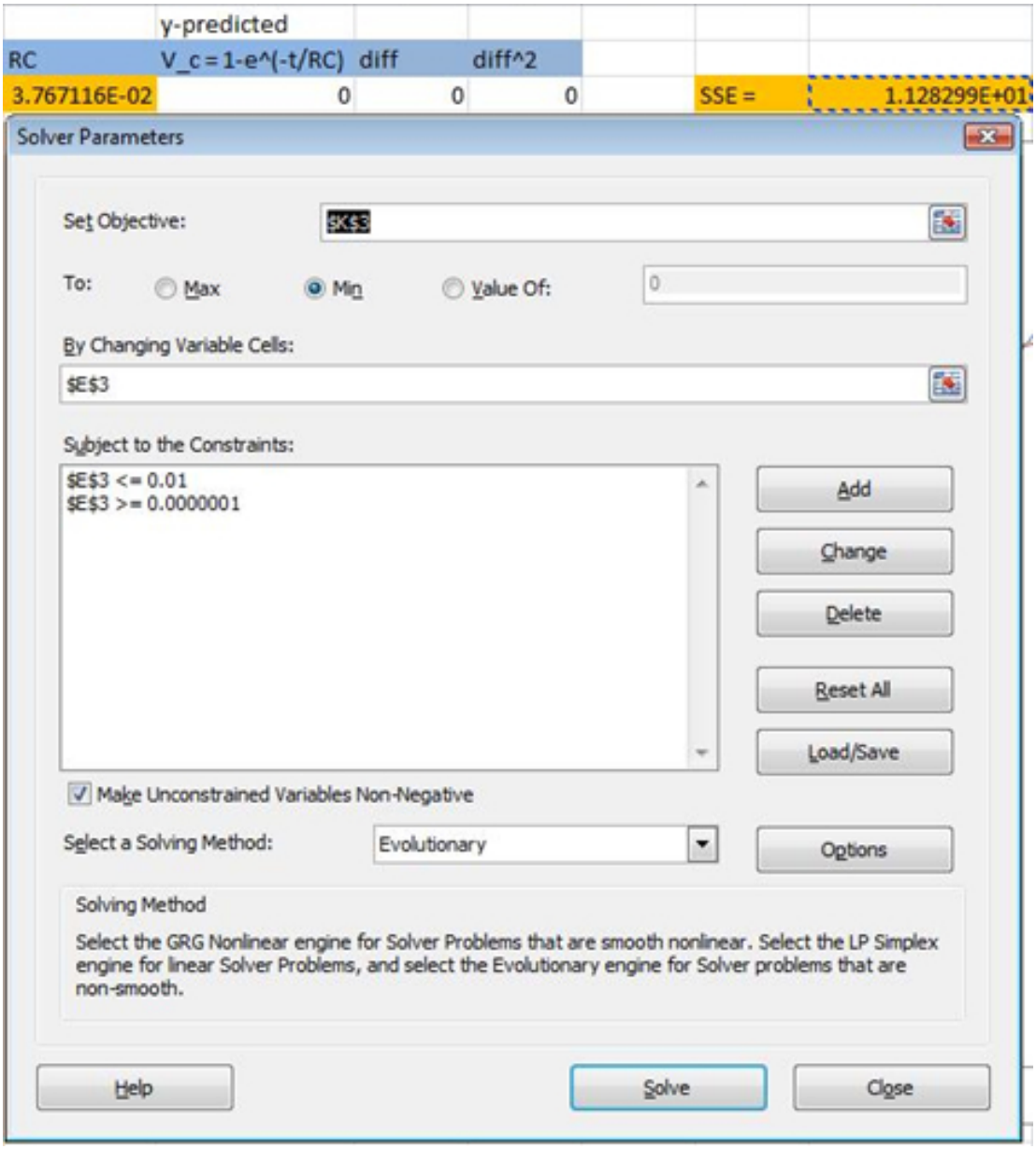

Figure C.3: Solver Parameters dialogue box

After calculating the Min SSE the corresponding RC value is saved in the corresponding cell. (Figure C.1)

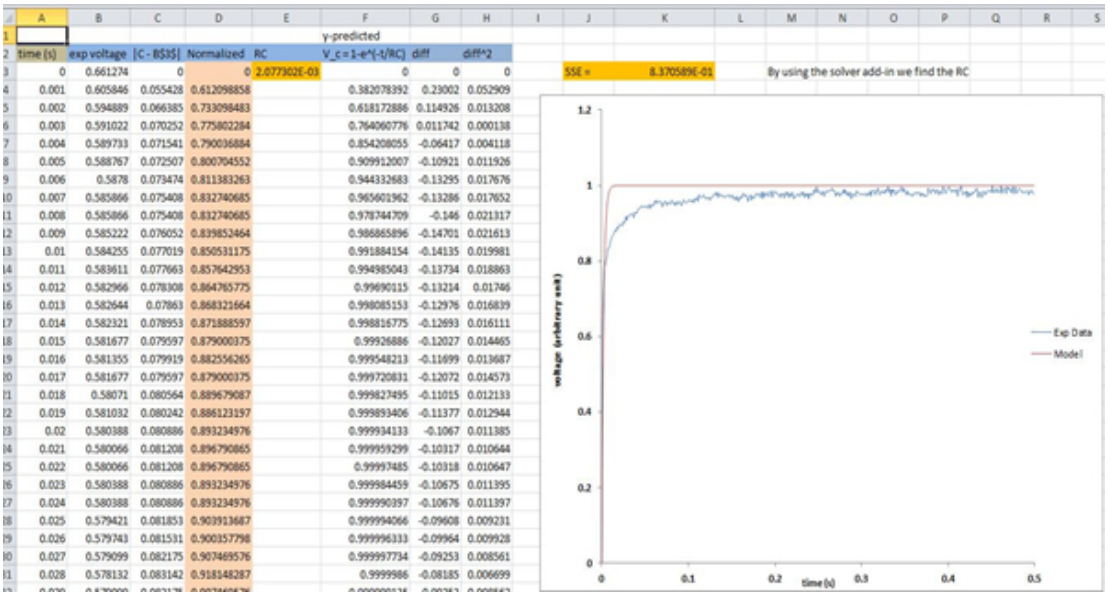

	A	B	C	D	E	F	G	H
1						y-predicted		
2	time (s)	exp voltage	|C - B3|	Normalized	RC	V_c = 1-e^(-t/RC)	diff	diff^2
3	0	0.661274	0	0	2.077302E-03	0	0	0
4	0.001	0.605846	0.055428	0.612098858		0.382078392	0.23002	0.052909
5	0.002	0.594889	0.066385	0.733098483		0.618172886	0.114926	0.013208
6	0.003	0.591022	0.070252	0.775802284		0.764060776	0.011742	0.000138
7	0.004	0.589733	0.071541	0.790036884		0.854208055	-0.06417	0.004118
8	0.005	0.588767	0.072507	0.800704552		0.909912007	-0.10921	0.011926
9	0.006	0.5878	0.073474	0.811383263		0.944332683	-0.13295	0.017676
10	0.007	0.585866	0.075408	0.832740685		0.965601962	-0.13286	0.017652
11	0.008	0.585866	0.075408	0.832740685		0.978744709	-0.146	0.021317
12	0.009	0.585222	0.076052	0.839852464		0.986865896	-0.14701	0.021613
13	0.01	0.584255	0.077019	0.850531175		0.991884154	-0.14135	0.019981
14	0.011	0.583611	0.077663	0.857642953		0.994985043	-0.13734	0.018863
15	0.012	0.582966	0.078308	0.864765775		0.99690115	-0.13214	0.01746
16	0.013	0.582644	0.07863	0.868321664		0.998085153	-0.12976	0.016839
17	0.014	0.582321	0.078953	0.871888597		0.998816775	-0.12693	0.016111
18	0.015	0.581677	0.079597	0.879000375		0.99926886	-0.12027	0.014465
19	0.016	0.581355	0.079919	0.882556265		0.999548213	-0.11699	0.013687
20	0.017	0.581677	0.079597	0.879000375		0.999720831	-0.12072	0.014573
21	0.018	0.58071	0.080564	0.889679087		0.999827495	-0.11015	0.012133
22	0.019	0.581032	0.080242	0.886123197		0.999893406	-0.11377	0.012944
23	0.02	0.580388	0.080886	0.893234976		0.999934133	-0.1067	0.011385
24	0.021	0.580066	0.081208	0.896790865		0.999959299	-0.10317	0.010644
25	0.022	0.580066	0.081208	0.896790865		0.99997485	-0.10318	0.010647
26	0.023	0.580388	0.080886	0.893234976		0.999984459	-0.10675	0.011395
27	0.024	0.580388	0.080886	0.893234976		0.999990397	-0.10676	0.011397
28	0.025	0.579421	0.081853	0.903913687		0.999994066	-0.09608	0.009231
29	0.026	0.579743	0.081531	0.900357798		0.999996333	-0.09964	0.009928
30	0.027	0.579099	0.082175	0.907469576		0.999997734	-0.09253	0.008561
31	0.028	0.578132	0.083142	0.918148287		0.9999986	-0.08185	0.006699

	J	K	L	M	N	O	P	Q	R	S
3	SSE =	8.370589E-01		By using the solver add-in we find the RC						

Figure C.4: RC value resulting in the minimal squared difference for a single pulse.

References

[1] Kissinger, P. T.; Heinman, W. R. *Laboratory techniques in electroanalytical chemistry*, 2nd ed.; Marcel Dekker, Inc.: New York, 1996.

[2] Bard, A. J.; Faulkner, L. R. *Electrochemical methods fundamentals and applications*, 2nd ed.; Wiley: Hoboken, 2001.

[3] Lubert, K. H.; Kalcher, K. *Electroanalysis* **2010**, *22*, 1937–1946.

[4] Oja, S. M.; Wood, M.; Zhang, B. *Anal. Chem.* **2013**, *22*, 473–486.

[5] Kimmel, D. W.; LeBlanc, G. M. M. E.; Cliffel, D. E. *Anal. Chem.* **2012**, *84*, 685–707.

[6] Tutulea, M. D.; Cretescu, I.; Sibiescu, D.; Stan, C. *Environ. Eng. Manag. J.* **2012**, *11*, 463–470.

[7] Yantasee, W.; Lin, Y.; Pryxell, G. E. In *Environmental applications of nanomaterials*, 2nd ed.; Fryxell, G. E., Cao, G., Eds.; World Scientific, 2012; pp 523–559.

[8] Kirchev, A. Z.; Diem, B.; Mattera, F. Miniature reference electrode with a proton exchange membrane. Patent WO 2012007660 A1 20120119, 2012.

[9] Ahmad, R. A.; Alva, S. T.; Nur, A.; Shuib, M. R.; Yahaya, M. F. Reusable miniaturized reference electrode. Patent WO 2011155815 A1 20111215, 2011.

[10] Blauw, M.; Gonzalo Ruiz, J.; Crego Calama, M.; Brongersma, S. H. Microfabricated liquid-junction reference electrode for miniaturized electrochemical sensors as part of microfluidic system. Patent US 20110192720 A1 20110811, 2011.

[11] Huber, B.; Roling, B. *Elecim. Acta* **2011**, *56*, 6569–6572.

[12] Weingarth, D.; Foelske-Schmitz, A.; Wokaun, A.; Koetz, R. *Electrochem. Commun.* **2012**, *18*, 116–118.

[13] Ruch, P. W.; Cericola, D.; Hahn, M.; Koetz, R.; Wokaun, A. *Electroanal. Chem.* **2009**, *636*, 128–131.

[14] Rahimi, M.; Mikkelsen, S. R. *Anal. Chem.* **2010**, *82*, 1779–1785.

[15] Foulk, C. W.; Bawden, A. T. *J. Am. Chem. Soc.* **1926**, *48*, 2045–2051.

[16] Vorlicek, J.; Vydra, F. *Talanta* **1965**, *12*, 671–676.

[17] Kekedy, L.; Makkay, F. *Stud. U. Babes-Bol. Che.* **1970**, *15*, 129–133.

[18] Montgomery, F. C.; Larson, R. W.; Richardson, W. H. *Anal. Chem.* **1973**, *45*, 2258–2260.

[19] Shukla, U.; Prasad, B. B. *Chem. Anal. (Warsaw)* **1988**, *33*, 639–642.

[20] Fatibello-Filho, O.; Capelato, M. D.; Calafatti, S. A. *Analyst* **1995**, *120*, 2407–2412.

[21] Nair, P. R.; Xavier, M.; Aggarwal, S. K. *Radiochim. Acta.* **2009**, *97*, 419–422.

[22] Evans, D. H. *J. Chem. Educ.* **1968**, *45*, 88–90.

[23] Tougas, T. P.; Jannetti, J. M.; Collier, W. G. *Anal. Chem.* **1985**, *57*, 1377–1381.

[24] Hill, B. Accu-Chek Advantage: Electrochemistry for Diabetes Management. http://www.currentseparations.com/issues/21-2/cs21-2c.pdf, Accessed: Nov 27, 2012.

[25] Wang, Y.; Yao, G.; Zhu, P.; Hu, X.; Xu, Q.; Yang, C. *Talanta* **2010**, *82*, 1500–1504.

[26] Kamimori, T.; Nagai, J.; Mizuhashi, M. *Sol. Energ. Mater.* **1987**, *16*, 27–38.

[27] Harris, D. C. *Quantitative Chemical Analysis*, 7th ed.; W. H. Freeman and Company: New York, 2007.

[28] Rahimi, M.; Mikkelsen, S. R. *Anal. Chem.* **2011**, *83*, 7555–7559.

[29] Sanderson, D. G.; Anderson, L. B. *Anal. Chem.* **1985**, *57*, 2388–2393.

[30] Elsholz, B.; Worl, R.; Blohm, L.; Albers, J.; Feucht, T.; Grunwald, T.; Jurgen, B.; Schweder, T.; Hintsche, R. *Anal. Chem.* **2006**, *78*, 4794–4802.

[31] Morita, M.; Niwa, O.; Horiuchi, T. *Electrochim. Acta* **1997**, *42*, 3177–3183.

[32] Kim, S. K.; Hesketh, P. J.; Li, C.; Thomas, J. H.; Halsall, H. B.; Heineman, W. R. *Biosens. Bioelectron.* **2004**, *20*, 887–894.

[33] Goluch, E. D.; Wolfrum, B.; Singh, P. S.; Zevenbergen, M. A.; Lemay, S. G. *Anal. Bioanal. Chem.* **2009**, *394*, 447–456.

[34] Nishizawa, M.; Uchida, I. *Electrochim. Acta* **1999**, *44*, 3629–3637.

[35] Berger, P. R. *Proc. SPIE* **2001**, *4258*, 198–207.

[36] Chidsey, C. E.; Feldman, B. J.; Lundgren, C.; Murray, R. W. *Anal. Chem.* **1986**, *58*, 601–607.

[37] Boden, N.; Bushby, R. J.; Clements, J.; Movaghar, B. *J. Mater. Chem.* **1999**, *9*, 2081– 2086.

[38] Wu, J.; Zunzhong, Y.; Yibin, Y.; Feng, J. *Electroanalysis* **2007**, *19*, 1939–1943.

[39] Li, L. J.; Chen, Q. F.; Cheng, H.; Yu, L. B.; Wu, J. L. *Chin. Chem. Lett.* **2008**, *19*, 703–706.

[40] Ertl, P.; Unterladstaetter, B.; Bayer, K.; Mikkelsen, S. R. *Anal. Chem.* **2000**, *72*, 4949–4956.

[41] Ertl, P.; Robello, E.; Battaglini, F.; Mikkelsen, S. R. *Anal. Chem.* **2000**, *72*, 4957–4964.

[42] Ding, T.; Schmid, R. D. *Anal. Chim. Acta.* **1990**, *234*, 247–251.

[43] Ertl, P.; Mikkelsen, S. R. *Anal. Chem.* **2001**, *73*, 4241–4248.

[44] Mann, T. S.; Mikkelsen, S. R. *Anal. Chem.* **2008**, *80*, 843–848.

[45] Voet, D.; Voet, J. G. *Biochemistry*, 2nd ed.; John Wiley & Sons, Inc.: New York, 1995.

[46] Atlas, R. M. *Principles of microbiology*, 2nd ed.; Wm. C. Brown: Dubuque, 1997.

[47] Karasinski, J.; White, L.; Zhang, Y.; Wang, E.; Andreescu, S.; Sadik, O. A.; Lavine, B. K.; Vora, M. *Biosens. Bioelectron.* **2007**, *22*, 2643–2649.

[48] Nakamura, H.; Suzuki, K.; Ishikuro, H.; Kinoshita, S.; Koizumi, R.; Okuma, S.; Gotoh, M.; Karube, I. *Talanta* **2007**, *72*, 210–216.

[49] Pyle, B. H.; Broadaway, S. C.; McFeters, G. A. *Appl. Environ. Microbiol.* **1995**, *61*, 2614–2619.

[50] Jahn, B.; Martin, E.; Stueben, A.; Bhakdi, S. *J. Clin. Microbiol.* **1995**, *33*, 661–667.

[51] Baker, C. N.; Banerjee, S. N.; Tenover, F. C. *J. Clin. Microbiol.* **1994**, *32*, 1261–1267.

[52] Tsai, H.; Tsai, S.; Deng, H.; Bor Fuh, C. *Electroanalysis* **2013**, *25*, 1005–1009.

[53] Rabinowitz, J. D.; Vacchino, J. F.; Beeson, C.; McConnell, H. M. *J. Am. Chem. Soc.* **1998**, *120*, 2464–2473.

[54] Barile, F. A. *J. Pharmacol. Toxicol.* **2010**, *61*, 136–145.

[55] Draize, J. H.; Woodard, G.; Calvery, H. O. *J. Pharmacol.* **1944**, *82*, 377–390.

[56] Eye Irritancy by Research Defence Society. http://web.archive.org/web/20070928111042/http://www.rds-online.org.uk/pages/page.asp?i_ToolbarID=4&i_PageID=149, Accessed: June 8, 2013.

[57] Bosshard, E. *Food Chem. Toxicol.* **1985**, *23*, 149–154.

[58] Calabrese, E. J. *Principles of Animal Extrapolation*; Wiley: New York, 1984.

[59] H., S. G. D. L. K. J. N. J. M. L. M. *J. Clin. Epidemiol.* **1985**, *49*, 711–717.

[60] Hackett, R. B.; Stern, M. E. In *Dermal and Ocular Toxicology Fundamentals and Methods*; Hobson, D. W., Ed.; CRC Press: Boca Raton, 1991; pp 607–626.

[61] Leopold, I. H.; Wong, E. K. In *Cutaneous Toxicity*; Drill, V., Lazar, P., Eds.; Raven: New York, 1984; pp 99–108.

[62] Eskes, C.; Bessou, S.; Bruner, L.; Curren, R.; Harbell, J.; Jones, P.; Kreiling, R.; Liebsch, M.; McNamee, P.; Pape, W. *ATLA: Altern. Lab Anim.* **2005**, *33*, 47–81.

[63] McNamee, P.; Hibatallah, J.; Costabel-Farkas, M.; Goebel, C.; Araki, D.; Dufour, E.; Hewitt, N. J.; Jones, P.; Kirst, A.; Le Varlet, B. *Regul. Toxicol. Pharm.* **2009**, *54*, 197–209.

[64] Borenfreund, E.; Puerner, J. A. *Methods Cell Sci.* **1985**, *9*, 7–9.

[65] Harbell, J. W.; Koontz, S. W.; Lewis, R. W.; Lovell, D.; Acosta, D. *Food Chem. Toxicol.* **1997**, *35*, 79–126.

[66] Blackwell, V.; O'Hara, R.; Clothier, R. H.; Griffin, G.; Balls, M. *ATLA: Altern. Lab. Anim.* **1989**, *17*, 28–37.

[67] Muir, C. K.; Flower, C.; Van Abbe, N. J. *Toxicol. Lett.* **1983**, *18*, 1–5.

[68] Kruszewski, F. H.; Walker, T. L.; Ward, S. L.; DiPasquale, L. C. *Comments Toxicol.* **1995**, *5*, 203–224.

[69] Cottin, M.; Zanvit, A. *Toxicol. In Vitro* **1997**, *11*, 399–405.

[70] Bruner, L. H.; Miller, K. R.; Owicki, J. C.; Parce, J. W.; Muir, V. C. *Toxicol. In Vitro* **1991**, *5*, 277–284.

[71] McConnell, H. M.; Owicki, J. C.; Parce, J. W.; Miller, D. L.; Baxter, G. T.; Wada, H. G.; Pitchford, S. *Science* **1992**, *257*, 1906–1912.

[72] Catroux, P.; Rougier, A.; Dossou, K. G.; Cottin, M. *Toxicol. In Vitro* **1993**, *7*, 465–469.

[73] Ramirez, C. N.; Antczak, C.; Djaballah, H. *Expert Opin. Drug Dis.* **2010**, *5*, 223–233.

[74] McNamee, P.; Hibatallah, J.; Costabel-Farkas, M.; Goebel, C.; Araki, D.; Dufour, E.; Hewitt, N. J.; Jones, P.; Kirst, A.; Le Varlet, B. *Regul. Toxicol. Pharm.* **2009**, *54*, 197–209.

[75] Edinger, A. *Cancer Biol. Ther.* **2010**, *10*, 1262–1265.

[76] Gonzalez, R. J.; Tarloff, J. B. *Toxicol. In Vitro* **2001**, *15*, 257–259.

[77] O'Brien, J.; Wilson, I.; Orton, T.; Pognan, F. *Eur. J. Biochem.* **2000**, *267*, 5421–5426.

[78] Mosmann, T. *J. Immunol. Methods* **1983**, *65*, 55–63.

[79] Berridge, M. V.; Herst, P. M.; Tan, A. S. *Biotechnol. Annu. Rev.* **2005**, *11*, 127–152.

[80] Wilson, A. P. In *Animal Cell Culture, A Practical Approach*, 3rd ed.; Masters, J. R. W., Ed.; Oxford University Press, 2000; Chapter 7, pp 185–191.

[81] Cory, A. H.; Owen, T. C.; Barltrop, J. A.; Cory, J. G. *Cancer Commun.* **1991**, *3*, 207–212.

[82] Water Soluble Tetrazolium Salts (WSTs). http://www.interchim.fr/ft/F/F98881.pdf, Accessed: Jul 15, 2013.

[83] Rahimi, M.; Youn, H.-Y.; McCanna, D. J.; Sivak, J. G.; Mikkelsen, S. R. *Anal. Bioanal. Chem.* **2013**, *405*, 4975–4979.

[84] Lu, Q.; Zhao, J.; Wang, M.; Wang, Z. *Int. J. Electrochem. Sc.* **2011**, *6*, 3868–3877.

[85] Kostesha, N. V.; Almeida, J. R. M.; Heiskanen, A. R.; Gorwa-Grauslund, M. F.; Hahn-Hagerdal, B.; Emneus, J. *Anal. Chem.* **2009**, *81*, 9896–9901.

[86] Zhao, J.; Wang, Z.; Fu, C.; Liu, J.; He, Q. *Anal. Lett.* **2008**, *41*, 2963–2971.

[87] Spegel, C. F.; Heiskanen, A. R.; Kostesha, N.; Johanson, T. H.; Gorwa-Grauslund, M.; Koudelka-Hep, M.; Emneus, J.; Ruzgas, T. *Anal. Chem.* **2007**, *76*, 8919–8926.

[88] Mauzeroll, J.; Bard, A. J. *PNAS* **2004**, *101*, 7862–7867.

[89] Chen, Q.; Cederbaum, A. I. *Mol. Pharmacol.* **1997**, *52*, 648–657.

[90] Olsen, K. W.; Bantseev, V.; Choh, V. *Mol. Vis.* **2011**, *17*, 270–278.

[91] Zhao, J.; Wang, M.; Yang, Z.; Wang, Z.; Wang, H.; Yang, Z. *Ana.l Chim. Acta.* **2007**, *597*, 67–74.

[92] Papa, S.; Guerrieri, F.; Izzo, G.; Boffoli, D. *FEBS Lett.* **1983**, *157*, 15–20.

[93] Koyama, K.; Shimazu, Y. In *Drugs and Poisons in Humans*; Suzuki, O., Watanabe, K., Eds.; Springer, 2005; pp 407–413.

[94] Cheng, W.; Wang, C.-H.; Chen, J.-C. *Dis. Aquat. Org.* **2003**, *53*, 223–229.

[95] Ayaki, M.; Iwasawa, A.; Inoue, Y. *Clin. Ophthalmol.* **2010**, *4*, 1217–1222.

[96] Xu, K.; Zhang, J.; Yu, F.-S. X. *J. Toxicol-Cutan. Ocul.* **2004**, *1*, 29–40.

[97] Ishiyama, M.; Tominaga, H.; Shiga, M.; Sasamoto, K.; Ohkura, Y.; Ueno, K. *Biol. Pharm. Bull.* **1996**, *11*, 1518–1520.

[98] Konynenbelt, B. J.; Mlnarik, D. S.; Ubels, J. L. *Eye Contact Lens* **2011**, *37*, 286–297.

[99] Gautheron, P.; Dukic, M.; Alix, D.; Sina, J. F. *Fund. Appl. Toxicol.* **1992**, *18*, 442–449.

[100] Burton, A. B. G.; York, M.; Lawrence, R. S. *Food Cosmet. Toxicol.* **1981**, *19*, 471–480.

[101] Prinsen, M. K. *Food Chem. Toxicol.* **1996**, *34*, 291–296.

[102] Sivak, J. G.; Stuart, D. D.; Herbert, K. L.; Van Oostrom, J. A.; Segal, L. *Toxicol. Method.* **1992**, *2*, 280–294.

[103] Sivak, J. G.; Herbert, K. L. *J. Toxicol-Cutan. Ocul.* **1997**, *16*, 173–187.

[104] Luepke, N. P. *Food Chem. Toxicol.* **1985**, *23*, 287–291.

[105] Leighton, J.; Nassauer, J.; Tchao, R. *Food Chem. Toxicol.* **1985**, *23*, 293–298.

[106] Worth, A.; Balls, M. *ATLA: Altern. Lab Anim.* **2002**, *30*, 1–125.

[107] Doucet, O.; Lanvin, M.; Thillou, C.; Linossier, C.; Pupat, C.; Merlin, B.; Zastrow, L. *Toxicol. In Vitro* **2006**, *20*, 499–512.

[108] Gettings, S. D.; Lordo, R. A.; Hintze, K. L.; Bagley, D. M.; Casterton, P. L.; Chudkowski, M.; Curren, R. D.; Demetrulias, J. L.; Dipasquale, L. C. *Food Chem. Toxicol.* **1996**, *34*, 79–117.

[109] Bufo, M.; Ulmer, R. *SOFW J.* **2008**, *134*, 18–20, 22–23.

[110] Muir, C. K. *Toxicol. Lett.* **1985**, *24*, 157–162.

[111] Hardin, J.; Bertoni, G.; Kleinsmith, L. J. *Becker's World of the Cell*, 8th ed.; Pearson: New York, 2012.

[112] Balda, M. S.; Gonzalez-Mariscal, L.; Contreras, R. G.; Macias-Silva, M.; Torres-Marquez, M. E.; Garcia Sainz, J. A.; Cereijido, M. *J. Membr. Biol.* **1991**, *122*, 193–202.

[113] Oliver, G. J. A.; Pemberton, M. A.; Rhodes, C. *Food Chem. Toxicol.* **1986**, *24*, 507–512.

[114] Shasby, D. M.; Hampson, F. *Exp. Lung Res.* **1989**, *15*, 345–357.

[115] Froemter, E.; Diamond, J. *Nature* **1972**, *235*, 9–13.

[116] Bacallao, R.; Garfinkel, A.; Monke, S.; Zampighi, G.; Mandel, L. J. *J. Cell Sci.* **1994**, *107*, 3301–3313.

[117] Janecki, A.; Jakubowiak, A.; Steinberger, A. *Toxicol. Appl. Pharm.* **1992**, *102*, 51–57.

[118] Welsh, M. J.; Shasby, D. M.; Husted, R. M. *J. Clin. Invest.* **1985**, *76*, 1155–1168.

[119] Cavet, M. E.; VanDerMeid, K. R.; Harrington, K. L.; Tchao, R.; Ward, K. W.; Zhang, J. Z. *Cont. Lens Anterior Eye* **2010**, *33*, S18–23.

[120] Ward, S. L.; Walker, T. L.; Dimitrijevich, S. D. *Toxicol. In Vitro* **1997**, *11*, 121–139.

[121] Pasternak, A. S.; Miller, W. M. *Biotechnol. Bioeng.* **1996**, *50*, 568–579.

[122] Zieske, J. D.; Mason, V. S.; Wasson, M. E.; Meunier, S. F.; Nolte, C. J. M.; Fukai, N.; Olsen, B. R.; Parenteau, N. L. *Exp. Cell. Res.* **1994**, *214*, 621–633.

[123] Toropainen, E.; Ranta, V.-P.; Vellonen, K.-S.; Palmgren, J.; Talvitie, A.; Laavola, M.; Suhonen, P.; Hamalainen, K. M.; Auriola, S.; Urtti, A. *Eur. J. Pharm. Sci.* **2003**, *20*, 99–106.

[124] Toropainen, E.; Ranta, V. P.; Talvitie, A.; Suhonen, P.; Urtti, A. *Invest. Ophth. Vis. Sci.* **2001**, *42*, 2942–2978.

[125] Holbrook, K. A.; Hennings, H. *J. Invest. Dermatol.* **1983**, *81*, 11s–24s.

[126] Lillie, J. H.; MacCallum, D. K.; Jepsen, A. *Exp. Cell. Res.* **1980**, *125*, 153–165.

[127] Youn, H.-Y.; McCanna, D. J.; Sivak, J. G.; Jones, L. W. *Mol. Vis.* **2011**, *17*, 237–246.

[128] Ward, S. L.; Walker, T. L.; Dimitrijevich, S. D. *Toxicol. In Vitro* **1997**, *11*, 121–139.

[129] Hochman, J.; Artursson, P. *J. Control. Release* **1994**, *29*, 253–267.

[130] Nakamura, T.; Yamada, M.; Teshima, M.; Nakashima, M.; To, H.; Ichikawa, N.; Sasaki, H. *Biol. Pharm. Bull.* **2007**, *30*, 2360–2364.

[131] Chang, J. E.; Basu, S. K.; Lee, V. H. L. *Pharm. Res.* **2000**, *17*, 670–676.

[132] McCanna, D. J.; Harrington, K. L.; Driot, J.-Y.; Ward, K. W.; Tchao, R. *Eye Contact Lens* **2008**, *34*, 6–12.

[133] EC. Manual of Decisions for Implementation of the 6th and 7th Amendments to Directive 67/548/EEC on Dangerous Substances (Updated Version 2006). http://www.reach-compliance.eu, Accessed: May 8, 2013.

[134] Swanson, J. E.; Lake, L. K.; Donnelly, T. A.; Harbell, J. W.; Huggins, J. *J. Toxicol-Cutan. Ocul.* **95**, *14*, 179–195.

[135] Rachui, S. R.; Robertson, W. D.; Duke, M. A.; Paller, B. S.; Ziets, G. A. *In Vitro Toxicol.* **1994**, *7*, 45–52.

[136] Barker, G. C.; Faircloth, R. L.; Gardner, A. W. *Nature* **1958**, *181*, 247–248.

[137] Eggleston, D. L. *Basic Electronics for Scientists and Engineers*; Cambridge University Press: Cambridge, UK, 2011.

[138] Dirkse, T. P.; Shoemaker, R. *J. Electrochem. Soc.* **1968**, *115*, 784–786.

[139] Kolb, D. M.; Schneider, J. *Electrochim. Acta.* **1986**, *31*, 929–936.

[140] Valette, G. *Electroanal. Chem.* **1982**, *138*, 37–54.

[141] Grahame, D. C. *Chem. Rev.* **1947**, *41*, 441–501.

[142] Wang, J. *Analytical electrochemistry*, 2nd ed.; Wiley: New York, 2000.

[143] Cavalcanti, I. T.; Guedes, M. I. F.; Sotomayor, M. D. P. T.; Yamanaka, H.; Dutra, R. F. *Biochem. Eng. J.* **2012**, *67*, 225–230.

[144] Das, J.; Cederquist, K. B.; Zaragoza, A. A.; Lee, P. E.; Sargent, E. H.; Kelley, S. O. *Nat. Chem.* **2012**, *4*, 642–648.

[145] Cui, Y.; Tang, D.; Liu, B.; Chen, H.; Zhang, B.; Chen, G. *Analyst* **2012**, *137*, 1656–1662.

[146] Adams, R. N. *Electrochemistry at Solid Electrodes*; Marcel Dekker, Inc.: New York, 1969.

[147] Pei, X.; Xu, Z.; Zhang, J.; Liu, Z.; Tian, J. *Anal. Method.* **2013**, *5*, 3235–3241.

[148] Tang, J.; Zhou, J.; Li, Q.; Tang, D.; Chen, G.; Yang, H. *Chem. Commun.* **2013**, *49*, 1530–1532.